Exploring long-term determinants of chronological lifespan using system-wide approaches

StJohn Townsend

A dissertation submitted in partial fulfillment of the requirements for the degree of

Doctor of Philosophy

of

University College London.

Department of Genetics, Evolution & Environment
University College London

March 16, 2021

I, StJohn Townsend, confirm that the work presented in this thesis is my own. Where information has been derived from other sources, I confirm that this has been indicated in the work.

Abstract

Ageing is a great research challenge. Age is the primary risk factor for many complex diseases, including cardiovascular disease, neurodegeneration and cancer. Anti-ageing interventions aim to delay the onset of these diseases and extend health span. Ageing remains enigmatic, however, and its proximal cause and mechanisms are not understood. This partly reflects the laborious nature of ageing experiments, typically requiring large timeframes and numerous individuals, which creates a bottleneck for systematic ageing studies.

Yeast can be grown under highly parallelised experimental platforms and are well suited to systematic studies. However, ageing research is a notable exception, with the traditional colony-forming unit (CFU) assay for chronological lifespan being notoriously time- and resource-consuming. I present two alternative assays which circumnavigate this bottleneck. One is a high-throughput CFU assay that is automated by robotics and supported by an R package to estimate culture viability by constructing a statistical model based on colony patterns. The second assay employs barcode sequencing to monitor strain viability in competitively ageing pools of deletion libraries, providing genome-scale functional insights into the genetics of lifespan. I employ this assay to dissect the genetic basis of rapamycin-mediated longevity, providing insights into the condition-specific nature of lifespan-extending mutations and the anti-ageing action of rapamycin.

Experimental reproducibility is essential for research. Ageing studies, including those in yeast, are notably sensitive to batch effects: genetically identical cells grown under identical conditions can exhibit substantial phenotypic

Abstract 4

differences. I systematically test typically neglected factors, and demonstrate that chronological lifespan is strongly affected by pre-culture protocol such as the amount of colony picked for the pre-culture – suggesting a 'memory' which is passed across cell divisions from pre-culture to non-dividing, ageing cells. Hence, this work addresses key issues in yeast ageing research, both technological and biological, establishing a platform to robustly perform future studies at large scales.

Impact Statement

Age is the number on risk factor for a variety of chronic diseases, including cancer, neurodegeneration, diabetes and cardiovascular disease. However, anti-ageing interventions offer great promise as they simultaneously delay the onset of these diseases and increase healthspan. Despite many exciting developments in ageing research, we are still far from understanding this enigmatic component of the human condition.

This is in part because ageing research is notoriously challenging. By its nature, an ageing experiment lasts the entire lifespan of an organism, which may be several years. Furthermore, lifespan is one of the most complex phenotypes in biology, meaning that lifespan experiments tend to get complicated very quickly, and it is often difficult to disentangle cause, correlation and effect. To make matters worse, lifespan is one of the most sensitive and variable phenotypes in biology, probably because of the complex interactions between processes which determine lifespan. As a result, ageing experiments require large number of individuals and also suffer from a lack of reproducibility. Collectively, this makes for a rather challenging field of research: the complexity of ageing necessitates large-scale, systematic studies; the resource-intensive, labour-intensive and often wasteful nature of these experiments prohibits large-scale studies.

Yeast, being well-suited to systematic studies, offer promise to solving these issues. However, there are still major bottlenecks which must be overcome. In this work, I present two methods which can accurately measure fission yeast lifespan in a high-throughput manner, expanding the toolkit available for generating systematic ageing datasets. I also apply these methods to dissect various aspects of fission yeast lifespan. In one case, I use a method called barcode sequencing to map the genetics associated with the anti-ageing drug rapamycin, which works by tricking cells into thinking they are starving and mimicking the beneficial effects of dietary restriction. In doing so, I reveal a huge number of genetic components which interact with rapamycin, from the molecular machinery which is at the centre of rapamycin's effects, to the numerous processes which rapamycin targets as part of its anti-ageing effects. Using another high-throughput lifespan method, I explore the reasons why lifespan experiments are so irreproducible. The results revealed some unexpected findings about the factors which determine yeast lifespan – the yeast "talk to each other" using a process called quorum sensing, and in doing so, can establish "memories" which determine their lifespan. It turns out that yeast have far more control over their lifespan than is generally appreciated, and although this sounds rather quirky, it actually makes perfect sense when you consider the ecological needs of yeast.

Hence, this research tackles multiple challenges in yeast ageing, and establishes a platform from which robust, large-scale ageing studies can be readily conducted. By overcoming bottlenecks which hamper ageing research, we are a step closer to generating datasets of sufficient complexity which may be used as a basis to develop mechanistic, as opposed to descriptive, model of ageing. Such models will have dramatic repercussions for our understanding of disease and ageing.

Acknowledgements

First and foremost, I would like to acknowledge my supervisors, Professor Jürg Bähler and Professor Markus Ralser, for the independence they have afforded me to pursue my own research, to test my hunches, to make mistakes, to figure out what kind of scientist I am, and to provide me with the tools to grow into that scientist. I would also like to acknowledge members of the Bähler and Ralser labs for their continuous support, collaboration and motivation, including Babis Rallis, Mar´ıa Rodr´ıguez-López, Clara Correia-Melo, Catalina-Andreea Romila, Olivia Hillson, Shajahan Anver, Michal Malecki, Shaimaa Hassan, Cristina Cotobal, Mimoza Hoti, Enrica Calvani, Christoph Messner and Michael Mülleder. I have also had the wonderful opportunity to be part of research from other fields, and I would like to acknowledge Carina Kern, Christopher Minnis and Joanna Kirkpatrick for those experiences. Working with each and every one of these colleagues has been a pleasure. They have inspired me and my science. I thank them for that.

I would also like to acknowledge my mother, my father and my brother. They have supported me throughout my life. They have fought to remove barriers in my life, fought to ensure that I always had the best opportunities possible, and in doing so have allowed me to follow my dreams. They have always been there. I would not have achieved what I have thus far in life without their support. I thank them for that.

Finally, I would like to acknowledge the many wonderful friends who have been part of my life throughout my PhD. They are the ones who have been by my side when things were difficult, the ones who have kept motivating me to move forward, and the ones who have reminded me that there is more to life than science. I thank them for that.

We shall not cease from exploration

And the end of all our exploring

Will be to arrive where we started

And know the place for the first time

Contents

Intr	roduction 17				
1.1	An ageing population				
1.2	A brief history of ageing research				
1.3	Challenges in ageing research				
1.4	Fission yeast as an ageing model				
1.5	High-throughput ageing studies in yeast				
1.6	Towards an integrated view of yeast ageing				
1.7	Contributions of this work				
_	•				
	-				
2.1	Introduction				
2.2	Methods & Results				
	2.2.1	Implementation of a high-throughput CFU assay	25		
	2.2.2	Image acquisition and analysis	27		
	2.2.3	Modelling of colony patterns	27		
	2.2.4	Estimation of viability from colony patterns	31		
	2.2.5	Validation of high-throughput CFU assay	32		
	2.2.6	Analysis of deletion mutant lifespan curves	34		
	2.2.7	Development of an R package to analyse high-			
		throughput CFU assays	36		
2.3	Discussion		36		
	2.3.1	Differences between the high-throughput and traditional			
		CFU assays	36		
	1.1 1.2 1.3 1.4 1.5 1.6 1.7 Dev 2.1 2.2	 1.1 An ag 1.2 A brie 1.3 Challe 1.4 Fission 1.5 High- 1.6 Towar 1.7 Contri Developm 2.1 Introd 2.2 Method 2.2.1 2.2.2 2.2.3 2.2.4 2.2.5 2.2.6 2.2.7 2.3 Discus 	1.2 A brief history of ageing research		

		2.3.2	Mutants with altered CLS	37
	2.4	Concl	usion	38
3	Esta	ablishi	ng a platform for genome-scale chronological lifespa	n
			fission yeast via barcode sequencing	39
	3.1	Introd	luction	39
	3.2	Metho	ods & Results	41
		3.2.1	Decoding of deletion mutant barcodes	41
		3.2.2	Persistence of DNA from dead cells necessitates re-	
			growth of stationary phase cultures prior to barcode se-	
			quencing	46
		3.2.3	Culture re-growth introduces a sampling bottleneck	
			which must be accounted for in order to model mutant	
			abundance correctly	49
		3.2.4	Detecting mutants with altered chronological lifespan	51
		3.2.5	Validaiton of Bar-seq screen against high-throughput	
			CFU assay	51
		3.2.6	Late stationary phase pools become dominated by short-	
			lived mutants	52
	3.3	Discus	ssion & Conclusion	55
4	Dis	secting	the genetic basis of rapamycin-mediated lifespan	
	ext	ension	recapitulates the spatial organisation of TOR sig-	
	nal	ling		57
	4.1	Introd	luction	57
	4.2	Metho	ods & Results	60
		4.2.1	Pooling and ageing of deletion mutants	60
		4.2.2	Library preparation and sequencing	61
		4.2.3	Analysis of sequencing data	62
		4.2.4	Identification of mutants with altered response to ra-	
			pamycin	64

	4.3	Discu	ssion	71
		4.3.1	The lifespan extension conferred by rapamcyin is medi-	
			ated by autophagy	71
		4.3.2	Diverse aspects of endosome function are required for	
			rapamycin-mediated lifespan extension	72
		4.3.3	Rapamycin-mediated lifespan extension is dependent on	
			Class III PI3K signalling to initiate autophagy	76
		4.3.4	Class III PI3K signalling is also mediates nutrient sens-	
			ing upstream of TORC1	77
		4.3.5	Distinct interaction profiles of PI3K mutants may reflect	
			interconnected positive and negative feedback loops in-	
			volved in TORC1 control of autophagy	78
		4.3.6	Inhibition of clathrin-mediated endocytosis can further	
			extend lifespan following rapamycin treatment	78
		4.3.7	TORC1 and PKA coordinate different temporal aspects	
			of starvation response	79
4.4		Concl	usion	81
5	Cor	nclusio	ns & Future Directions	102
Appendix 1			105	
Analysis of high-throughput colony forming units assays 10			105	
References 1			112	

List of Figures

2.1	Schematic depiction of traditional CFU assay	<u>2</u> 4
2.2	Resource usage comparison for traditional vs high-throughput	
	CFU assays2	26
2.3	Schematic depiction of high-throughput CFU assay2	26
2.4	Image analysis pipeline for high-throughput CFU assay2	28
2.5	Probability distributions for colony patterns in high-throughput	
	CFU assay	30
2.6	Analysis of colony patterns for wild-type cells grown in YES	32
2.7	Comparison of traditional and high-throughput CFU measure	e-
	ments	33
2.8	Proxy calculation for 48 strains.	35
3.1	Systematic construction of barcoded deletion mutants in fissio	m
3.1	yeast4	
2.2		
3.2	Manual curation of barcodes by viewing aligned reads in	
	genome browser	13
3.3	Chronological lifespan curves of pooled mutants4	ŀ7
3.4	Correlation of barcode frequencies from chronologically agein	ıg
	mutant pools.	18
3.5	Comparison of re-growth bottleneck size to library size for age-	
	ing pools4	19
3.6	Volcano plot showing changes in pool composition through sta	a-
	tionary phase.	52
3.7	Validaiton of Bar-seq screen against high-throughput CFU assay. 53	3

3.8	Late stationary phase pools become dominated by short-li	ved
	mutants	54
4.1	CLS of rapamycin-treated and -untreated pools	61
4.2	Pairwise correlations of read counts in rapamycin-treated and	
	-untreated pools	63
4.3	Identification of mutants with altered CLS	66
4.4	Functional enrichments involved in rapamycin-mediated lifes-	
	pan extension.	67

List of Tables

1 1	TP: 1 (1 C 1 1	•	- 1
41	Limenoints selected for harcode	sequencing6	١I
1.1	Time points selected for bareode	bequerien g	,,

Chapter 1

Introduction

1.1 An ageing population

The world is undergoing dramatic demographic shifts, with the proportion of elderly increasing in nearly every country [1]. Age is the biggest risk factor in a variety of chronic diseases, including cancer, autoimmune diseases, neurodegenerative disorders and cardiovascular diseases [2]. The increased incidence of these diseases is becoming a hallmark of 21st century life, meaning that ageing presents great biomedical, economic and social challenges. Whilst it is critical to treat individual diseases as they arise, an anti-ageing intervention promises to simultaneously delay the onset of all of these diseases and increase healthspan. Hence, ageing research aims to fundamentally discern the nature of ageing, and in doing so identify pharmacological and dietary interventions which may increase healthspan.

1.2 A brief history of ageing research

Ageing, due to its intimate relationship with death, has always been one of the most enigmatic aspects of the human condition. For much of history, ageing was viewed as an inevitable consequence of entropy [3]. However, research in the 1990s demonstrated that simple genetic perturbations could have produce dramatic increases in the lifespan on nematode worms [4, 5]. Not only did these results challenge the view that age-associated decline is inevitable, but they legitimised ageing as a field of research. Studies utilising various model

systems continued to demonstrate that age-associated decline is plastic, and ageing was consolidated as a field when it became apparent that ageing in eukaryotes is regulated by a conserved regulatory system of nutrient sensing pathways [6]. Ageing research has continued to dissect these pathways and it has become clear that many chronic diseases associated with ageing share a common regulation and are interwtined [2].

1.3 Challenges in ageing research

Ageing research is notoriously challenging. By its nature, an ageing experiment lasts the entire lifespan of an organism, which is several years in most vertebrate model systems. Furthermore, large cohorts of individuals are required because there is substantial phenotypic variability in lifespan even between genetically identical individuals maintained under identical environmental conditions [7]. There can also be great variability in lifespan between repeats of the same experiment, and it requires a great deal of work to identify the sources of this experimental irreproducibility [8]. Hence, ageing research is laborious, slow and resource-intensive, and the identification of even a single factor which robustly increases lifespan is a challenging endeavor [9].

Ageing is also a difficult process to study due to its multifactorial nature [10, 11]. This is true for both the factors which regulate ageing and the physiological consequences of ageing, which are often confounded due to regulatory feedback mechanisms [12, 13]. This complexity means that it is extremely difficult to develop mechanistic (as opposed to descriptive) models of ageing. Consequently, there has been much debate, and little consensus, as to how to define the proximal cause of ageing [10, 11, 12, 13, 14, 15, 16].

1.4 Fission yeast as an ageing model

The fission yeast *Schizosaccharomyces pombe* (*S. pombe*) is a proven eukaryotic model organism; it is simple, can be studied under tightly controlled environmental conditions, and has a low complexity, well-annotated genome. Additionally, its short lifespan carries clear advantages in ageing research, making

it possible to complete an ageing experiment over the course days or weeks. Whilst most research in the field of yeast ageing has been carried out in the budding yeast *Saccharomyces cerevisiae* [17], fission yeast has emerged as a potent alternative model system [18]. Approximately 70% of its genes have identifiable human orthologs [19], making *S. pombe* an excellent model to study conserved biological processes which play fundamental roles in eukaryotic ageing. In addition, *S. pombe* is only distantly related to *S. cerevisiae*, having diverged around 400 million years ago [20], and can thus provide complementary insights [18]. Indeed, the genetic, environmental and pharmacological interventions which can extend lifespan are remarkably well conserved from yeast to humans [17, 18], suggesting that ageing is conserved across eukaryotes.

Two forms of ageing have been described in yeast: replicative and chronological ageing [17, 18, 21]. Replicative lifespan (RLS) is defined as the number of times a mother cell can divide before senescence [22], and is used as a model for ageing in mitotically active cells. In budding yeast, which divide asymmetrically, mother and daughter cells can be easily distinguished under the microscope and RLS can be measured [17]. In fission yeast, which divide symmetrically, there is no clear mother or daughter cell, and it is disputed whether replicative ageing exists in fission yeast [23, 24].

Chronological lifespan (CLS) is defined as the amount of time a cell can remain viable in a non-dividing state, and is used as a model for ageing in post-mitotic cells. Chronological ageing is usually induced by allowing cultures to reach stationary phase, where cells enter a non-dividing state following glucose exhaustion [25]. However, chronological ageing can also be induced by restricting the cells of a key nutrient, such as the carbon [26] or nitrogen [27] source, or even by physically restricting the cells such that they cannot divide [28]. Furthermore, CLS assays can vary in their definition of viability; traditionally, viability is measured by determining the number of colony-forming units (CFUs) in the ageing culture, defining cells as viable if they are able to re-enter

the cell cycle upon return to growth-favourable conditions [25]. Alternative measures of viability involve using fluorescent dyes such as propidium iodide and MTT, which report cell membrane integrity [29] and metabolic activity [30] respectively. These dyes are typically measured using a flow cytometer, fluorescent microscope or fluorescent plate reader.

1.5 High-throughput ageing studies in yeast

Yeast can be cultured under tightly controlled conditions in parallelised experimental platforms, making them well suited for high-throughput, systematic studies [31]. However, both the traditional RLS [22] and CLS [25] assays are laborious and do not scale well to high-throughput studies. Hence, the development of novel assays which circumnavigate these bottlenecks is a critical prerequisite to systematic ageing studies which have the potential to dissect the complexity of ageing.

Determination of RLS requires prolonged observation of a mother cell under the microscope. High-throughput approaches to determination of RLS typically employ a microfluidic device which can trap mother cells whilst allowing daughter cells to be removed via fluid flow [23, 32]. High-throughput CLS assays are more varied, and can differ substantially in the platform used to culture many samples in parallel and the way in which CLS is measured. The first high-throughput CLS assay developed involved growing and ageing cultures in a 96-well plate, and then using a small aliquot of the ageing culture to inoculate a re-growth culture [33]. The optical density of the re-growth culture after a defined period of time can be measured using a plate reader, serving as an indication of the number of viable cells in the inoculum. A conceptually similar approach is to competitively age two strains labelled with different fluorophores (for example, a mutant and a wild-type control), and to measure relative fluorescence of a re-growth culture to indicate relative survival [34, 35]. Another approach involves growing and ageing cells in a 96-well plate and then using high-throughput flow cytometry to measure the proportion of

cells stained with a dye which indicates viability [30, 36].

Genome-wide collections of non-essential deletion mutants are powerful tools for investigating gene function. In both the *S. cerevisiae* [37] and *S. pombe* [38] deletion collections, each individual gene has been deleted and replaced with an antibiotic resistance cassette flanked by specific DNA barcodes (UpTag and DnTag). Hence, deletion mutants can be pooled and the abundance of each mutant can be measured using DNA microarrays [39] or next-generation sequencing, termed barcode sequecning, or Bar-seq [40, 41]. These approaches have been adapted to monitor mutant survival in chronologically ageing pools of deletion mutants [27, 42], providing quantitative, genome-scale insights into the genetic basis of lifespan in a highly parallelised manner.

1.6 Towards an integrated view of yeast ageing

The vast majority of genetic factors which alter lifespan have been found in yeast, worms and flies. Many of these factors are shared, suggesting that a conserved system regulating ageing arose early in eukaryotic evolution [6], perhaps even earlier [43, 44]. Of particular note are the stress response genes and nutrient sensors [45]. These genes integrate numerous extracellular and intracellular signals to determine whether an organism is experiencing stress, and are responsible for inducing a physiological shift towards cell maintenance and protection when conditions are not favourable to growth.

However, ageing is still a poorly understood process, and there remains much work to uncover all genes which affect ageing and to understand the interactions between them [46]. High-throughput lifespan screens in yeast have uncovered hundreds of genetic factors which are involved in ageing, but the overlap between these screens is surprisingly poor [35]. Indeed, the genetic variants associated with longevity differ substantially based on environmental conditions [36], with even subtle changes in culture conditions leading to marked changes in the genetic basis of lifespan [47]. This is concordant with

the high degree of irreproducibility observed in ageing research [8], suggesting that lifespan is a highly sensitive phenotype which is tightly regulated in a context-dependent manner.

1.7 Contributions of this work

In this work, I present a variety of experimental and analytical advancements which facilitate systematic ageing studies in yeast. The first of these is a high-throughput CFU assay which can be largely automated using robotics. This provides a day-to-day alternative to the notoriously labour- and resourceintensive traditional CFU assay which can be used for CLS determination of batch cultures. The second is a refinement of Bar-seq in order to identify mutants with alterned CLS. This involved decoding the barcodes for the majority of mutants in the latest version of the Bioneer deletion library [38], allowing parallel profiling of a substantially higher proportion of the fission yeast non-essential genome than previously possible, in addition to addressing key technical and statistical biases which arise when Bar-seq is used to study CLS. I then apply Bar-seq to dissect the genetic basis of rapamycin-mediated lifespan extension, providing insights into the genetic components which interact with rapamycin in an ageing context. Collectively, this thesis tackles many of the bottlenecks in yeast ageing, establishing a platform from which robust ageing studies can be readily conducted in a high-throughput manner.

Chapter 2

Development of a high-throughput colony-forming unit assay

2.1 Introduction

Chronological lifespan (CLS) is defined as the amount of time a cell can remain viable in a non-dividing state, and is regarded as a model for ageing in post-mitotic tissues [25]. More generally, CLS assays are one of the workhorses of ageing research, allowing the effect of a genetic, environmental or pharmacological perturbation on lifespan to be assessed with relative ease compared to other ageing models [48]. Hence, many genes associated with ageing have been identified using the traditional CFU assay for CLS in both budding yeast [17] and fission yeast [18, 49].

The traditional CFU assay involves diluting and spreading aliquots of ageing cultures on agar and counting the number of colony-forming units (CFUs), which can be used to calculate the number of viable cells in the ageing culture (Figure 2.1) [17, 18]. Whilst this is far more tractable than most ageing research, it is still slow by yeast standards, and does not leverage the amenability of yeast to high-throughput approaches. In particular, since the viability of the culture is not known, the dilution factor which will result in a quantifiable

number of CFUs is also not known, so multiple dilution factors must be plated out in order to ensure that at least one dilution factor is quantifiable. This underpins the laborious and resource-intensive nature of this assay.

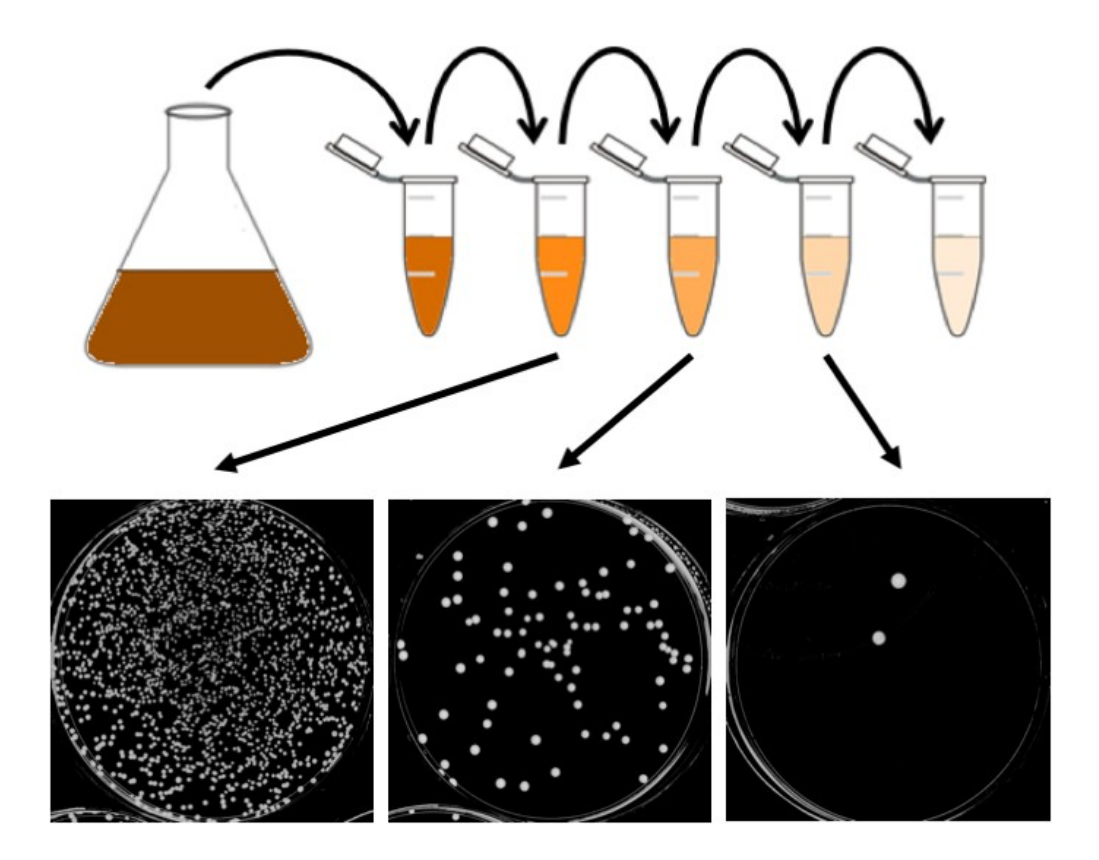


Figure 2.1: Schematic depiction of traditional CFU assay. An aliquot of an ageing culture is serially diluted (in this case 10-fold), and the dilution factors are spread on solid agar. After 2-4 days growth, colonies can be counted for one of the dilution factors, allowing the number of CFUs to be calculated for the ageing culture.

As a result, there has been much focus on developing CLS assays which circumnavigate the bottlenecks imposed by the traditional CFU assay, as discussed in Chapter 1. However, these assays are highly specialised, and often limited to a particular application. For example, some are only compatible with specific mutant libraries [27, 34, 42]. And none directly measure the ability for a cell to re-enter the cell cycle - that is, measure the number of CFUs instead relying on re-growth kinetics [33, 34] or fluorescent dyes which measure a feature associated associated with viability such as metabolic activity [30]

or cell membrane integrity [36]. Hence, there is a need for an alternative CFU assay which does not suffer from the drawbacks of the traditional assay and can serve as a replacement for the traditional assay in day-to-day applications.

One such assay does already exist - the spot assay, where cultures are serially diluted and spotted onto agar. This assay has already been adapted to measure CLS [50], and carries several advantages compared to the traditional CFU assay - all dilution factors for a culture are spotted on the same agar plate, and multiple cultures can be spotted in parallel on the same plate, making this assay far less resource-intensive than the traditional assay. However, a major disadvantage of this assay is that it is qualitative, not quantitative, in nature. Hence, differences in CLS must be assessed by eye, meaning that this assay is not a suitable alternative for high-throughput, systematic ageing studies.

In this chapter, I present a novel high-throughput CFU assay which can be largely automated by robotics. This assay is in essence a spot assay, but by pinning each dilution factor multiple times, a digital pattern of colonies can be extracted for each culture. By modelling the dilution and pinning process, it is possible to analyse the digital pattern of colonies and quantitatively estimate the number of CFUs for each culture. I validate this assay by measuring CFUs for a variety of mutants with different lifespans using both the traditional and novel high-throughput methods. CFU measurements from both methods are highly correlated, but the high-throughput method can capture the same amount of information using far less plates (Figure 2.2).

2.2 Methods & Results

2.2.1 Implementation of a high-throughput CFU assay

Ageing cultures are processed in batches of 8 (Figure 2.3). 150 μ L aliquots of cultures are loaded into the first column of a 96-well plate. Other wells are filled with 100 μ L YES. By taking 50 μ L of the ageing cultures, the ageing cultures are serially diluted 3-fold across the plate using an ASSIST automated multichannel pipette (INTEGRA Biosciences Ltd, UK), ensuring that each



Figure 2.2: Resource usage comparison for traditional *vs* high-throughput CFU assays.

Left: 1944 agar plates are required in order to measure CFUs for 24 cultures at 9 different time points using the traditional assay. For this, 3 dilution factors are plated in triplicate for each culture. Right: 108 agar plates can capture the same information using the high-throughput CFU assay, pinning each dilution factor in replicates of 16. Future refinements to the assay demonstrated that the same information can be acquired using only quadruplicate replicate pins, meaning that in fact only 27 plates are required.

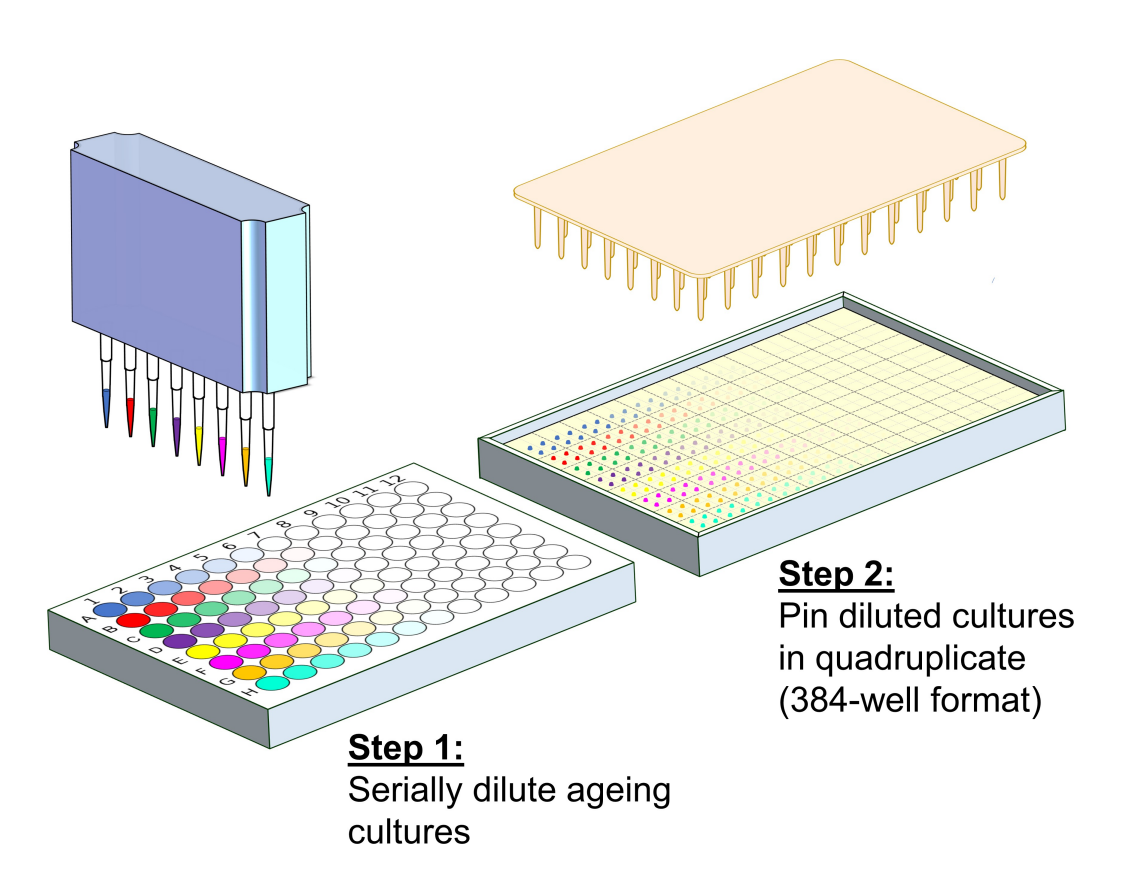


Figure 2.3: Schematic depiction of high-throughput CFU assay. Aliquots of ageing culture are serially diluted across a 96-well plate. Droplets of diluted culture are arrayed on agar in quadruplicate (384-well format) using a pinning robot.

dilution factors is well mixed before proceeding to the next. Diluted cultures are immediately pinned on YES agar in quadruplicate using a ROTOR HDA

pinning robot (Singer Instruments, UK). For this, 96-well format long pins are used to array droplets of diluted cultures in 384-well format, ensuring that the source plate is revisited before each pin onto agar. Agar plates are incubated at 32°C until patterns of colonies are clearly visible.

2.2.2 Image acquisition and analysis

Images of plates are acquired using an Epson V700 scanner in transmission mode. The first step to quantifying CFUs for each measurement is to determine whether or not there is a colony in each position on the agar plate using the gitter package in R [51]. For this, it is essential to provide a reference image of colonies in 384-well format which can be used to align colonies correctly in sparsely population regions of the agar plate (Figure 2.4A). For each raw image analysed (Figure 2.4B), gitter will then identify colonies and provide colony size measurements for each position on the agar plate (Figure 2.4C). The distribution of log-transformed colony sizes can be analysed and thresholded using Otsu thresholding [52] in order to classify colonies are present or absent for each position on the agar plate (Figure 2.4D). Using this, it is possible to extract a digital vector for each measurement representing how many colonies are present at each dilution factor (Figure 2.4E).

2.2.3 Modelling of colony patterns

In order to estimate CFUs for each measurement, the number of CFUs per droplet of ageing culture is modelled, with a droplet being the amount dispensed by a 96-well format long pin. As cultures are serially diluted, the mean number of CFUs per droplet will exponentially decrease across the 96-well plate. The number of CFUs in a single droplet can be modelled as Poisson distributed according to the mean number of CFUs per droplet. In the case that there are 1 or more CFUs in a droplet, a colony will grow, and if there are 0 CFUs, there will be no colony. Hence, from the Poisson distribution it is possible to calculate the probability of observing or not observing a colony according to the mean number of CFUs per droplet. Given that each dilu-

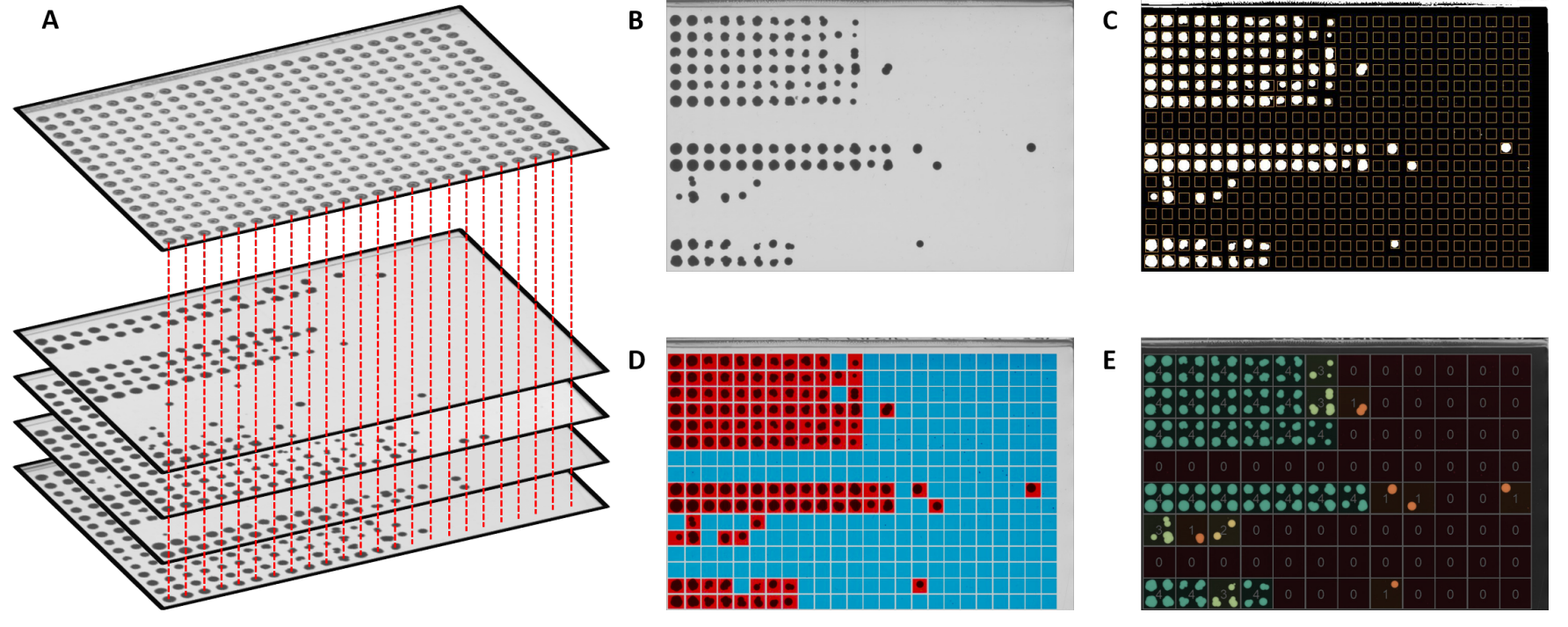


Figure 2.4: Image analysis pipeline for high-throughput CFU assay.

A: A reference image containing colonies arrayed in 384-well format must be provided for each batch of images analysed. This ensures that colonies in sparsely populated regions of the plate can be aligned to the reference image in order to correctly determine their positions in 384-well format. In order for the images to be aligned correctly, all images must be of the same dimensions and acquired in exactly the same positioning. B: A raw image of colony patterns for 8 ageing cultures of different viabilities. C: A 384-well grid is aligned to the raw image according to the reference image and colonies are identified. This image is produced by gitter [51]. D: The distribution of colony sizes for a batch of plates is analysed and thresholded in order to classify colonies as present or absent in each position on the 384-well plate. Red indicates present, blue indicates absent. E: The number of colonies present at each dilution factor for each culture is counted and indicated at the centre of each quadruplicate. Colonies are coloured from red through amber to green according to the number of colonies which grew in each quadruplicate. This creates a vector for each sample indicating how many colonies are present at each dilution factor.

tion factor is pinned in quadruplicate, the number of colonies present at each dilution factor can be modelled as binomially distributed according to the probability of observing a colony.

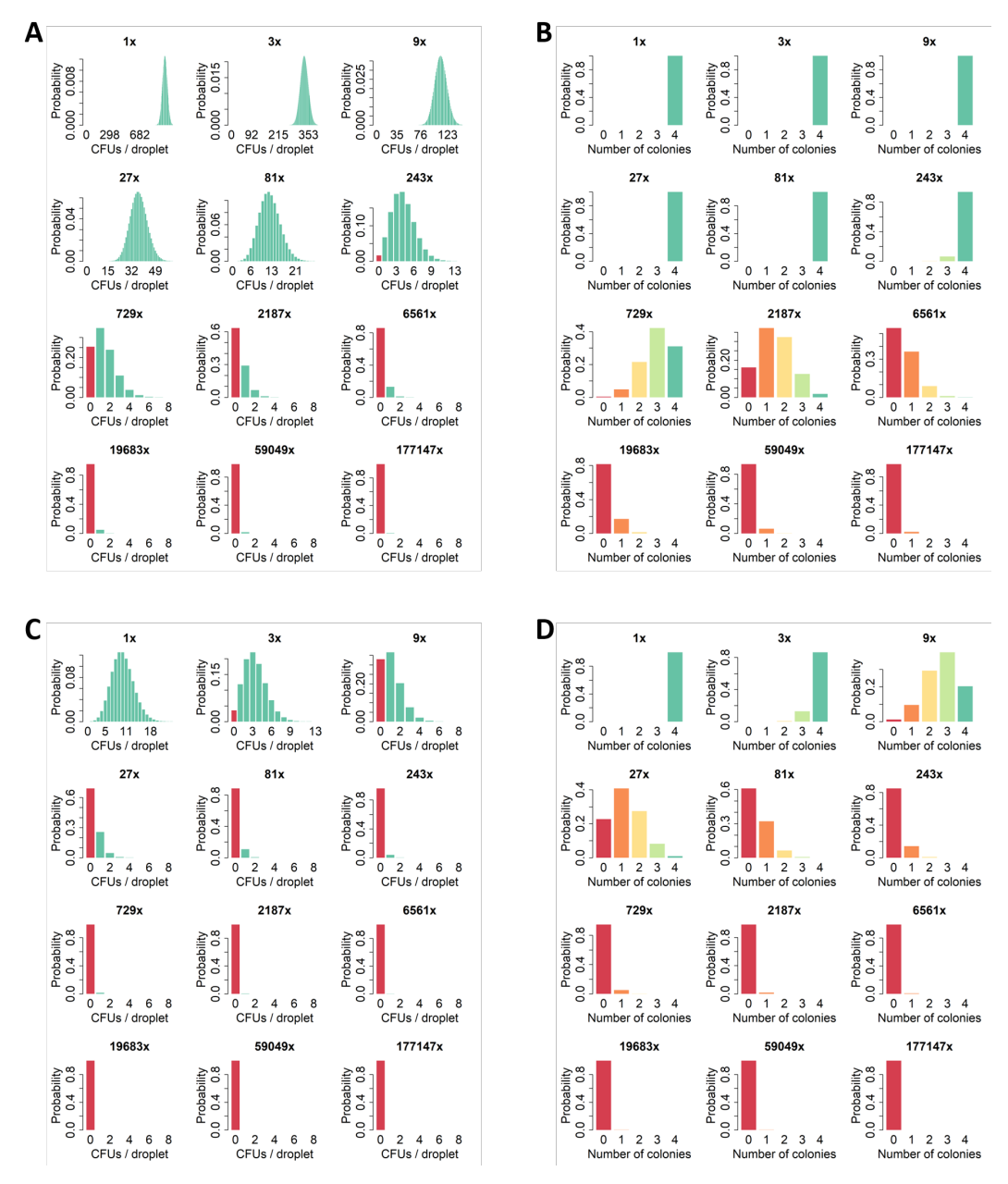


Figure 2.5: Probability distributions for colony patterns in high-throughput CFU assay.

A: In the case that there is a mean of 1000 CFUs per droplet in an ageing culture, probability distributions for the number of CFUs per droplet according to the Poisson distribution is shown for all dilution factors in a 3-fold serial dilution. For this, it is assumed that the mean number of CFUs per droplet exponentially decreases with each dilution factor, which hence changes the shape of the distribution for each dilution factor. Green bars indicate that there is at least 1 CFU in a droplet, in which case a colony will grow. Red bars indicate there are 0 CFUs in a droplet, in which case no colony will grow. B: For the same case as in A, probability distributions for the number of colonies colonies at each dilution factor is shown according to the binomial distribution if serial dilutions are pinned in quadruplicate. The shape of the distribution changes as a function of the probability of observing a colony (i.e. the sum of all green bars for the equivalent dilution factor in A). Bars are coloured from red through amber to green according to the number of colonies grown. C: Same as A, for the case of a mean of 10 CFUs per droplet. D: Same as B, for the case of a mean of 10 CFUs per droplet.

Using this model, it is hence possible to calculate the probability of observing a particular colony pattern if the mean number of CFUs per droplet is known. For example, in the hypothetical case that there is a mean of 1000 CFUs per droplet in an ageing culture, Figure 2.5A shows the probability distributions for the number of CFUs pinned at each dilution factor according to the Poisson distribution, from which the probability of a colony growing can be calculated. Likewise, Figure 2.5B shows the probability distributions for the number of colonies which grow at each dilution factor according to the binomial distribution. Conversely, Figures 2.5C & 2.5D respectively show equivalent Poisson and binomial probability distributions in the hypothetical case that there is a mean of 10 CFUs per droplet in an ageing culture. From the distributions, it is clear in this case that a colony pattern generated from 10 CFUs per droplet will span less dilution factors than a pattern generated from 1000 CFUs per droplet, consistent with what is expected in a spot assay.

2.2.4 Estimation of viability from colony patterns

The model described in the previous section allows colony patterns to be predicted if the mean number of CFUs per droplet is known. In order to quantify CFUs from colony patterns, the model is used to perform a maximum likelihood estimation - that is, to determine the mean number of CFUs per droplet which is most likely to give rise to the observed colony pattern. For this, Brent optimisation [53] is used to find the value of mean CFUs per droplet which maximises the log-likelihood function. Maximum likelihood estimators are known to be highly sensitive to anomalous data points [54]. In this context, anomalous data points may arise due to a colony being misclassified as present or absent in the image analysis pipeline, a contamination on the plate, or pinning errors. To account for this, an error checking algorithm is implemented, which identifies and removes data points which are extremely unlikely to observe, greatly improving the stability of the maximum likelihood estimator. Measurements for which several data points had to be removed in order to achieve a stable maximum likelihood estimator can be excluded from

downstream analyses. Confidence intervals for the estimate of mean CFUs per droplet are calculated using likelihood ratio testing [55]. This represents the statistical error associated with the maximum likelihood estimator, and does not include other technical sources of error (such as errors in the serial dilutions). Figure 2.6A shows a timelapse of colony patterns for chronologically ageing wild-type cells (972 *h*-) in YES. Corresponding maximum likelihood estimates, in addition to 95% confidence intervals, are plotted as a function of time in Figure 2.6B.

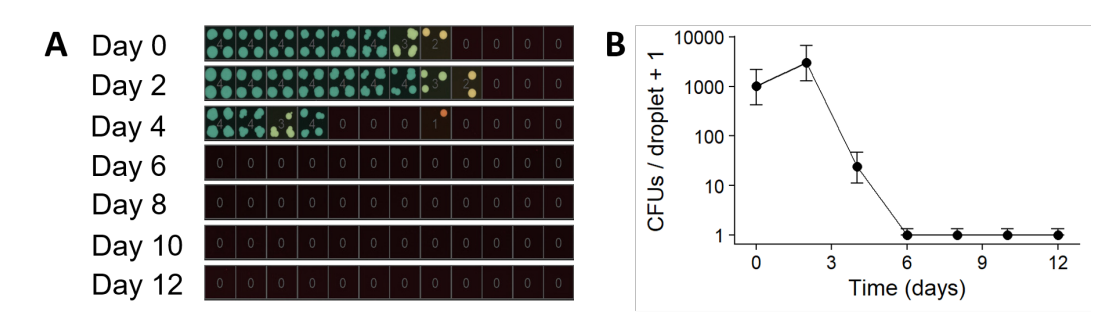


Figure 2.6: Analysis of colony patterns for wild-type cells grown in YES. **A:** Timelapse of colony patterns for chronologically ageing wild-type cells grown in YES. Colonies are coloured from red through amber to green according to the number of colonies grown at each dilution factor. The number of colonies grown at each dilution factor is shown in the centre of each quadruplicate. **B:** The number of CFUs per droplet is estimated via maximum likelihood based on the colony patterns in A, and is used to generate a lifespan curve. Error bars represent 95% confidence intervals based on likelihood ratio testing.

2.2.5 Validation of high-throughput CFU assay

To validate this assay, I measured lifespan curves for 6 strains with known lifespan differences using both the traditional and high-throughput assays. For wild-type, the 972 h- strain was used, gsk3::natMX6 h- was generated in a previous study [56], whilst reb1::natMX6 h-, atf1::natMX6 h-, php2::natMX6 h- and pka1::kanMX4 h- are unpublished strains from the Bähler laboratory strain collection and were generated as described previously [57]. For CLS experiments, strains were streaked to single colonies on YES agar. After 2 days growth at 32°C, a single colony of each strain was picked and used to inoculate YES pre-cultures. These were grown for 1 day at 32°C, shaking at

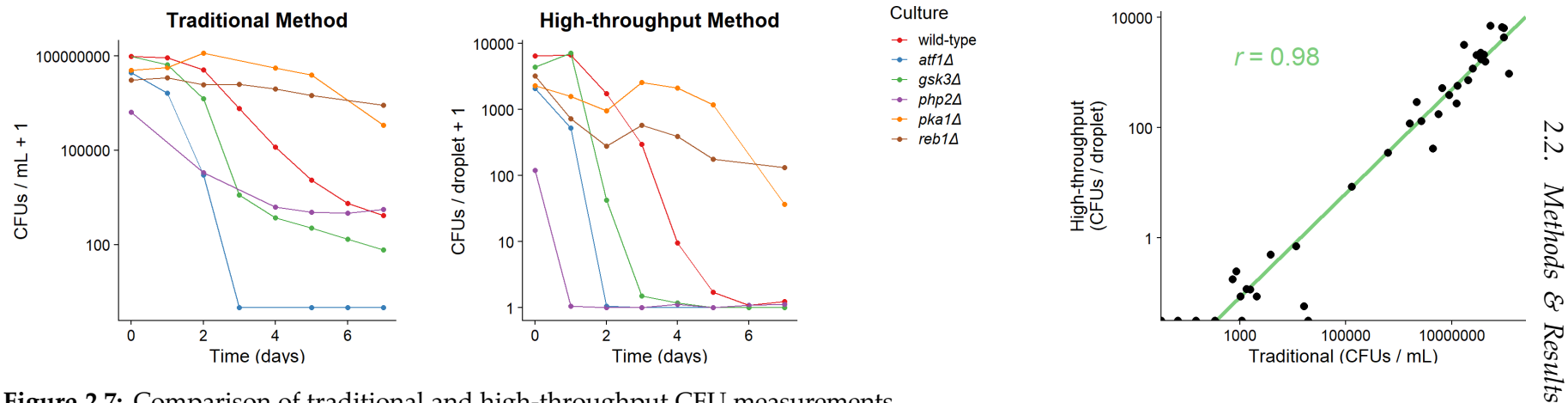


Figure 2.7: Comparison of traditional and high-throughput CFU measurements.

A: Lifespan curves for 6 strains with different CLS measured used the traditional methods. B: For the same cultures as in A, lifespan curves measured using the high-throughput method. C: Scatter plot comparing CFU measurements for all strains across all timepoints. Green line shows a linear regression of log-transformed CFU values (traditional vs high-throughput). Pearson correlation coefficient is also shown in green.

170rpm, after which YES cultures were inoculated. Cultures were grown at 32°C, shaking at 170 rpm. After 2 days cultures had reached stationary phase, which is taken to be day 0 of the lifespan curve. For each culture, CFUs were measured using the high-throughput method, and using the traditional method as described previously [58].

Figure 2.7A shows lifespan curves for these 6 strains measured using the traditional method. Lifespan curves for the same cultures measured using the high-throughput method show good agreement (Figure 2.7B) - $pka1\Delta$ and $reb1\Delta$ are both long-lived relative to the wild-type according to both methods, whilst $gsk3\Delta$, $atf1\Delta$ and $php2\Delta$ are all short-lived relative to the wild-type according to both methods. In order to quantify the extent of the agreement, all traditional method CFU measurements (all strains across all timepoints) are plotted against the corresponding high-throughput measurement in Figure 2.7C, with the two methods showing excellent agreement (r = 0.98).

2.2.6 Analysis of deletion mutant lifespan curves

In order to facilitate downstream analyses and integration with other datasets, I have developed a proxy which summarises the lifespan of a culture as a single number - in essence, a dimensionality reduction. To demonstrate this, I use CLS data for 47 deletion mutants with different lifespans, in addition to the wild-type (the 972 h- strain) [59]. Colony patterns and maximum likelihood estimates of CFUs per droplet for this wild-type sample were previously shown in Figure 2.6. The deletion mutants originated from a prototroph deletion library, constructed as described previously [27]. The 47 selected mutants were picked manually, re-streaked to single colonies on YES, and incubated at 32°C for 2 days. The wild-type was also streaked to single colonies on YES and incubated at 32°C for 2 days. YES pre-cultures were inoculated by picking single colonies of each strain, and were grown for 1 day at 32°C, shaking at 170 rpm. YES cultures were inoculated from pre-cultures and grown at 32°C, shaking at 170 rpm. After 2 days cultures had reached stationary phase, which is taken to be day 0 of the lifespan curve. CFUs were measured for each strain

using the high-throughput method.

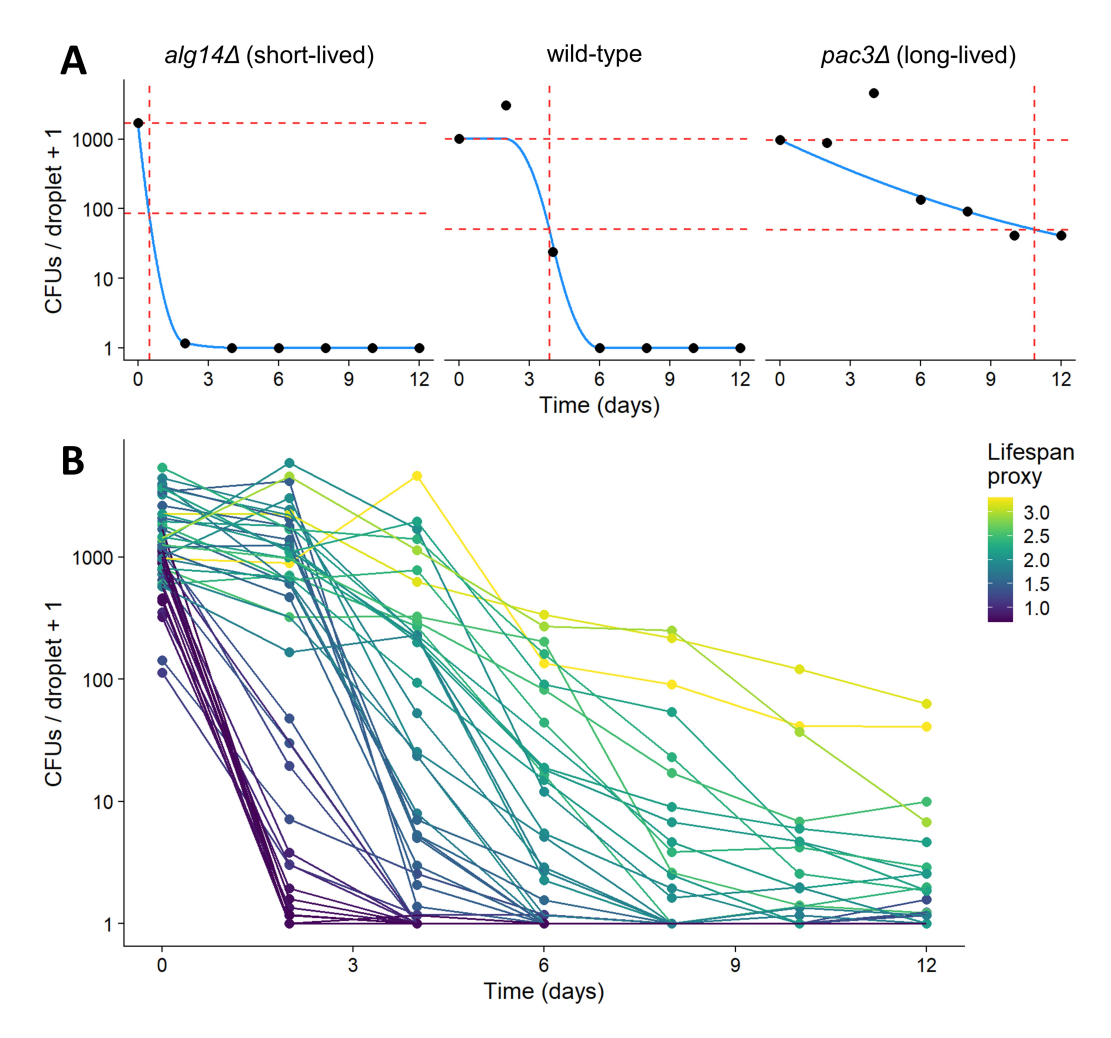


Figure 2.8: Proxy calculation for 48 strains.

A: Lifespan curves for 3 strains of different lifespan. For each strain, a constrained smoothing spline is fitted to the CFU measurements, shown in blue. Horizontal dashed lines in red indicate 100% viability and 5% viability according to the fitted values. Red vertical dashed lines indicate the time at which 5% viability is reached according to the fitted values. The square root of this value is used as the lifespan proxy. **B:** CLS curves are plotted for 48 strains of different lifespans. Lifespan curves are coloured according to the proxy calculated for each curve.

For each strain, a smoothing spline was fitted to the lifespan curve using the cobs package in R [60]. This spline was constrained such that the fitted values must always decrease. For each strain, the time taken for viability to decrease to 5% was calculated according to the fitted values. The square root of the time taken for viability to decrease to 5% is used as the proxy. Figure 2.8A shows the smoothing spline fit and proxy calculation for 3 strains: the $alg14\Delta$ (short-lived), wild-type and $pac3\Delta$ (long-lived). Lifespan curves for all 48 strains are shown in Figure 2.8B. Lifespan curves are coloured by proxy, demonstrating that the proxy effectively discriminates long- and short-lived mutants in a quantitative manner.

2.2.7 Development of an R package to analyse highthroughput CFU assays

In order to facilitate usage of the high-throughput CFU method, I developed an R package, *DeadOrAlive*, containing functions for image analysis, extraction of colony patterns, maximum likelihood estimation and plotting/analysis of lifespan curves. This can be used to construct an analysis pipeline for high-throughput CFU data, as outlined in the *DeadOrAlive* tutorial (Appendix A). In addition, the functions allow a great deal of flexibility; colonies can be arrayed in different density formats, different dilution factors can be analysed, and the proxy can be customised. Hence, the analysis pipeline can easily be tailored for different experimental setups. The package can be downloaded and installed from GitHub (www.github.com/JohnTownsend92/DeadOrAlive).

2.3 Discussion

2.3.1 Differences between the high-throughput and traditional CFU assays

I validate this assay by measuring CLS for strains with different lifespans using both the traditional and high-throughput assays in parallel. Despite excellent agreement between the CFU measurements for both assays (Figure 2.7C),

there are some notable differences in the shapes of the CLS curves measured using the traditional (Figure 2.7A) and high-throughput (Figure 2.7B) assays. The reason for this is that the limit of detection for the high-throughput assay is substantially higher than for the traditional assay. The limit of detection for the high-throughput assay is slightly lower that 1 CFU per droplet, as a droplet is the amount of culture which is pinned onto agar. However, the limit of detection in the traditional assay is approximately 10 CFUs per mL. This is because, at the lowest dilution factor, 100 µL of undiluted culture is spread onto solid agar. Hence, the high-throughput assay is not suitable for recording CFUs at very low concentrations. However, this is not a problem in the context of chronological ageing studies, as this concentration of CFUs is only reached after the vast majority of cells have died. At this point in stationary phase, nutrients released from dead cells support survival and growth of the remaining cells, a phenomenon described in bacteria [61] and recently in *S. pombe* [62]. Hence, CFU measurements at this concentration reflect factors unrelated to chronological ageing.

2.3.2 Mutants with altered CLS

This assay has been used to record CLS curves for a variety of mutants. In order to validate this assay, CLS curves were recorded for mutants which have previously been described to differ in CLS (Figure 2.7B). The majority of mutants show good agreement with published results. $pka1\Delta$ [63] and $reb1\Delta$ [64] have been previously annotated as long-lived, whilst $gsk3\Delta$ [56] and $atf1\Delta$ [63] have previously been annotated as short-lived.

A notable discrepancy was for $php2\Delta$, which was short-lived according to both the traditional (Figure 2.7A) and high-throughput (Figure 2.7B) assays, yet has previously been described as long-lived [65]. Php2 is a subunit of the evolutionary conserved CCAAT-binding complex, a transcription factor which positively regulates respiratory genes [66, 67]. Upregulation of respiration (and downregulation of fermentation) is required for stationary phase survival, as cells must switch to a more efficient metabolism upon glucose exhaustion [68,

69]. Hence, it is unsurprising that $php2\Delta$ cells display an altered CLS, although it is unclear why opposite effects can be observed. One possibility is that differences in media composition can alter the effect that Php2 has on CLS, as experiments in this study were performed in rich medium whilst the previous study used minimal medium [65]. This difference may be critical, as cells grown in rich medium do not require respiration, whilst cells grown in minimal medium must upregulate respiration in order to synthesise amino acids [70]. Hence, it is plausible that a respiratory-deficient mutant such as $php2\Delta$ would behave differently when cultured in rich vs minimal media, which may explain the opposite CLS effects observed. Another important consideration is the presence of auxotrophies, with the $php2\Delta$ mutant from the previous study [65] also containing *leu1-32 ade6-M216* selectable markers. Leucine auxotrophies and leucine supplementation have both been shown to affect CLS in budding yeast in a respiration-dependent manner [71]. Hence, the presence of a leucine auxotrophy, in addition to leucine supplementation in minimal medium [65], may also affect the CLS of a respiratory-deficient mutant such as $php2\Delta$.

2.4 Conclusion

In this chapter, I show that by adapting the spot assay to produce a digital pattern of colonies which can be modelled using simple probability distributions, a quantitative CFU assay can be established. This can be largely automated via liquid handling and pinning robots, creating an assay which is vastly less resource-intensive and laborious than the traditional CFU assay. Hence, this assay can serve as an efficient alternative in day-to-day CFU measurements, in addition to providing a platform from which high-throughput, systematic CLS studies can be conducted.

Chapter 3

Establishing a platform for genome-scale chronological lifespan studies in fission yeast via barcode sequencing

3.1 Introduction

Genome-scale deletion collections of non-essential mutants are powerful tools for interrogating genome function. In a typical screen, each mutant is arrayed on solid agar in a high-density format using a pinning robot, and the colony size of each mutant is used as a fitness readout [51]. This technology has been applied to uncover insights into how the genetic basis of fitness changes with respect to genetic, environmental or pharmacological perturbations, which can serve as a platform for systematically dissecting genetic pathway structure [72]. However, this approach is limited in that it can only be used to investigate growth-related phenotypes. CLS is an example of a phenotype which cannot be studied by using colony size as a readout, as lifespan describes the death, not growth, of cells. Hence, an alternative approach is required to study CLS using genome-scale deletion collections.

In both the budding yeast [37] and fission yeast [38] deletion collections,

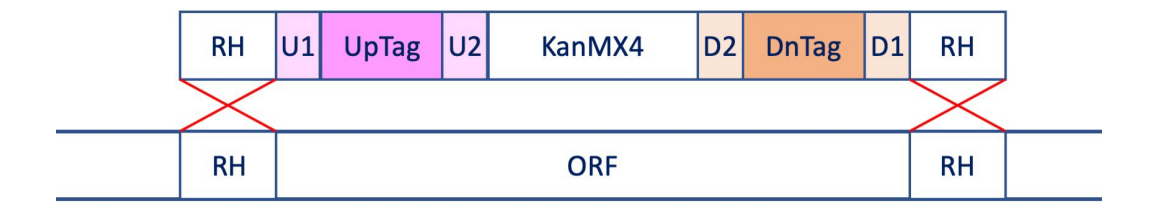


Figure 3.1: Systematic construction of barcoded deletion mutants in fission yeast. Each open reading (ORF) is deleted and replaced with an antibiotic resistance cassette which is used as a selectable marker (KanMX4). For each ORF, the targeting cassette contains regions of homology (RH) to the DNA sequences flanking the ORF, facilitating deletion of the ORF by homologous recombination. Each targeting cassette also contains two DNA barcodes - the UpTag and DnTag. These are flanked by universal priming sequences - U1 and U2 for the UpTag, and D1 and D2 for the DnTag, which allow each barcode to be amplified via polymerase chain reaction (PCR).

each mutant contains unique DNA barcodes which can be amplified and sequenced. In order to achieve this, each non-essential open reading frame was deleted and replaced with an antibiotic resistance cassette flanked by two unique DNA barcodes - the UpTag, upstream of the resistance cassette, and the DnTag, downstream of the resistance cassette (Figure 3.1). Hence, all mutants from the collection can be pooled and the relative abundance of each mutant in the pool can be quantified by barcode sequencing (Bar-seq). This greatly increases the versatility of the deletion collections, extending their functionality beyond colony-based fitness screens.

In this chapter, I present key steps required in order to establish a platform for genome-scale CLS studies using Bar-seq, building on previous work [27]. The first step of this involved decoding the barcodes for the fission yeast deletion collection, as the barocdes for mutants generated in the latest version of the deletion collection were previously uncharacterised. I also address key technical and biological biases which arise from the re-growth protocol necessitated by the persistence of DNA from dead cells.

3.2 Methods & Results

3.2.1 Decoding of deletion mutant barcodes

Barcodes were decoded for each mutant using a PCR-based genome walking strategy, as described in Romila et al., 2021 [59]. Briefly, pools of mutants from the Bioneer deletion library (version 5, Bioneer, South Korea) were generated. DNA was extracted from the pools and a primer extension procedure was used to amplify the barcodes alongside the adjacent genomic region. PCR products were sequenced and reads were analysed using an in-house Python script, *Barcount* (www.github.com/Bahler-Lab/barcount), which extracted barocdes and genomic sequences from the reads. Genomic sequences were mapped to the genome using Bowtie2 [73], and the nearest upstream/downstream gene was identified using BEDTools [74], accounting for the directionality of the gene and the type of barcode (UpTag or DnTag) as required. Reads for which a barcode could not be extracted or the genomic sequence could not be uniquely mapped were discarded.

In order to match barcodes to genes with high confidence, I identified barcode-gene pairs which appeared with high frequency and were specific. This was performed separately for UpTags and DnTags. To account for possible mutations which are known to appear in synthetic barcode sequences [75], pairwise Levenshtein distance was calculated between all barcodes, and barcodes were assembled into clusters where they differed by no more than 3 mutations. A consensus barcode was defined for each cluster as the average sequence of the cluster. A consensus barcode was automatically assigned to a gene if the following 3 criteria were met:

- 1. The barcode-gene pair was observed at least 10 times.
- 2. The barcode was specific to the gene at least 80% of the reads containing the barcode mapped to the gene.
- 3. The gene was specific to the barcode at least 80% of the reads which mapped to the gene contained the barcode.

Barcodes were decoded for the majority of mutants using this approach.

However, there were numerous reasons for which a barcode could not be automatically decoded for a mutant. The first was that not every mutant was revived from the cryostock and hence some were not sequenced, which is a typical caveat when working with mutant libraries. The second was that sometimes the same barcode was associated with two different mutants. Hence, even though the barcodes are known for these mutants, they are not suitable for use in Bar-seq experiments as the barcode cannot be uniquely associated to a mutant, a phenomenon described previously when barcodes for earlier versions of the Bioneer library were decoded [41]. The third reason was that sometimes the genomic region could not be uniquely mapped to the genome, or could not be mapped at all. In these cases, it was not possible to associate the barcode with a mutant. The final reason was that sometimes the correct gene was not automatically identified, which was often the case in regions of the genome containing many genes in close proximity. These cases required manual inspection of the mapped genomic reads in order to correctly associate a barcode with a mutant. For this, I developed a genome browser which shows the mapped reads with respect to the position of mutants from the deletion library, allowing for manual curation of barcodes. Figure 3.2A shows the mapped reads for a simple case where automatic assignment of both UpTag and DnTag were possible for a mutant, whilst Figure 3.2B shows a more complex case which required manual curation. This browser is part of the BarSeqTools R package (www.github.com/Catalina37/Barcount_ BarSeqTools_Pipelines/tree/master/BarSeqTools).

Using a combination of automatic and manual barcode curation, it was possible to decode both UpTag and DnTag for 3011 mutants. In addition, 96 mutants were decoded for UpTag only, and 99 for DnTag only. Hence, at least one barcode was decoded for 3206 mutants, which represents 94% of mutants in the latest version of the Bioneer library. In comparison, previous attempts to decode older versions of the Bioneer library managed to decode 2560 [41]

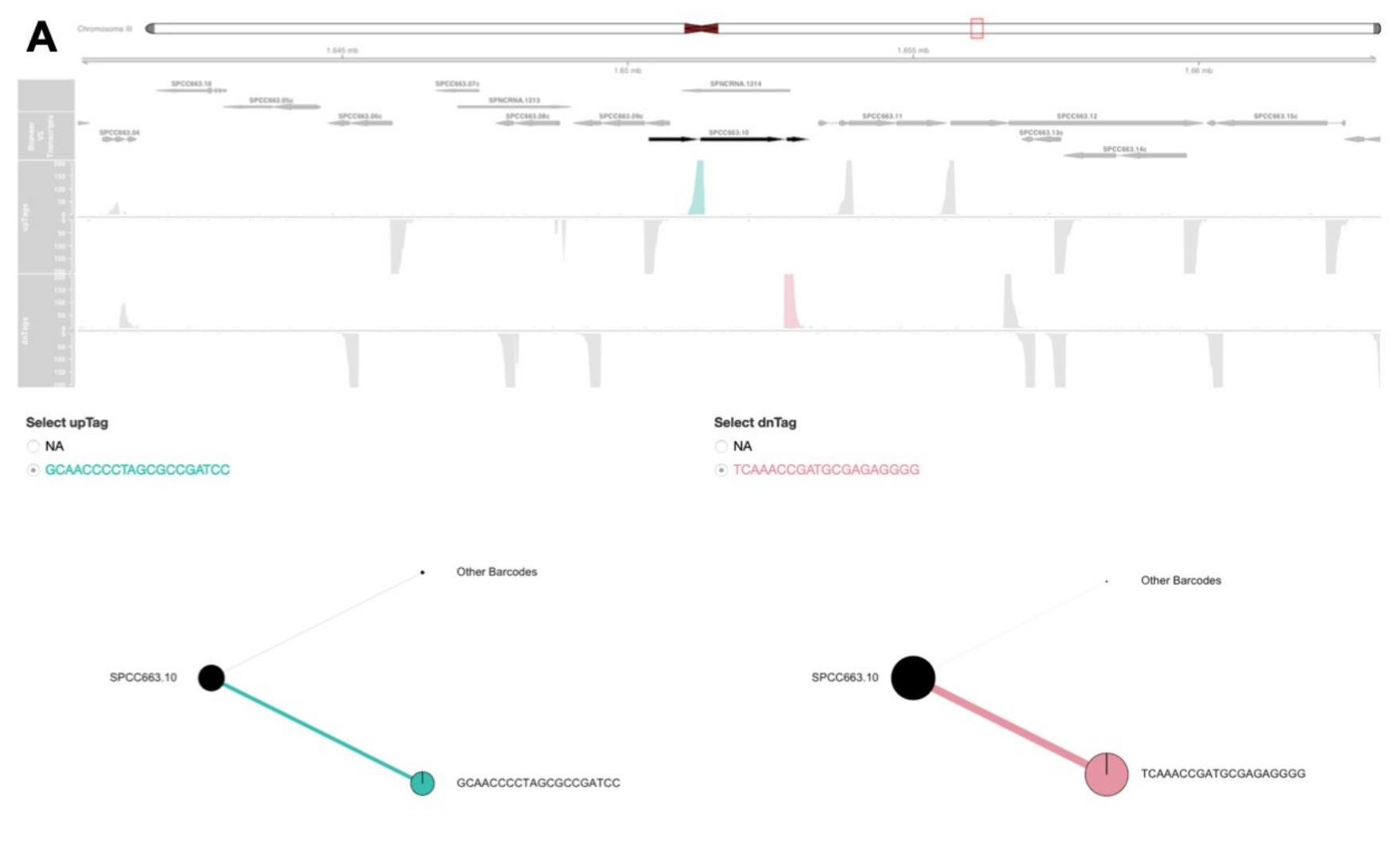


Figure 3.2: Manual curation of barcodes by viewing aligned reads in a genome browser.

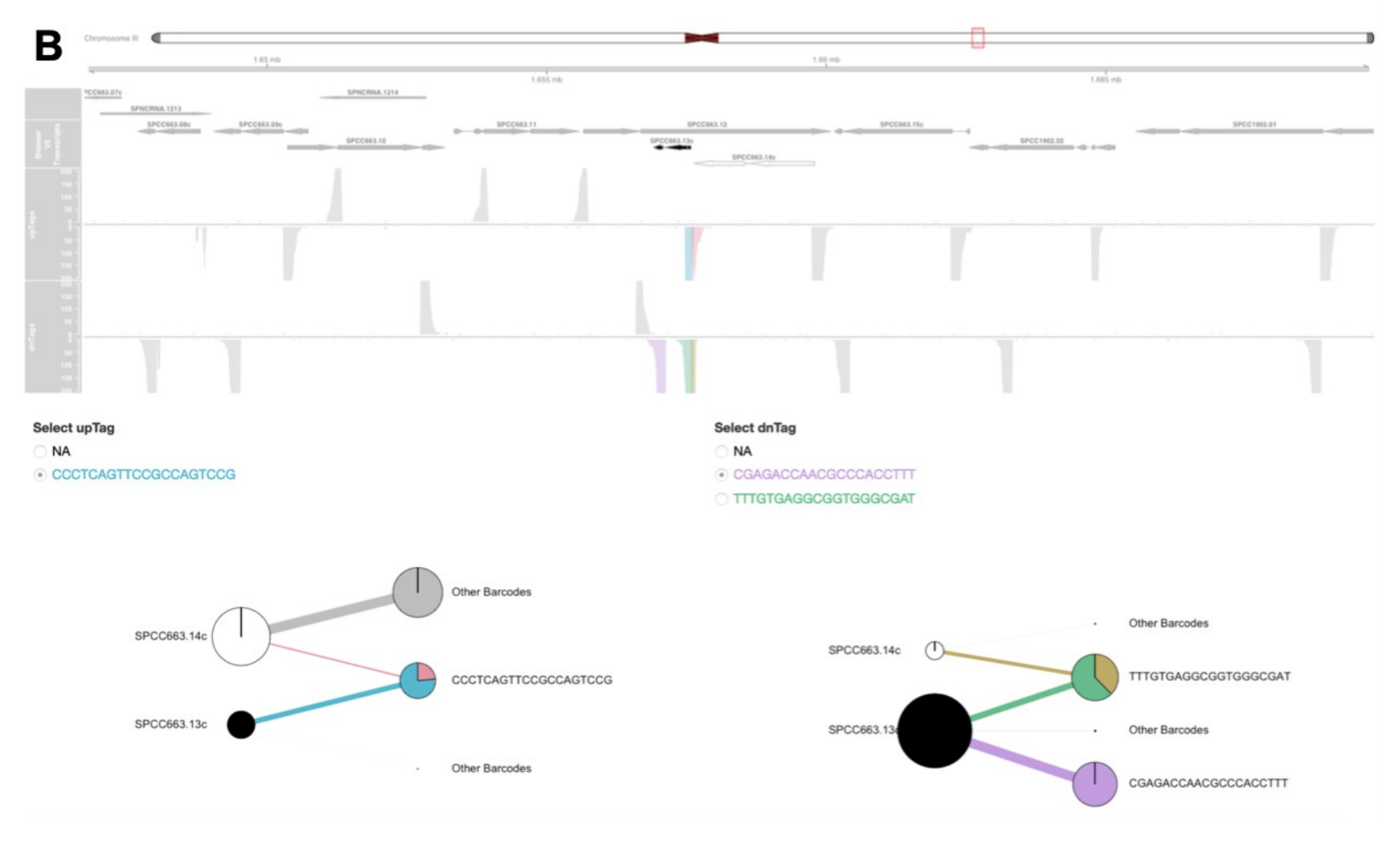


Figure 3.2: Manual curation of barcodes by viewing aligned reads in a genome browser.

Figure 3.2: Manual curation of barcodes by viewing aligned reads in a genome browser.

Tracks from top to bottom are:

- 1. chromosomal position
- 2. non-Bioneer genes
- 3. Bioneer genes (with the selected Bioneer gene shown in black)
- 4. histogram of aligned genomic fragments associated with UpTags
- 5. histogram of aligned genomic fragments associated with dnTags

For the UpTag and DnTag tracks, the direction of the aligned genomic fragment is represented by the direction of the peak. Below are two bipartite networks (one for UpTag and one for DnTag) showing the relevant barcodes associated with the selected mutant, and the mutants with which those barcodes are associated. For genes, the size of the node represents the number of reads which contained a genomic fragement which mapped to that gene. For barcodes, the size of the node represents the number of reads which contained that barocde. The selected mutant is shown in black, and other mutants in white. Barcodes are coloured based on the gene to which the corresponding genomic fragment was mapped, with each unique gene-barcode pair being coloured differently. A: Barcodes associated with SPCC663.10, a mutant for which both UpTag and DnTag were automatically assigned. **B**: Barcodes associated with SPCC663.13c, a mutant which required manual curation because another Bioneer gene, SPCC663.14c, was located almost immediately adjacent to this gene. In the case of the UpTag, many reads were correctly assocated with SPCC663.13c (blue). However, some of the genomic fragments were long enough to extend into the neighbouring gene, and were hence incorrectly mapped to SPCC663.14c (red). In the case of the DnTag, all reads were correctly associated with SPCC663.13c (purple). However, due to the close proximity of the neighbouring gene, many reads which should have been associated with SPCC663.14c were incorrectly associated with SPCC663.13c (green). Thus, two different barcodes were associated with SPCC663.13c. Some genomic fragments from the other barcode were correctly associated with SPCC663.14c (gold).

and 2473 [27] mutants. Consequently, a substantially greater proportion of the fission yeast non-essential proteome can now be interrogated in Bar-seq screens.

3.2.2 Persistence of DNA from dead cells necessitates re-growth of stationary phase cultures prior to barcode sequencing

In order to apply Bar-seq to detect mutants with altered CLS, the typical Bar-seq approach used to profile mutant fitness [41] must be adapted to deal with biological and technical biases introduced by the CLS protocol. For this, I analysed a Bar-seq dataset of chronologically ageing mutant pools, as described in Romila et al., 2021 [59]. This consisted of 3 independent prototroph pools of Bioneer mutants grown to stationary phase in 3% glucose YES. At days 0, 2, 3, 5, 7, 9 and 11 of stationary phase, the following was performed:

- CFUs were measured using the traditional method.
- DNA was extracted from cells.
- An aliquot of ageing culture was used to inoculate a re-growth culture in 3% glucose YES. These cultures were grown to stationary phase and DNA was extracted from cells.

UpTags and DnTags were amplified from the extracted DNA using PCR. Following next generation sequencing, barcodes were extracted from reads and assigned to a gene based on the look-up table compiled, using an in-house Python script, *Barcount* (www.github.com/Bahler-Lab/barcount). For each gene, counts for UpTag and DnTag were summed to create a total count for each gene. Figure 3.3 shows the viability curves based on CFU measurements for the 3 pool replicates.

It has been previously assumed that persistence of DNA from dead cells can introduce a bias when barcode abundance is used to infer CLS. One approach to dealing with this was to re-grow cells on solid agar prior to sequencing

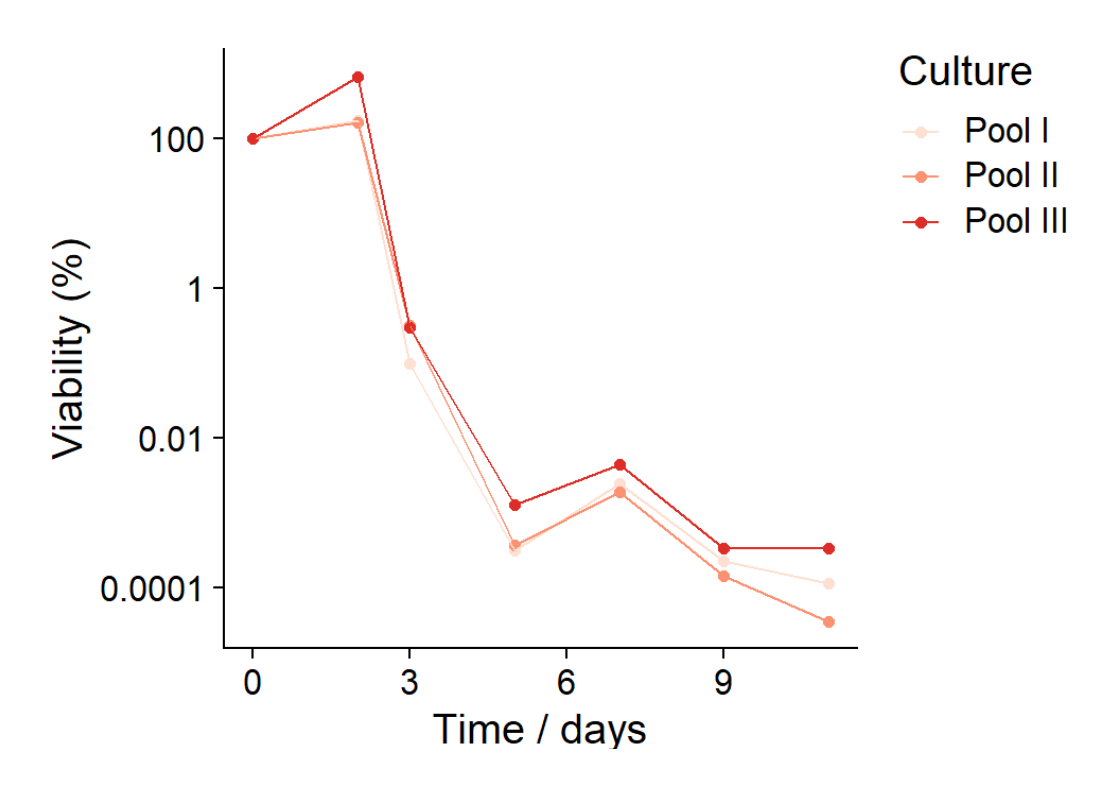


Figure 3.3: Chronological lifespan curves of pooled mutants.

[42], whilst in another study which investigated CLS in quiescent cells following nitrogen starvation, such an approach was not required as quiescent cells survive for several weeks, far longer than DNA is expected to persist [27]. In the current study, which investigates CLS in stationary phase cells grown in rich medium, it was expected that persistence of DNA from dead cells would be a severe bias, and this is confirmed by the pairwise correlations of barcode frequencies in stationary phase cells (Figure 3.4A). Barcode frequencies for all replicates across all timepoints were almost perfectly correlated, with very little changes in barcode frequencies being observed throughout 11 days of stationary phase. This is corroborated by measurements of DNA levels throughout stationary phase, which were reported to change very little throughout stationary phase in the Romila et al., 2021 study [59].

Conversely, pairwise correlations in barcode frequencies from re-growth cultures were much more varied (Figure 3.4B), indicating that culture regrowth captured differences in mutant survivial throughout stationary phase.

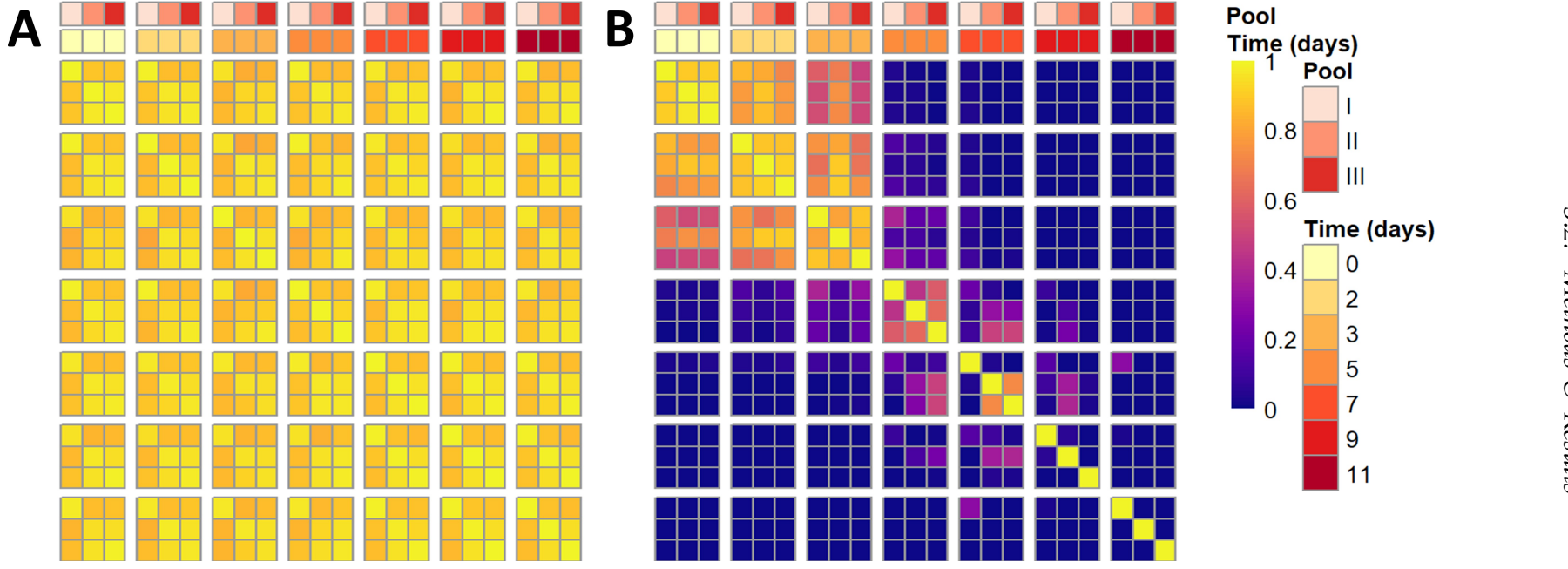


Figure 3.4: Correlation of barcode frequencies from chronologically ageing mutant pools. Pairwise correlations of barcode frequencies are displayed as a heatmap. Data is shown for 3 independently generated mutant pools, as indicated by the upper side bar. The age of the pool is indicated in the lower side bar. **A:** Pairwise correlations of reads sequenced from stationary phase cultures. **B:** Pairwise correlations of reads sequenced from re-growth cultures.

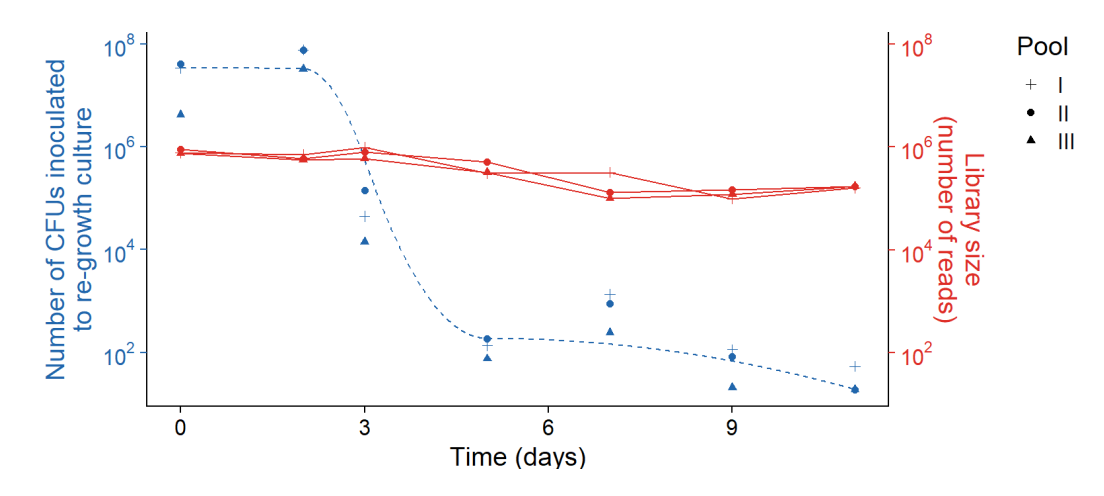


Figure 3.5: Comparison of re-growth bottleneck size to library size for ageing pools.

The number of CFUs used to inoculate the re-growth cultures is shown in blue, which represents the size of the sampling bottleneck when re-growth cultures are inoculated. Blue dashed line shows a constrained smoothing spline fitted to this data. The size of each library is shown in red. The pool is indicated by the shape.

Specifically, correlations were high between days 0 and 2, suggesting that most mutants remained viable at these timepoints. These correlations began to fall apart at day 3, suggesting that short-lived mutants began to die and long-lived mutants were starting to become enriched. This is consistent with the drop in pool viability observed between days 2 and 3 (Figure 3.3). These analyses show that chronologically ageing pools of mutants must be re-grown in order to minimise the contribution of barcodes which persist from dead cells.

3.2.3 Culture re-growth introduces a sampling bottleneck which must be accounted for in order to model mutant abundance correctly

The re-growth pools at day 5 were poorly correlated with those from the beginning of the experiment, suggesting that the vast majority of mutants were dead at this point, consistent with the viability curve for the pools. Beyond day 5, pools showed poor correlations even between replicates at the same time point, suggesting that re-growth pool composition at these timepoints is driven by stochastic sampling of the few remaining mutants.

Bar-seq datasets, being genome-scale count data, can be analysed using statistical models developed for RNA-seq datasets. This assumes that read counts follow a negative binomial distribution [76]. However, in the case of the re-growth protocol, we are not interested in modelling the counts per se, but instead modelling the number of surviving cells in the ageing stationary phase culture. Hence, it is important to note that there is a sampling bottleneck when an aliquot of ageing culture is used to inoculate a re-growth culture, and this bottleneck becomes increasingly severe as culture viability decreases. Based on the number of CFUs / mL and the volume of ageing culture used to inoculate the re-growth culture, it is possible to estimate the size of this bottleneck (Figure 3.5). For day 5 and beyond, I estimate the size of this bottleneck to be 100 cells. This is many orders of magnitude lower than the corresponding library sizes for the re-growth pools. Hence, it is clear from this that the clonal descendants of the cells in the inoculum have been sequenced multiple times. Given that statistical power increases with the number of counts under the negative binomial distribution, the result of this clonal amplification is in an overestimation of statistical power. Similar conclusions have arisen from a recent study, where it has been demonstrated that barcode count data does not follow a negative binomial distribution in cases where there is high degree of clonal amplification as a result of a strong selection bottleneck [77]. This problem is analogous to the the well known problem of PCR duplicates which arise in RNA-seq experiments, where multiple reads can originate from the same RNA molecule [78]. Given that the size of the bottleneck is known based on the CFU data, I implement a simple normalisation strategy where read counts are scaled such that the library size equals the bottleneck size in cases where the library size is greater than the bottleneck size. In this case, the normalisation applies to all re-growth libraries from day 3 to day 11 (Figure 3.5). This ensures that, on average, each normalised read represents one stationary phase cell.

3.2.4 Detecting mutants with altered chronological lifespan

In order to detect mutants with altered CLS, barcode counts for the normalised re-growth libraries at day 3 were comparied to those at day 0. This is because barcode counts at day 3 should capture differences in lifespan for both longand short-lived mutants as the pool had substantially decreased in viability but was not completely dead (Figure 3.3). Conversely, barcode counts at day 2 do not differentiate long-lived mutants from the population average as the majority of mutants were still alive at this point, whilst barcode counts at day 5 and beyond do not differentiate short-lived mutants from the population average as the majority of mutants were dead at this point. In addition, library sizes from day 5 onwards are too small to perform differential fitness analysis following normalisaiton for the sampling bottleneck.

Differential fitness analysis based on normalised barcode counts in the regrowth cultures was performed using edgeR (version 3.24.3) [76]. Only data for day 0 and day 3 were used. In order to account for differences in mutant frequency between replicate pools at day 0, pool was included as a term in the model. Read counts were analysed using a negative binomial generalised linear model, and likelihood ratio testing was used to determine p-values for differences in barcode frequencies between days 0 and 3. Using a fold change (FC) cut-off of $|\log_2 FC| > \log_2 1.5$ and a false discovery rate (FDR) cut-off of FDR < 0.05, 341 long-lived mutants and 1246 short-lived mutants were identified (Figure 3.6).

3.2.5 Validaiton of Bar-seq screen against high-throughput CFU assay

In order to validate the results from the Bar-seq screen, I use the data from the 47 mutants for which lifespan curves were recorded using the high-throughput CFU method (Figure 2.8). \log_2 FC (day 3 vs day 0) are well correlated with proxy scores for the 47 mutants (r = 0.76, Figure 3.7). This is reassuring con-

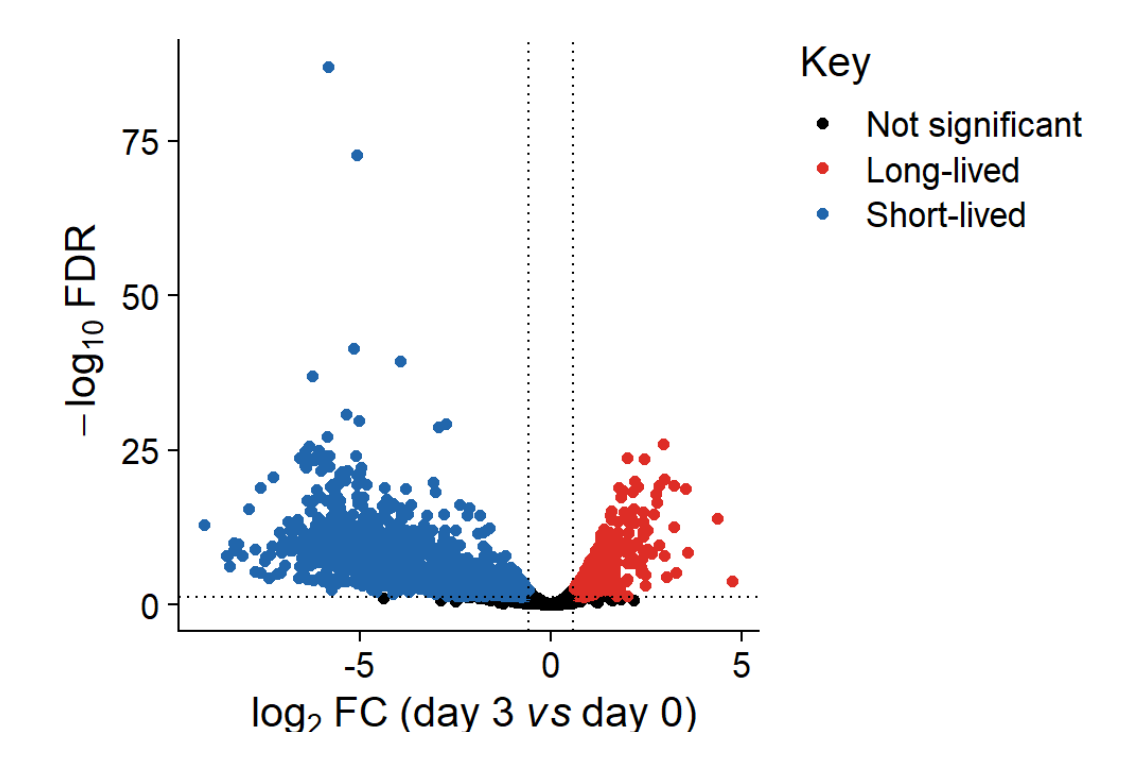


Figure 3.6: Volcano plot showing changes in pool composition through stationary phase.

 \log_2 FC in barcode abundance for day 3 vs day 0 is plotted against - \log_{10} FDR. A fold change (FC) cut-off of $|\log_2$ FC $|>\log_2$ 1.5 and a false discovery rate (FDR) cut-off of FDR < 0.05 were used to define mutants as long- or short-lived. 341 long-lived mutants are shown in red, and 1246 short-lived mutants are shown in blue. All other mutants are shown in black.

sidering there are substantial differences in the biological contexts and analytical approaches employed by the two methods. For example, all mutants in the pool share the same extracellular environment, and so differences in lifespan must be caused by cell-intrinsic factors. However, lifespan differences between mutants grown in batch cultures may reflect cell-intrinsic or cell-extrinsic factors.

3.2.6 Late stationary phase pools become dominated by short-lived mutants

Each of the re-growth libraries for late stationary phase pools (days 9 and 11) was dominated by a small number of mutants, although this was highly stochastic (Figure 3.4, Figure 3.8A. 29 mutants which contributed to at least

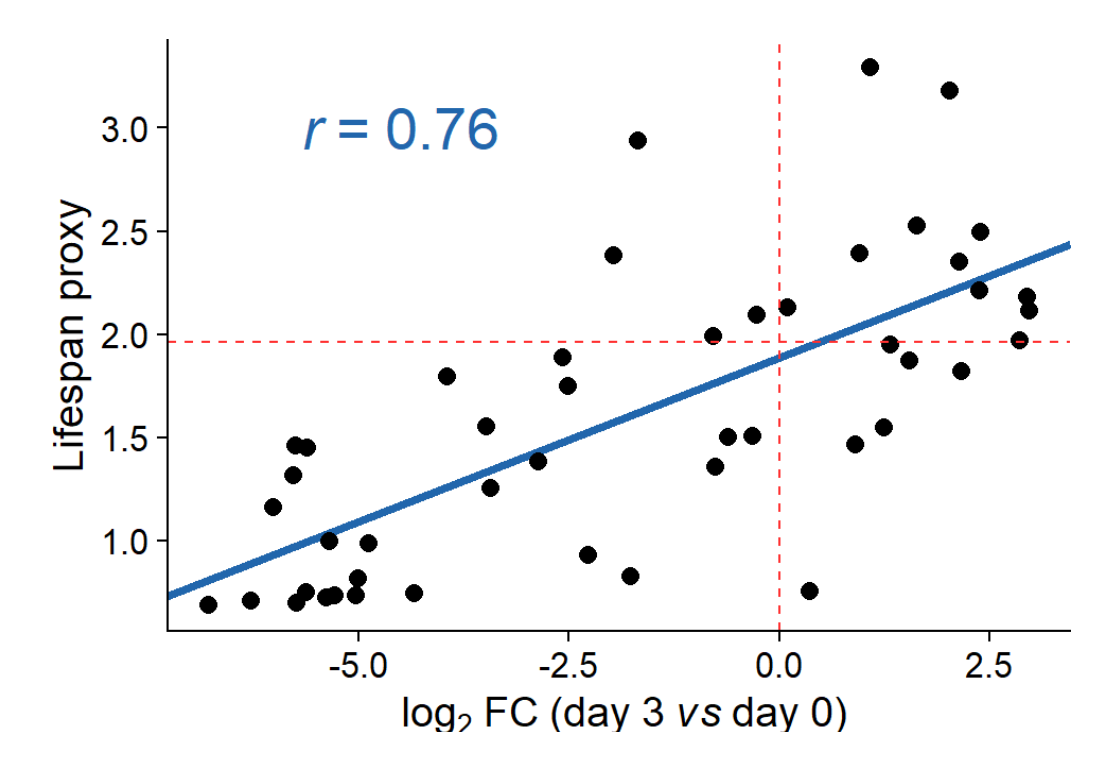


Figure 3.7: Validaiton of Bar-seq screen against high-throughput CFU assay. In order to validate the Bar-seq CLS screen, lifespan proxies calculated for 47 mutants using the high-throughput CFU method (Figure 2.8) are compared to their respective \log_2 FC (day 3 vs day 0) calculated from the Bar-seq screen. A linear regression between \log_2 FC (day 3 vs day 0) and the lifespan proxy alongside Pearson correlation coefficient, r, is shown in blue. Red horizontal dashed line shows the lifespan proxy for the wild-type, whilst red vertical dashed line shows \log_2 FC (day 3 vs day 0) = 0, which represents the average lifespan of the pool.

1% of the reads in at least 1 of the replicate pools at days 9 or 11 were defined as highly abundant in late stationary phase. In order to investigate this further, normalised read counts for re-growth pools across all timepoints were analysed using edgeR (version 3.24.3) [76], treating time as a categorical variable and including pool as a variable in the model. As before, read counts were analysed using a negative binomial generalised linear model, and likelihood ratio testing was used to determine p-values for differences in barcode frequencies. These 29 mutants typically decreased in abundance in early stationary phase and increased in abundance in late stationary phase (Figure 3.8B). The early decrease in abundance between days 0 and 3 was statistically significant for 21 of these mutants (Figure 3.8C). Furthermore, the \log_2 FC (day 3 vs day 0)

Not abundant in late stationary phase

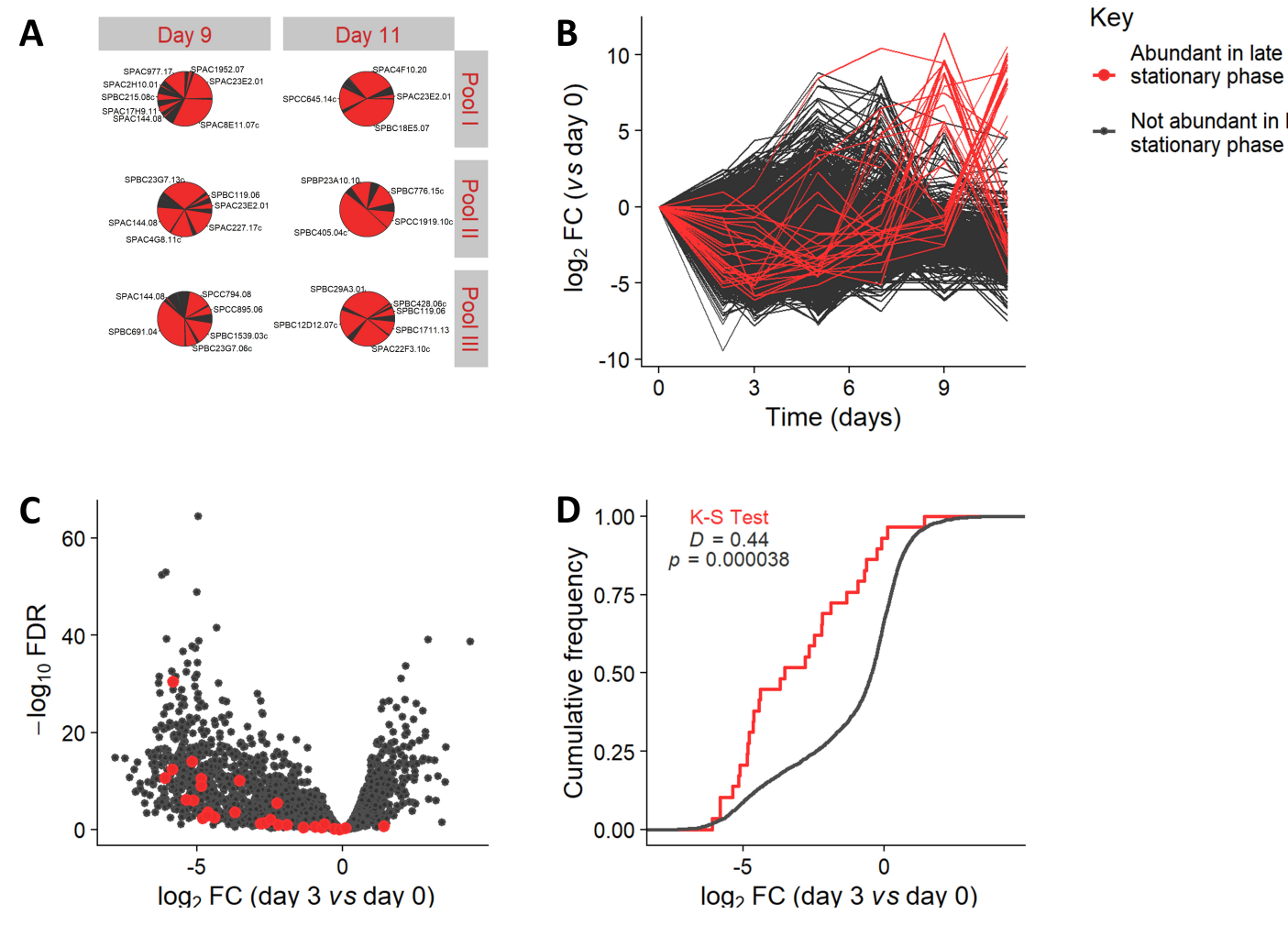


Figure 3.8: Late stationary phase pools become dominated by short-lived mutants.

Figure 3.8: Late stationary phase pools become dominated by short-lived mutants.

A: Pie charts showing mutant abundances in re-growth pools in late stationary phase (days 9 and 11). There were 29 mutants which contributed to at least 1% of the reads in at least 1 of the replicate pools at either of these timepoints, which I define as highly abundant in late stationary phase. These mutants are shown in red, all other mutants in dark grey. B: Line plot where log₂ FC of barcode abundace for each timepoint (vs day 0) is shown for each mutant. Mutants which dominate late stationary phase pools typically decrease in abundance in early stationary phase and increase in abundance in late stationary phase. C: Volcano plot where log2 FC in barcode abundance for day 3 vs day 0 is plotted against -log₁₀ FDR. 21 of the 29 mutants which are defined as highly abundant in late stationary phase significantly decrease in abundance between days 0 and 3, using an FC cut-off of log₂ FC < log₂ 1.5 and an FDR cut-off of FDR < 0.05. **D:** Cumulative frequency plot showing the distributions of log₂ FC (day 3 vs day 0) for mutants defined as highly abundant in late stationary phase and for all other mutants. Mutants which dominate late stationary phase pools have a significantly lower log₂ FC than all other mutants (Kolmogorov-Smirnov test, D = 0.44, p = 0.00004). This indicates that late stationary phase pools become dominated by mutants which are classified as short-lived according to the analysis of earlier timepoints.

for these 29 mutants was significantly lower than for all other mutants (Figure 3.8D), indicating that late stationary phase pools become dominated by mutants which were classified as short-lived according to an analysis of earlier timepoints. This indicates that pool composition is dynamic throughout stationary phase, and that late stationary phase pool composition may reflect factors unrelated to longevity. Indeed, it is known in bacteria that nutrients released by dead cells may support the survival of other cells in late stationary phase [61], and a similar phenomenon has recently been described in fission yeast during quiescence [62].

3.3 Discussion & Conclusion

In this chapter, I present an analysis of a Bar-seq dataset which I use to establish a pipeline for the identification of long- and short-lived mutants in CLS screens of pooled deletion mutants, which addresses key technical, statistical and biological biases. In particular, persistence of barcodes from dead cells necessitates re-growth of ageing cultures prior to sequencing. This introduces a sampling bottleneck that becomes increasingly more severe as viability de-

creases, which must be accounted for in order to ensure that read counts reflect stationary phase pool composition and that statistical analyses are valid. An effective and simple approach for the detection of long- and short-lived mutants is to compare normalised read counts at the beginning of stationary phase to those at a timepoint where viability has substantially decreased, but not all cells are dead. At this timepoint, pool composition reflects both long- and short-lived mutants, there are a sufficient number of reads following normalisation to perform differential fitness analysis, and results are not confounded by other biological phenomena which can cause changes in pool composition in late stationary phase. Enrichment analyses of long- and short-lived mutants identified and subsequent discussions are not presented, as mutants with altered chronological lifespan are discussed in the context of rapamycin-mediated lifespan extension in Chapter 4.

Chapter 4

Dissecting the genetic basis of rapamycin-mediated lifespan extension recapitulates the spatial organisation of TOR signalling

4.1 Introduction

Rapamycin is a macrolide isolated from *Streptomyces hygroscopicus* and was first characterised as an antifungal agent [79]. Its growth-inhibitory properties were later found to extend to eukaryotic cells in general, leading to its use as an anticancer drug and as an immunosuppressant to prevent tissue rejection in organ transplants [80]. Investigations into the molecular mechanisms underlying rapamycin's anti-proliferative properties led to the identification of the protein target of rapamycin (TOR) in budding yeast [81], with subsequent studies identifying the mammalian ortholog [82, 83, 84]. Interest continued to grow following reports that rapamycin treatment or genetic interventions which suppress TOR signalling could extend lifespan in a variety of invertebrate model systems, including budding yeast (both RLS [85] and CLS [33]),

nematode worms [86] and fruit flies [87]. These studies helped consolidate the view that the genetics of ageing is conserved across eukaryotes [45]. It was subsequently shown that rapamycin treatment could extend also lifespan in mice [88]. This study was a significant milestone in the search of treatments for age-related diseases in humans, as it was the first reported case of a pharmacological agent which could significantly increase the lifespan of a mammal in both sexes, even when applied later in life. Following this, clinical trials are now beginning to show that the anti-ageing TOR inhibition also apply to humans [89].

TOR proteins are serine/threonine kinases which act as master regulators of cellular growth and metabolism in response to nutrient signals [90, 91, 92, 93, 94]. In animals, TOR signalling has also evolved to integrate hormonal cues [90, 91, 92]. Misregulation of TOR signalling is associated with a variety of chronic diseases including as cancer, obesity, autoimmune diseases, cardiovasular diseases and metabolic disorders [80, 90, 91]. TOR proteins exist as part of two structurally and functionally distinct complexes - TORC1 and TORC2. In mammals, a single TOR kinase associates with different regulatory subunits in order to form either complex [92]. Many unicellular eukaryotes, including budding yeast and fission yeast, contain two TOR kinases, and the affinities of each kinase to the two TOR complexes can differ [93, 94, 90]. TORC1 is acutely sensitive to rapamycin [95] and is the far better studied of the two complexes. In response to amino acid availability, TORC1 positively regulates growth-promoting processes such as ribosome biogenesis and translation, and negatively regulates starvation responses such as autophagy [90]. TORC2 is not sensitive to acute rapamycin treatment [95, 96], but does display some sensitivity in response to chronic rapamycin treatment [92]. Its functions are less well characterised but are clearly diverse, and include regulating aspects of plasma membrane homeostasis, cytoskeleton organisation and genome stability [97, 98, 99, 100].

Furthermore, the spatial organisation of the TOR complexes is related

to their distinct roles of TOR signalling. Whilst TORC2 is located at the plasma membrane [97, 98], two spatially and functionally distinct pools of TORC1 exist - one at the vacuole membrane (lysosome membrane in mammals) which positively regulates protein synthesis, and another at endosome membranes which negatively regulates autophagy [101]. This likely reflects the different information which is conveyed by amino acid concentrations at the vacuole and in the cytoplasm. The vacuole serves as an amino acid reservoir [102, 103], and hence amino acid concentrations at the vacuole reflect the potential for the cell to synthesise new proteins. Upon activation, vacuolar TORC1 phosphorylates the S6 kinase(s), resulting a global induction of ribosome biogenesis and protein translation [101, 104]. On the other hand, cytoplasmic amino acid concentrations are much more tightly regulated in order to maintain cytoplasmic homeostasis, and only begin to drop during times of nutrient depletion [105]. Concordantly, endosomal TORC1 is responsible for initiating autophagy in response to a drop in cytoplasmic amino acid concentrations, allowing the cell to replenish its amino acid pool by degrading proteins [106, 107]. Hence, TORC1 achieves protein homeostasis by balancing protein synthesis and protein degradation in response to amino acid availability from two distinct subcellular locations.

Whilst a great deal of studies have dissected the TOR signalling pathway, this is the first genome-scale study to systematically dissect TOR signalling specifically in an ageing context. Consistent with several studies which have investigated rapamycin-mediated lifespan extension, I find a clear requirement for autophagy to mediate the beneficial effects of rapamycin, consistent with the notion that rapamycin mimics the effect of dietary restriction [108, 109]. Furthermore, rapamycin-mediated lifespan extension was also dependent on diverse aspects of endosome function, highlighting the intimate relationships between TORC1 signalling, endosomes and autophagy [101, 110, 111]. This included phosphatidylinositol 3-kinase (PI3K) signalling, which has a crucial role in coordinating multiple aspects of autophagy initiation and progression

in response to rapamycin treatment. This study demonstrates that TORC1 inhibition activates multiple downstream effectors, and the coordinated action of these effectors is required for rapamcyin-mediated lifespan extension via initiation of autophagy.

4.2 Methods & Results

4.2.1 Pooling and ageing of deletion mutants

3 independently generated prototrophic pools of Bioneer mutants were prepared as described previously [27]. 250 mL pre-cultures of pools in 3% glucose YES were grown for 15 hours at 25°C without shaking. Cells were centriguged for 3 minutes at 420 rcf and washed once in the same volume of 3% glucose YES. The optical density at 600 nm (OD600) was measured for each pool. From each pre-culture, a pair 50 mL cultures were inoculated in 3% glucose YES at OD600 = 0.1. To one of the cultures within each pair, 50 μ L of 100 μ g/mL rapamycin () in DMSO was added to give a final concentration of 100 ng/mL, whilst 50 μ L of DMSO was added to the other. These were grown at 32°C, shaking at 170 rpm, and cultures had reached stationary phase after 1 day, which was taken to be day 0 of CLS.

CFUs were measured for cultures at day 0 using the traditional method, as described previously [58]. CFUs were measured for cultures at days 0, 1, 2, 3, 4, 5, 6, 7, 9, 11, 13, 15, 17, 20 and 22 using the high-throughput method, as described in Chapter 2. At the same timepoints, 1 mL aliquots of ageing cultures were used to inoculate 50 mL re-growth cultures in 3% glucose YES, which were grown at 32°C, shaking at 170 rpm. When re-growth cultures reached stationary phase, 1.5 mL aliquots were centrifuged for 3 minutes at 1000 rcf, the supernatant was removed, pellets were snap frozen and stored at -80°C.

Colony patterns from the high-throughput CFU assay were analysed using the DeadOrAlive R package, as described in Chapter 2. For each culture, a smoothing spline which was constrained such that it must always decrease was

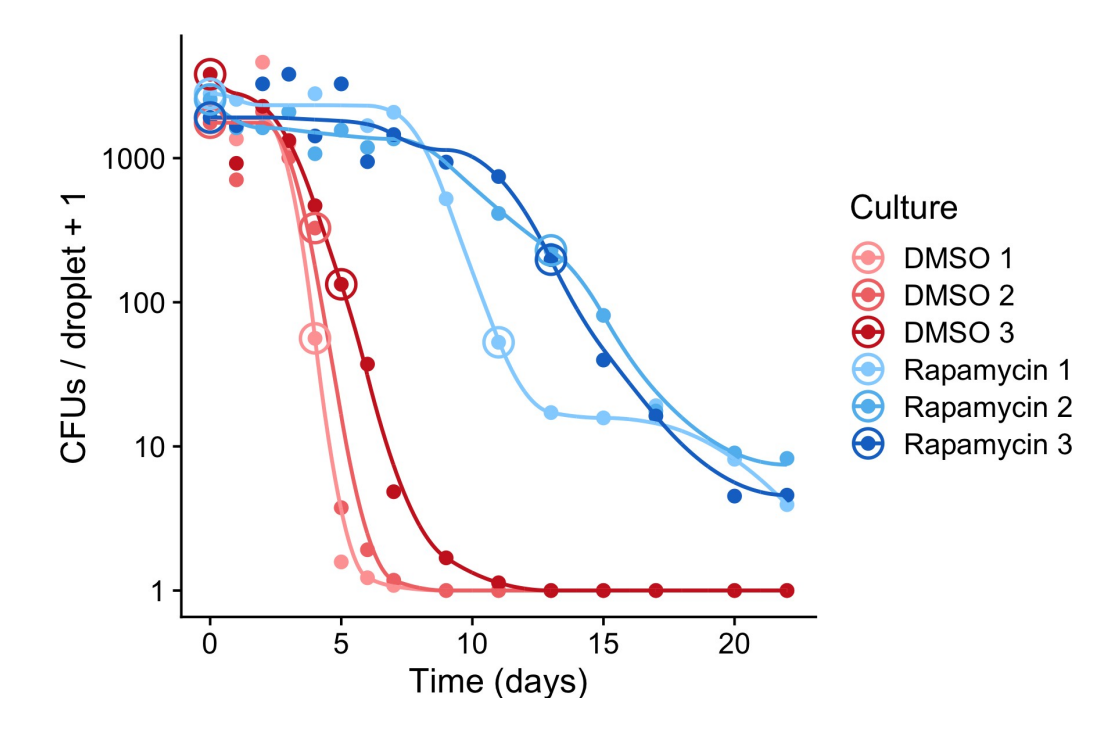


Figure 4.1: CLS of rapamycin-treated and -untreated pools. CFU measurements are plotted against time for cultures as indicated. A constrained smoothing spline is fitted to the CFU data for each culture. Samples selected for sequencing are circled.

fitted using the cobs package in R [60]. For all 3 replicate pools, rapamycin treatment substantially increased CLS (Figure 4.1).

4.2.2 Library preparation and sequencing

Culture	Time / days	Viability	-log ₁₀ Viability
DMSO 1	0	1.0	0.0
DMSO 2	0	1.0	0.0
DMSO 3	0	1.0	0.0
Rapamycin 1	0	1.0	0.0
Rapamycin 2	0	1.0	0.0
Rapamycin 3	0	1.0	0.0
DMSO 1	4	0.029	1.5
DMSO 2	4	0.10	1.0
DMSO 3	5	0.035	1.5
Rapamycin 1	11	0.019	1.7
Rapamycin 2	13	0.089	1.0
Rapamycin 3	13	0.10	1.0

Table 4.1: Timepoints selected for barcode sequencing.

Based on the CLS curves for the 6 cultures (Figure 4.1), 12 aliquots of re-growth cultures were selected for sequencing (Table 4.1). For this, each culture was sequenced at day 0, where every mutant is assumed to be 100% viable. In addition, a later timepoint for each culture was selected at a point where the viability was between 1% and 10%, allowing for the detection of long- and short-lived mutants.

DNA was extracted from the 12 re-growth samples using a phenol:chloroform protocol. Separate PCRs were performed to amplify UpTags and DnTags as described previously [59], resulting in 24 barcode libraries. These were pooled at a total concentration of 4 nM, and PhiX sequencing control v3 (Illumina, US) to increase the library complexity was added at a concentration of 5%. Libraries were sequenced on an Illumina MiSeq Instrument with 168 cycles using paired-end reads of 75 bp each and generating approximately 23 million reads.

4.2.3 Analysis of sequencing data

Pair-end reads were assembled using PEAR [112], and PCR duplicates removed using BBTools [113]. Barcount [59] was used to extract barcodes from reads and match them to genes according to the look-up tables assembled in Chapter 3. In order to ensure library size was never greater than the size of the selection bottleneck necessitated by culture re-growth as discussed in Chapter 3, traditional and high-throughput CFUs recorded on day 0 were analysed using an interceptless linear model in order to generate a calibration which could convert CFUs / droplet into CFU / mL, allowing the size of the selection bottlneck to be calculated. For all libraries, library size was greater than the size of the selection bottleneck, and so no normalisation was required.

An analysis of pairwise correlations of barcount counts revealed good clustering between libraries 3.4. Libraries clustered primarily based on culture viability, indicating that both rapamycin-treated and -untreated pools become enriched for long-lived mutants. However, within the older libraries, there was a clear separation of rapamycin-treated and -untreated pools, indicating that

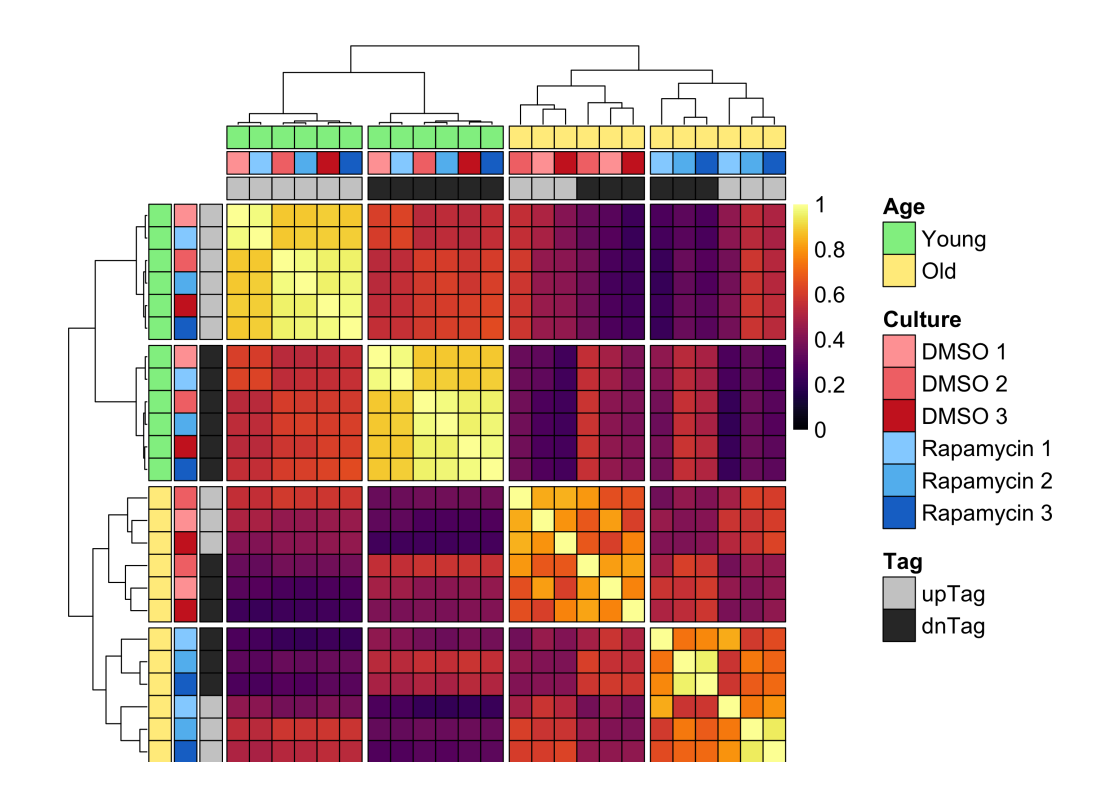


Figure 4.2: Pairwise correlations of read counts in rapamycin-treated and - untreated pools.

Sidebars indicate culture treatment, replicate, barcode type and culture age (with young representing 100% viability and old representing between 1% and 10% viability (Table 4.1).

rapamycin treatment causes different mutants become enriched during ageing. Subclustering in the young libraries was driven by barcode type, suggesting the presence of PCR bias. There was also some clustering based on replicate, suggesting the mutant composition differs between pools. There was no evidence of clustering based on rapamycin treatment in the young libraries. It is likely that pool composition at the beginning of stationary phase was affected by rapamycin treatment, but these effects are likely to be subtle and blurred by the re-growth protocol, and hence not detected in this analysis.

4.2.4 Identification of mutants with altered response to rapamycin

Reads were modelled in edgeR (version 3.30.3) [76] using a negative binomial generalised linear model. Rapamycin treatment was included as a term in the model in order to account for differences in initial mutant abundance between DMSO and rapamycin pools. In order to quantify changes in barcode abundance during chronological ageing, -log₁₀ viability was included as a term in the model (Table 4.1). This also allows viability to be modelled in a more nuanced way, accounting for the fact that cultures were sequenced at different days and viabilities. In order to detect mutants which respond differently in ageing due to rapamycin treatment, an interaction term between rapamycin treatment and -log₁₀ viability is included. In order to account for technical biases such as PCR bias and differences in initial mutant composition between replicate pools, barcode type and replciate were also included as terms in the model. *p*-values for differential barcode representation were calculated using likelihood ratio testing and corrected for multiple testing according to FDR.

Hence, the design matrix is constructed using the following code:

```
design <- model.matrix( ~ Treatment + MinusLog10Viability +
    Treatment : MinusLog10Viability + Barcode + Replicate)</pre>
```

In the case of the data presented, this results in a model with the following coefficients (coefficients which represent lifespan effects are highlighted in bold):

- 1. Intercept
- 2. log₂ FC between DMSO and rapamycin at day 0
- 3. Lifespan score in DMSO
- 4. log₂ FC between UpTag and DnTag
- 5. log₂ FC between replicate 2 and replicate 1

6. log₂ FC between replicate 3 and replicate 1

7. Difference in lifespan score between DMSO and rapamycin

Hence, this model allows the identification of mutants which are long- and short-lived in DMSO, in addition to mutants which have a different lifespan effect in rapamycin, whilst controlling for techincal effects. However, there is an important contrast which is missing - the lifespan score in rapamcyin. In order to calculate this score, the following design matrix can be used:

```
design <- model.matrix( ~ Treatment + Treatment :

MinusLog10Viability + Barcode + Replicate)
```

This is known as a nested interaction formula, and fits exactly the same model as before. However, because the design matrix has been parameterised in a different way, different coefficients are extracted:

- 1. Intercept
- 2. log₂ FC between DMSO and rapamycin at day 0
- 3. log₂ FC between UpTag and DnTag
- 4. log₂ FC between replicate 2 and replicate 1
- 5. log₂ FC between replicate 3 and replicate 1
- 6. Lifespan score in DMSO

7. Lifespan score in rapamycin

The units of the lifespan score are $\log_2 FC / -\log_{10} V$ iability, which represents the $\log_2 FC$ in barcode abundance per order of magnitude of viability lost - reflecting the fact that barcode abundances change more dramatically as viability decreases. For instance, a lifespan score of 0 means than barcode abundance did not change throughout CLS (no lifespan effect), a lifespan score of 1 means than barcode abundance doubled between 100% and 10% viability

(long-lived mutant), and a lifespan score of -1 means that barcode abundance halved between 100% and 10% viability (short-lived mutant). It is also important to note that lifespan scores are condition-specific, and reflect lifespan relative to the average lifespan of the pool in that condition. To illustrate, if a mutant has a lifespan score of 0 in DMSO and a lifespan score of 0 in rapamycin, it would mean that it essentially behaves like the wild-type.

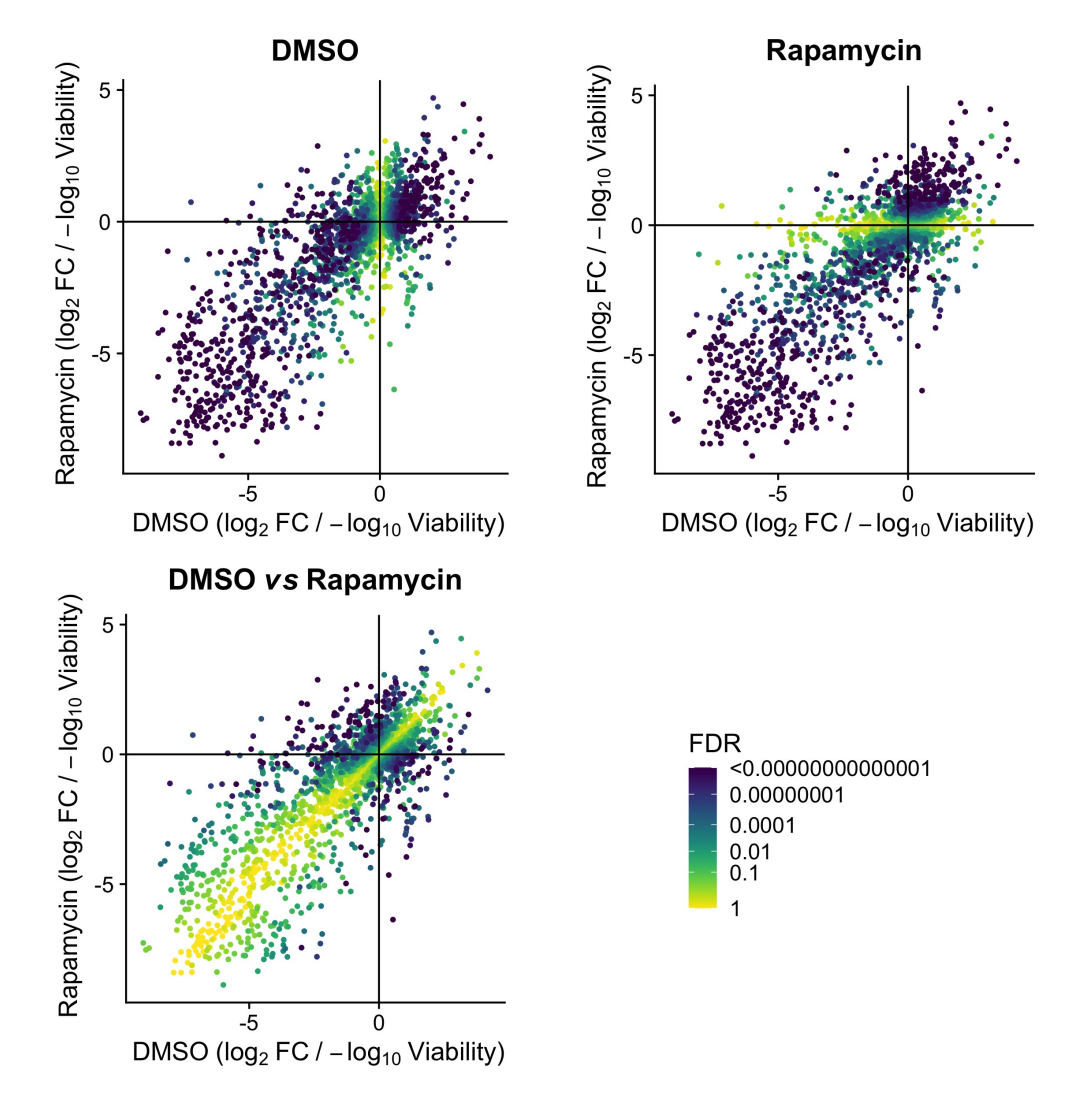


Figure 4.3: Identification of mutants with altered CLS. Lifespan score in DMSO is plotted against lifespan score in rapamycin. In each of the 3 panels, points are coloured based on FDR to identify mutants with altered lifespan in DMSO, mutants with altered lifespan in rapamycin, and mutants which behave differently in rapamycin *vs* DMSO.

Lifespan scores for DMSO and rapamycin are shown in Figure 4.3. To identify mutants with altered lifespan in DMSO, altered lifespan in rapamycin,

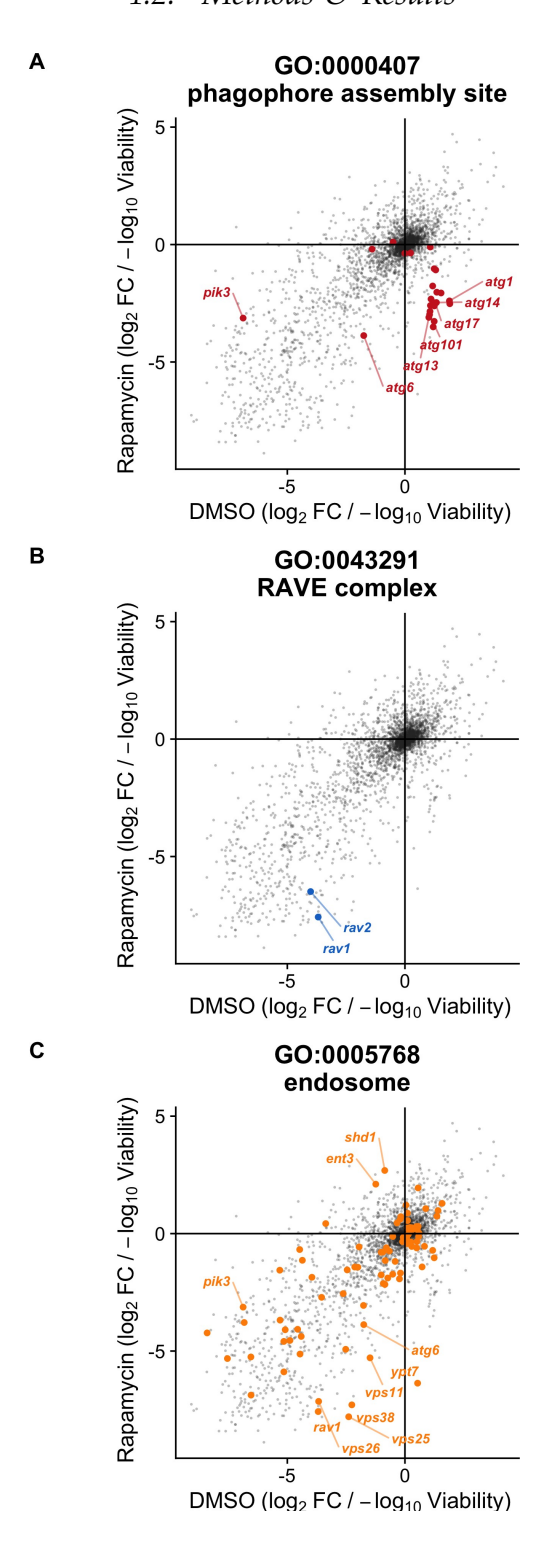


Figure 4.4: Functional enrichments involved in rapamycin-mediated lifespan extension.

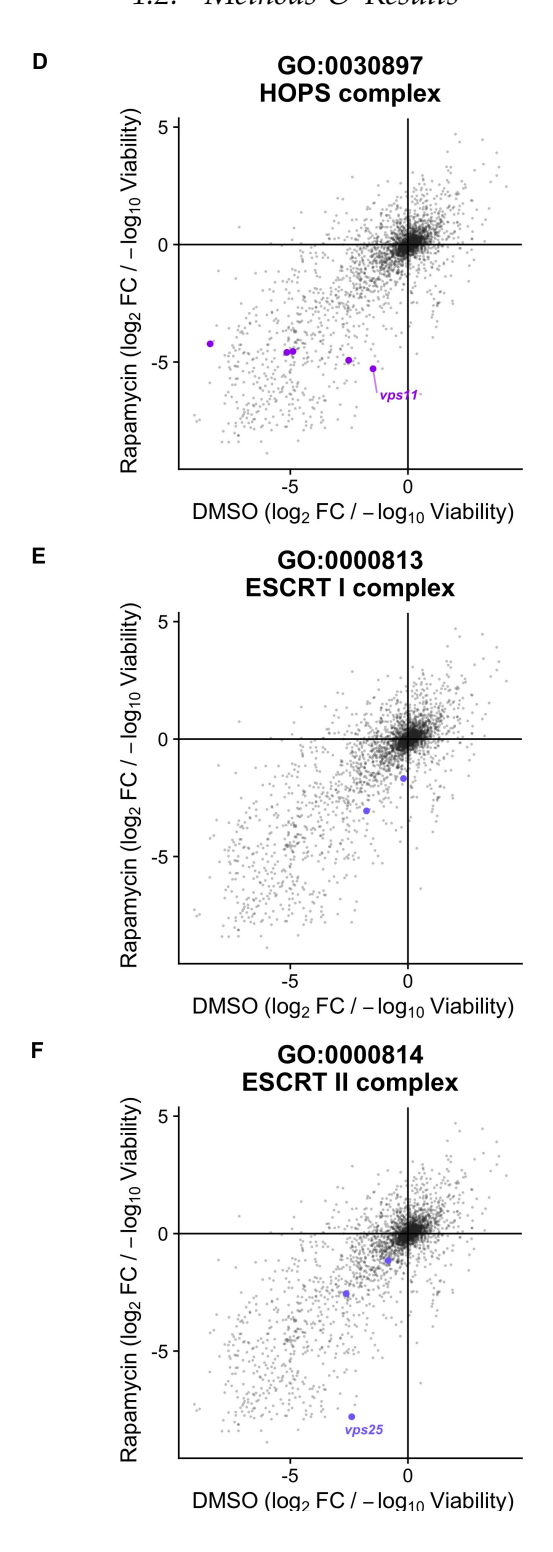


Figure 4.4: Functional enrichments involved in rapamycin-mediated lifespan extension.

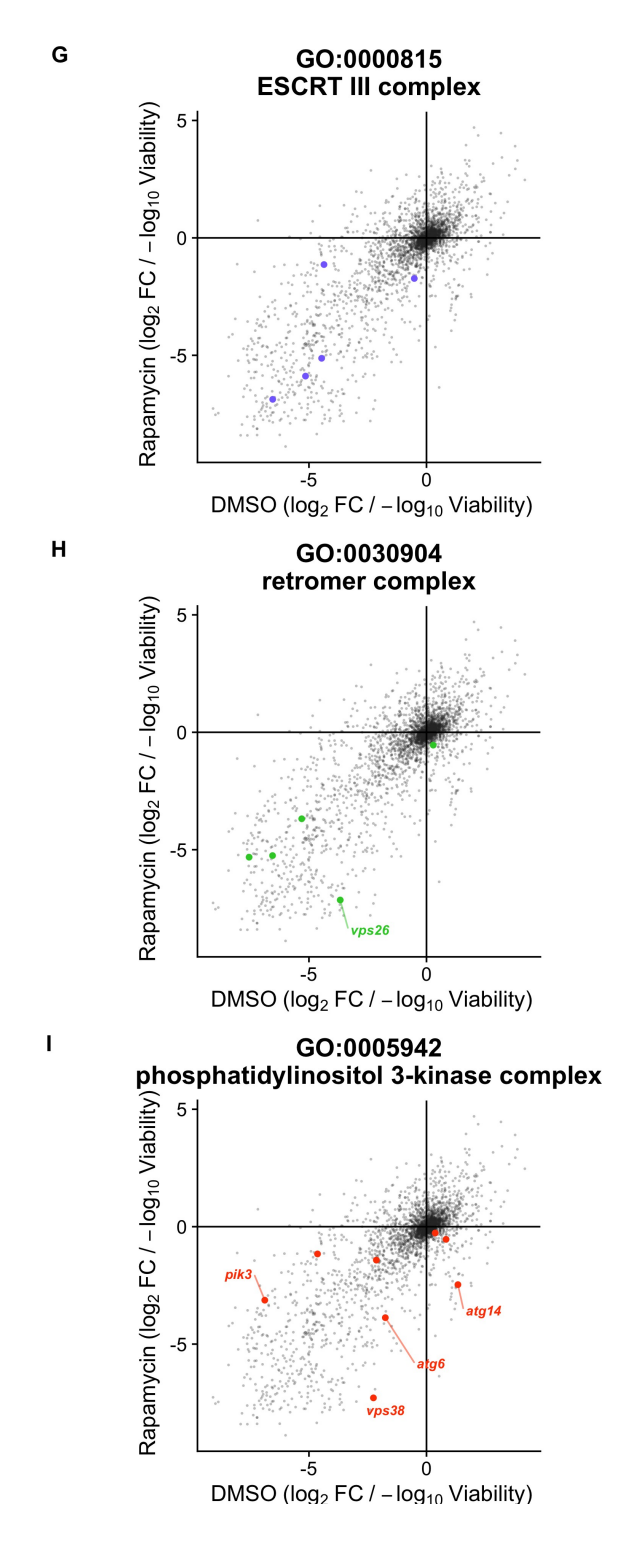


Figure 4.4: Functional enrichments involved in rapamycin-mediated lifespan extension.

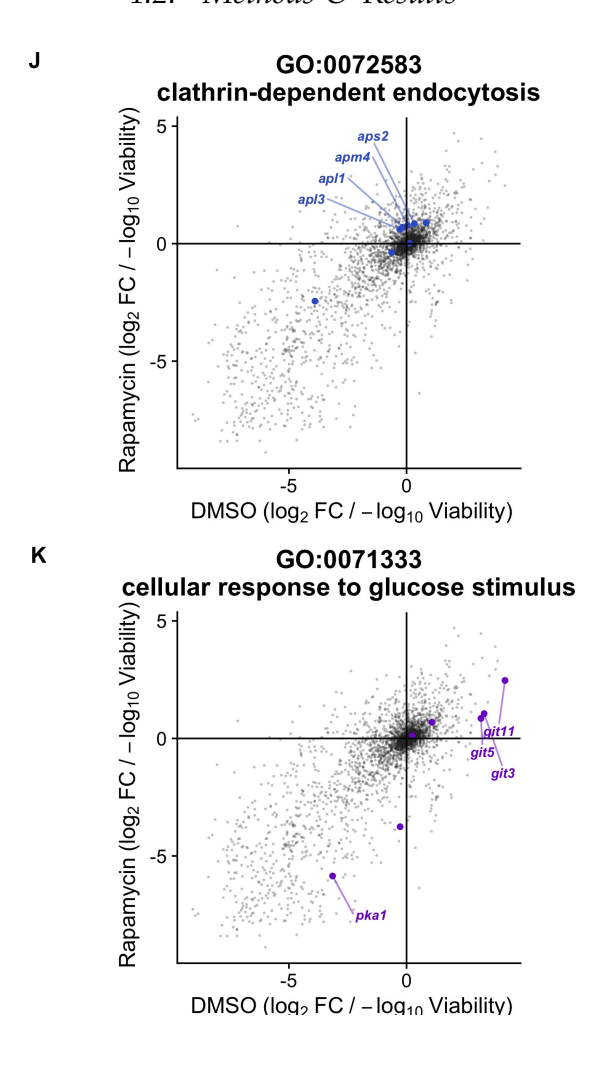


Figure 4.4: Functional enrichments involved in rapamycin-mediated lifespan extension.

and mutants which behave differently in rapamycin vs DMSO, the following cut-offs were applied: a fold change (FC) cut-off of $|\log_2 FC| > \log_2 1.5$ and a false discovery rate (FDR) cut-off of FDR < 0.05. Lists of mutants were analysed using gProfiler [114]. Figure 4.4 highlights selected terms and mutants which are subsequently discussed.

4.3 Discussion

4.3.1 The lifespan extension conferred by rapamcyin is mediated by autophagy

Mutants which respond differently in the rapamycin-treated pools compared to the DMSO-treated pools provide insights into the genetic components which interact with TORC1 in an ageing context. Some of the strongest negative interactions were observed in mutants annotated to the phagophore assembly site (Figure 4.4A). This included atg13, a conserved phosphorylation target of TORC1 [100, 104]. Atg13 becomes dephosphorylated upon TORC1 inactivation, leading to the assembly of the Atg1 complex and initiation of macroautophagy [115]. Indeed, all members of the fission yeast Atg1 complex (atg1, atg13, atg17 and atg101 [116]) were similarly rapamycin-insensitive. These results indicate that rapamycin extends fission yeast chronological lifespan by via autophagy. This is consistent with a numerous reports in other model systems, and highlights the benefits of degrading damaged proteins and organelles which accumulate during ageing [108, 109]. It is unclear why these mutants also show a slightly extended lifespan in the DMSO-treated pools, as this contradicts the notion that autophagy increases lifespan. However, autophagy can be detrimental to lifespan under certain contexts. For example, in both mice and nematode worms, mutations which cause the mitochondrial permeability transition pore to open result in decreased lifespan as a result of excessive clearance of dysnfunctional mitochondria [117]. Hence, it is possible that the increased lifespan of autophagy mutants in the absence of rapamycin could reflect a similar phenomenon. Indeed, it is notable that this study was performed in rich media, a condition where fission yeast has little requirement for mitochondrial function during exponential growth [70]. Irrespective of the mechanism, this result highlights that the genetic basis of lifespan is highly context-dependent, and that a process can be beneficial or detrimental to lifespan depending on physiological conditions.

In addition, rav1 and rav2 mutants were short-lived, and displayed a

strong insensitivity to rapamycin (Figure 4.4B). They encode subunits the RAVE complex, which is involved in the assembly of the vacuolar and endosomal ATPase [118, 119, 120]. The ATPase performs a variety of functions, most notably vacuolar and endosomal acidification [102]. Low pH in the vacuole is required to activate hydrolases which degrade cargos delivered to the vacuole and is hence an essential component of autopagy [121], which may underlie the reason why *rav1* and *rav2* are rapamycin-insensitive. If this were the case, then rapamycin-insensitivity can arise by disrupting autophagy at various stages, from autophagophore formation to hydrolysis of cargoes at the vacuole. However, it is important to note that vacuolar pH can also regulate a wide variety of other processes involved in ageing [118, 122].

4.3.2 Diverse aspects of endosome function are required for rapamycin-mediated lifespan extension

Negative interactions were also enriched for mutants annotated to endosomes, indicating that endosomes are mediators of rapamycin-mediated longevity. However, endosome mutants displayed a range of effects, with some endosome mutants displaying positive interactions and many others being short-lived but not displaying an interaction with rapamycin (Figure 4.4C). The interactions at endosomes are difficult to dissect as they reflect the complex regulatory functions which endosomes play in TORC1 signalling in addition to their roles as mediators of processes downstream of TORC1 [101, 110, 111]. The strongest negative interactors covered a range of conserved endosome functions. They included:

• *vps11*, encoding an E3 ubiquitin ligase which is a member of the HOPS and CORVET tethering complexes which coordinate membrane fusion events [123]. However, other members of the HOPS and CORVET complexes did not show a strong negative interaction with rapamycin, with many being short-lived (Figure 4.4D). Interestingly, a recent report using human cell lines indicates that VPS11 regulates other aspects of cellu-

lar signalling via ubiquitination independently of its role in membrane fusion events [124]. Furthermore, genetic leukoencephalopathies, a rare group of inherited disorders affecting the central nervous system, have been linked to defects in autophagy as a result of a mutation in *VPS11* [125].

- *vps*25, encoding a subunit of the ESCRT-II complex which is involved in sorting ubiquitinated cargo in endosome membranes into intraluminal vesicles, resulting in the formation of a multivesicular body which will deliver the ubiquitinated cargo to the vacuole for degradation [126, 127]. Deletion of *vps*25 in fruit flies leads to autophagosome accumulation and impaired autophagy [128], although this appears to be a general feautre of ESCRT mutants in higher eukaryotes [129]. Notably, other ESCRT mutants in this screen do not show strong negative interactions with rapamycin, and many are short-lived (Figure 4.4E-G).
- *vps26*, encoding a subunit of the retromer complex which is required for endosome-to-Golgi transport [130, 131]. An important function of the retromer complex is to retrieve and recycle hydrolase receptors such as Vps10 [132], which are essential for delivering hydrolytic enzymes to vacuoles [133, 134]. Hence, deletion of retromer complex components leads to dysfunctional autophagy in fruit flies [135] and pathogenic yeast [136]. Furthermore, a decrease in the expression of retromer complex components, including VPS26, is associated with Alzheimer's disease [137]. Notably, other components of the retromer complex do not show strong negative interactions with rapamycin, and many are short-lived (Figure 4.4H).
- ypt7, endocding a Rab GTPase which is a master regulator of membrane trafficking and organelle fusion [138]. Several studies have demonstrated that Ypt7 is required for proper autophagy progression in budding yeast.
 For example, deletion of ypt7 results in autophagosome accumulation and

vacuolar fragmentation [139], whilst *ypt7* was also identified in a screen for genes required for mitohpagy [140]. In addition, Ypt7 is invovled in the fusion of the autophagosome with the vacuole [141] and is linked to to retromer-mediated receptor recycling [142], suggesting that Ypt7 coordinates multiple aspects of autophagy.

There is an undoubtedly complex relationship between endosome trafficking and autophagy. Notably, TORC1 localises to endosomes where it regulates autophagy by inhibiting autophagosome formation in the presence of nutrients [101]. However, strong negative interactions between rapamycin and genes which cover diverse aspects of endosome function suggests that the relationship between autophagy and endosomes is far more intertwined. Defining the nature of these interactions requires differentiating between general aspects of endosome function which are required for autophagy and specific regulators of autophagy which reside on endosomes, which is not clear from the interaction profiles of these mutants alone. That only specific components of the HOPS/CORVRET, ESCRT and retromer complexes show strong negative interactions with rapamycin suggests that these may represent specialised regulatory functions which are carried out by these components. However, it is also notable that other components of these complexes are short-lived, indicating that HOPS/CORVET, ESCRT and retromer complexes in general are required for stationary phase survival under standard conditions. In the case of the retromer complex, a mechanism has already been established which may explain why this aspect of endosomal trafficking is required for lifespan [135, 136], but in the cases of other aspects of endosome function, it is less clear, at least in yeast.

Several lines of evidence suggest that endosome functions in general are required to mediate the downstream effects of TORC1 inhibition. For example, genome-scale metabolic profiling of deletion mutants in budding yeast clearly demonstrates that the metabolic signatures of many endosomal mutants, including vacuolar and endosomal ATPase, RAVE, HOPS/CORVRET, ESCRT

and retromer complex mutants mimic the metabolic signature of rapamycintreated cells [143]. Furthermore, autophagy and endosomal trafficking are closely linked in mammals. For instance, fusion of endosomes and autophagosomes to form an amphisome is a critical part of autophagosome maturation and is required for autophagy in mammals [144, 145, 146, 110, 147, 148]. In yeast, interactions between endosomes and autophagosomes are less well defined as it is difficult to distinguish between these structures owing to a lack of morpholological differences and a lack of well-defined marker proteins [110]. However, it seems that even in yeast, much of the molecular machinery involved in autophagy and endosomal function is shared [141]. Hence, it is plausible that the strong negative interactions observed between endosome mutants and rapamycin may reflect an interdependence between diverse endosome functions and autophagy, as is the case in mammals [144, 145, 146, 110, 147, 148].

What is puzzling is that many of HOPS/CORVET, ESCRT and retromer complex mutants, especially the short-lived ones, do not show a strong negative interaction with rapamycin, indicating that rapamycin treatment is capable of extending lifespan in these mutants. Indeed, it actually implies that rapamycin treatment may partially rescuse defects resulting from endosomal disruption. A possible explanation is that in the context of severe endosome disruption, alternative mechanisms of autophagy induction may be upregulated, which in turn leads to rapamycin-sensitivity. Indeed, such behaviour has often been described in many aspects of biology, especially ageing, where the effect of a mild perturbation can have the opposite effect of a severe perturbation [149, 150] and may reflect negative feedback loops which are involved in maintaining homeostasis in response to stress [151, 152]. Dissecting these interactions is beyond the scope of this study, although such contradicting interaction profiles are important to recognise and highlight that seemingly subtle changes in endosome function can have completely different effects on lifespan and rapamycin-sensitivity.

4.3.3 Rapamycin-mediated lifespan extension is dependent on Class III PI3K signalling to initiate autophagy

Lipid kinases such as PI3Ks play important roles in the regulation of many cellular functions, including autophagy [148, 153, 154]. They do so via the phosphorylation of lipids which act as second messengers, leading to the binding and recruitment of specific effectors to cell membranes [155, 156]. Class I PI3K signalling to TORC1 via AKT is a well characterised regulator in mammals [157], although this signalling pathway is not present in yeast [158, 159]. The Class III PI3K Vps34 is the only PI3K which shows a strong conservation across eukaryotes [153, 154]. In yeast, association of Vps34 with different subunits creates two spatially and functionally distinct PI3K complexes with diverse roles in both autophagy and endosome trafficking. Complex I contains Atg14 and is recruited to the phagophore assembly site via Atg8, an interaction which is essential for autophagy initiation [160, 161]. In mammalian cells it has been shown that TORC1 directly suppresses Complex I activity by phosphorylating Atg14 [162]. In addition, Complex I is involved in delivery of cargo to the vacuole for degradation, being required to recruit Ypt7 and subsequently the HOPS complex to the autophagosome, which mediates fusion of the autophagosome with the vacuole [141]. Complex II contains Vps38 and is a regulator of endosomal trafficking [155, 156]. The role of Complex II in autophagy is unclear, although a study in Arabadopsis has indicated that Vps38 is also required for autophagy [163]. Consistently, atg14, atg8, vps38 and atg6 (a subunit of both Complex I and Complex II) all showed strong negative interactions with rapamycin (Figure 4.4I), indicating that PI3K signalling at both the phagophore assembly site and endosomes is required for rapamycin-mediated lifespan extension. The requirement of Complex I for autophagy is well established [141, 160, 161], although the reason why Complex II is required for rapamycin-mediated lifespan extension is less clear. However, it is known that production of phosphatidylinositol 3-phosphate (PI3P)

via Complex II is required to recruit the retromer complex to endosomes and initiate endosome-to-Golgi retrograde transport [164, 165]. Hence, it is possible that the rapamycin-insensitive phenotype of *vps38* may be as a result of an inability to recycle hydrolases receptors via endosome-to-Golgi transport, leading to autophagy defects [135, 136]. It is notable that *vps38* mutants in *Arabadopsis* are phenotypically similar to retromer complex mutants [166].

4.3.4 Class III PI3K signalling is also mediates nutrient sensing upstream of TORC1

The interaction profile of *pik3*, the fission yeast ortholog of *vps34*, was markedly different to the interaction profiles of the subunits with which Pik3 physically interacts. Deletion of *pik3* causes a serious reduction in lifespan (Figure 4.4I). This is consistent with the sickness observed in budding yeast *vps34* mutants, which may be linked to their inability to accumulate any PI3P [167]. However, the pik3 mutant was hypersensitive to rapamycin, suggesting that rapamycin treatment can partially rescue the short lifespan associated with loss of Pik3. Consistently, rapamycin hypersensitivity has been observed in budding yeast vps34 mutants, with atg14 mutants showing the opposite phenotype of rapamycin resistance [168]. This may reflect the fact that Vps34 is also an upstream activator of TORC1, where Vps34 is activated by amino acids leading to recruitment of the PI3P-binding protein Pib2 which activates TORC1 [169, 170]. Indeed, pib2 showed a positive interaction with rapamycin, consistent with Pib2 being an upstream activator of TORC1 (Figure ??). The distinct interaction profile of the pik3 mutant is consistent with suggestions that Pik3 forms a third complex which is distinct from Complex I and II in order to relay amino acid signals to TORC1 [170]. Assuming that rapamycin increases lifespan of pik3 cells via the same mechanism as wild-type cells, this result suggests that rapamycin is able to initiate authophagy via alternative mechanisms in the absence of any Pik3 activity. This is in contrast to cells with Pik3 activity, in which case Pik3 activity must be correctly localised to the phagophore assembly site via Atg14 and to endosomes via Vps38 in order

to initiate autophagy in response to rapamycin treatment.

4.3.5 Distinct interaction profiles of PI3K mutants may reflect interconnected positive and negative feedback loops involved in TORC1 control of autophagy

PI3P is an upstream activator of TORC1 which is invovled in amino acid sensing [168, 169, 170]. PI3P also acts downstream to initiate autophagy in response to TORC1 inactivation [153, 154]. In essence, inhibition of TORC1 produces an activator of TORC1, which implies the presence of a negative feedback loop where TORC1 activity and PI3P abundance mutually regulate each other to coordinate autophagy initiation. Downstream of this, PI3P is also involved in a positive feedback loop to initiate autophagy at the phagophore assembly site via interactions with Atg8 [161]. This may reflect the distinct roles which positive and negative feedback loops play in biological systems. Negative feedback loops are important for maintaining homeostasis and have been extensively studied in the context of control theory [171]. In this case, negative feedback loops allow TORC1 activity to be tuned to reflect nutrient availability and other signals. Positive feedback loops on the other hand lead to bistability [172], and are important for establishing two distinct on/off states for autophagy in response to TORC1 activity [161]. This control architecture may facilitate precise regulation of autophagy and other TORC1-regulated processes in response to changes in nutrient availability.

4.3.6 Inhibition of clathrin-mediated endocytosis can further extend lifespan following rapamycin treatment

Mutants which were long-lived specifically in rapamycin were enriched for clathrin-dependent endocytosis (Figure 4.4J). In addition, two endosomal mutants which are involved in endocytosis, *ent3* [173] and *shd1* [174] also showed

a strong rapamycin-specific increase in lifespan 4.4C). As many positive regulators of TORC1 are hypersensitive to rapamycin [168], one possible explanation is that clathrin-mediated endocytosis is a positive regulator of TORC1. Given that endocytosis is a source of endosomes, to which TORC1 localises, and that TORC1 regulates endocytosis, it is plausible that endocytic flux may reciprocally regulate TORC1. However, an alternative possibility is that endocytosis itself may cause ageing via a mechanism distinct to autophagy. Indeed, it has been suggested that age-related increases in the abundance of endocytic proteins could be a factor Alzheimer's disease progression by facilitating the conversion of amyloid precursor protein into the disease-causing β -amyloid [175]. Furthermore, endocytosis is suppressed when nematode worms enter the longlived dauer diapause, particularly in neuronal cell types [176]. This suggests that reduced endocytosis is a general mechanism which promotes long-term survival of non-dividing cells. Indeed, it is sensible to presume that limiting a cell's interactions with the extracellular environment would benefit its longterm survival, especially if that environment becomes progressively more toxic with age.

4.3.7 TORC1 and PKA coordinate different temporal aspects of starvation response

The protein kinase A (PKA) signalling pathway is another important aspect of nutritional sensing which is highly conserved across eukaryotes [177, 178, 179]. The G protein coupled receptor (GPCR) Git3 is activated by extracellular glucose, which initiates a signalling cascade resulting in the production of cyclic adenosine monophosphate (cAMP), a cytosolic second messenger, via adenylate cyclase activity. cAMP activates Pka1, which in turn regulates a wide array of cellular processes. Indeed, TORC1 and PKA regulate many of the same targets, although appear to regulate different temporal aspects [180]: TORC1 allows cells to tune growth rate to internal metabolite concentrations, whilst PKA allows cells to rapidly respond to changes in glucose availability. Hence, it is unsurprising that deletion of *git3* or other components of the GPCR

(git5 and git11) increase lifespan, as previously described [179]. Furthermore, these mutants showed a reduced sensitivity to rapamycin (Figure 4.4K), which suggests that these mutants have an extended lifespan because they mimic the effect of rapamycin, which is consistent with the overlapping functionalities of TORC1 and PKA [180]. Indeed, budding yeast PKA has been shown to directly inhibit autophagy in parallel to TORC1 via Atg13 phosphorylation to prevent Atg1 complex formation at the phagophore assembly site [181].

However, pka1 showed a reduced lifespan (Figure 4.4K), which is not consistent with previous reports [63]. This result may serve to highlight critical differences in pool versus batch culture ageing experiments. pka1 mutants in batch culture experiments continue to grow at a low rate in early stationary phase (Figure 2.7, unpublished data), which is consistent with the idea that pka1 mutants prematurely enter into stationary phase due to an inability to properly detect low levels of glucose. This would mean that there are still low levels of glucose in batch cultures, which would support growth and survival. However, in pooled experiments, other mutants would still properly sense and consume glucose at low levels, meaning that this advantage to the pka mutant in batch cultures is gone in the pool. Furthermore, the short lifespan of *pka1* mutants in the pool is consistent with the idea that PKA signalling is important for responding to sudden changes in glucose availability [180]. This implies that the short lifespan of pka1 in the pool is due to an inability to adapt to stationary phase, and hence does not reflect the role of PKA in ageing. Consistent with this, pka1 cells show a negative interaction with rapamycin, which would be expected as rapamycin treatment would not compensate for the inability to adapt to stationary phase.

It must also be addressed why Git3 signalling mutants do not behave like *pka1* in the pool. In budding yeast and mammals, Ras signalling is able to sense intracellular energy levels via cytosolic pH and is the other major source of cAMP in cells, meaning PKA detects changes in glucose levels via two upstream regulators [118, 182, 183, 184]. However, it appears that Ras

signalling does not modulate adenylate cyclase activity in fission yeast, and hence does not signal to PKA [185]. However, it is still likely that PKA is able to respond to changes in glucose availability via other mechanisms in the absence of Git3 signalling. Indeed, fission yeast Pka1 phosphorylation status changes in response to glucose availability even in the absence of adenylate cyclase, demonstrating the existence of a cAMP-independent mechanism of PKA regulation [186]. That there are additional regulators of PKA activity in fission yeast offers a plausible explaination as to why Git3 signalling mutants behave differently to *pka1*.

4.4 Conclusion

This study systematically dissects the genetic basis of rapamycin-mediated lifespan extension, revealing a critical requirement of autophagy. Furthermore, the coordinated action of multiple effectors downstream of TORC1 is required to initiate autophagy. This included diverse aspects of endosome function, including PI3K signalling, membrane fusion complexes and retromer trafficking. In addition, an enormous number of mutants showed altered responses in rapamycin compared to DMSO, demonstrating that the genetic basis of lifespan is highly context-dependent, as previously suggested [36, 47]. However, it is often difficult to interpret these differences, as a genetic interaction may be interpreted differently depending on context [187]. The ability for a single screen to capture decades worth of regulatory connections highlights the potential value of Bar-seq. Indeed, Bar-seq captures information which other genome-scale technologies, such as RNA-seq or proteomics, cannot, revealing functional connections which may dissect complex phenotypes such as lifespan.

Chapter 6

Conclusions & Future Directions

One of the most remarkable discoveries in ageing research was that there are simple genetic, environmental and pharmacological perturbations which consistently increase lifespan across eukaryotes [6, 45]. This is somewhat surprising given the intricate complexity of lifespan as a phenotype, which is only beginning to be truly appreciated and dissected. Yeast remain a vital model system to tackle complex questions of fundamental biological important owing to their amenability to high-throughput methods [31], and hence may represent our best opportunity at modelling complex cellular processes [72]. However, there are still substantial obstacles which must be overcome before we can develop a mechanistic, as opposed to descriptive, model of ageing. This thesis addresses a number of these obstacles, establishing a platform from which high-throughput CLS assays can be readily in a reproducible manner.

This has involved the development of two high-throughput methods for determination of CLS at various experimental scales. The first is a high-throughput CFU assay which can be largely automated by robotics. This provides an attractive alternative to the labour- and resource-intensive traditional CFU assay for day-to-day lifespan experiments. The second establishes Barseq as a technology which can provide genome-scale insights into the genetic basis of lifespan in a specific context. This involved in the characterisation of barcodes associated with mutants from the Bioneer deletion library and the identification of key technical and biological biases which must be addressed

when Bar-seq is applied to CLS. For both methods, care has been taken to establish well-documented experimental and analytical pipelines which will facilitate use and deployment of these methods by the wider community, hence facilitating high-throughput ageing studies.

I have applied Bar-seq to dissect the genetic basis of rapamycin-mediated lifespan extension. The gene-drug interactions uncovered provide insights into the genetic components with which rapamycin interacts, specifically in an ageing context. Some of these interactions reflect the components which are functional partners of TORC1, and reveal that the coordinated actions of multiple aspects of endosome function are required to initiate autophagy in response to rapamycin treatment. Indeed, some of these interactions captured remarkably specific functional connections and summarise decades worth of research into TOR signalling, highlighting the insights which can be afforded by functional profiling which are not possible from other genome-scale technologies such as RNA-seq and proteomics. Other interactions may reflect interactions between different processes which are involved in determining fission yeast lifespan. Hence, the interactions uncovered may serve as a basis to constructing a mechanistic model of ageing, wherein the regulatory functions of nutrient sensing pathways such as TOR signalling are linked to processes which determine the lifespan of the organism. Indeed, developing a comprehensive model of fission yeast ageing will require dissecting the genetic basis of lifespan in far more contexts. However, given the relative ease with which Bar-seq CLS screens can now be conducted, generating such datasets is a realistic prospect. Such investigations may include ageing mutant pools under different environmental conditions, ageing mutant pools in the presence of other pharmacological agents, or using synthetic genetic array technology to create and age double mutant pools [27]. Indeed, such an approach can even be extended to create different mutants of the same gene, facilitating functional profiling at the level of individual amino acid residues. Furthermore, should enough Bar-seq CLS datasets be generated (or indeed any genome-scale lifespan datasets), machine

learning approaches may be able to construct representations which reflect the regulatory interactions encoded within interaction profiles, such as Bayesian networks [188]. Such a network would be a mechanistic model of ageing in a eukaryote, a milestone which would have significant repercussions in the biomedical sciences.

However, for all of this to be possible, it is essential that research is robust, reliable and reproducible. The irreproducible nature of ageing research likely reflects the complexity of ageing as a process and the number of factors which interact to determine an organism's lifespan. When working with simple model systems such as fission yeast, it is essential to consider all aspects of the organism's ecology and life history traits as important determinants of lifespan, not just those which may have transferable value to understanding human ageing. Indeed, investigations into the sources of experimental irreproducibility in fission yeast CLS revealed that yeast have a remarkable ability to regulate their own lifespan in response to population density, and will "remember" this for many rounds of division. In the lab, this manifests as irreproducibility owing to an inability to consistently pick exactly the same amount of colony from an agar plate. The amount of colony picked to inoculate a pre-culture seems like a trivial factor to the naive PhD student, but may be one of the most important sensory cues to the yeast. Indeed, after considering the ecology of a microbe, this kind of behavior is a rather sensible strategy to maximising fitness. However, the ecological context of an a model system is often neglected in research, and in some cases not even known [189]. Hence, in order to truly harness yeast as a model system, an integrated view of ageing must be established which appreciates the full range of factors involved in lifespan determination. It is only then that we will be able to pick apart how these factors interact, and in turn slowly build an understanding of what ageing is.

Appendix

Analysis of High-throughput Colony Forming Units Assays

Installation

Tutorial

```
library(DeadOrAlive)
library(ggplot2)
```

This tutorial will teach you how to analyse high-throughput colony forming unit (CFU) assay data as described in Romila et al., 2021. This assay facilitates high-throughput chronological lifespan (CLS) studies in microorganisms such as *Saccharomyces cerevisiae* or *Schizosaccharomyces pombe* by using robotics to automate CFU plating in a highly parallelisable manner (Figure 1).

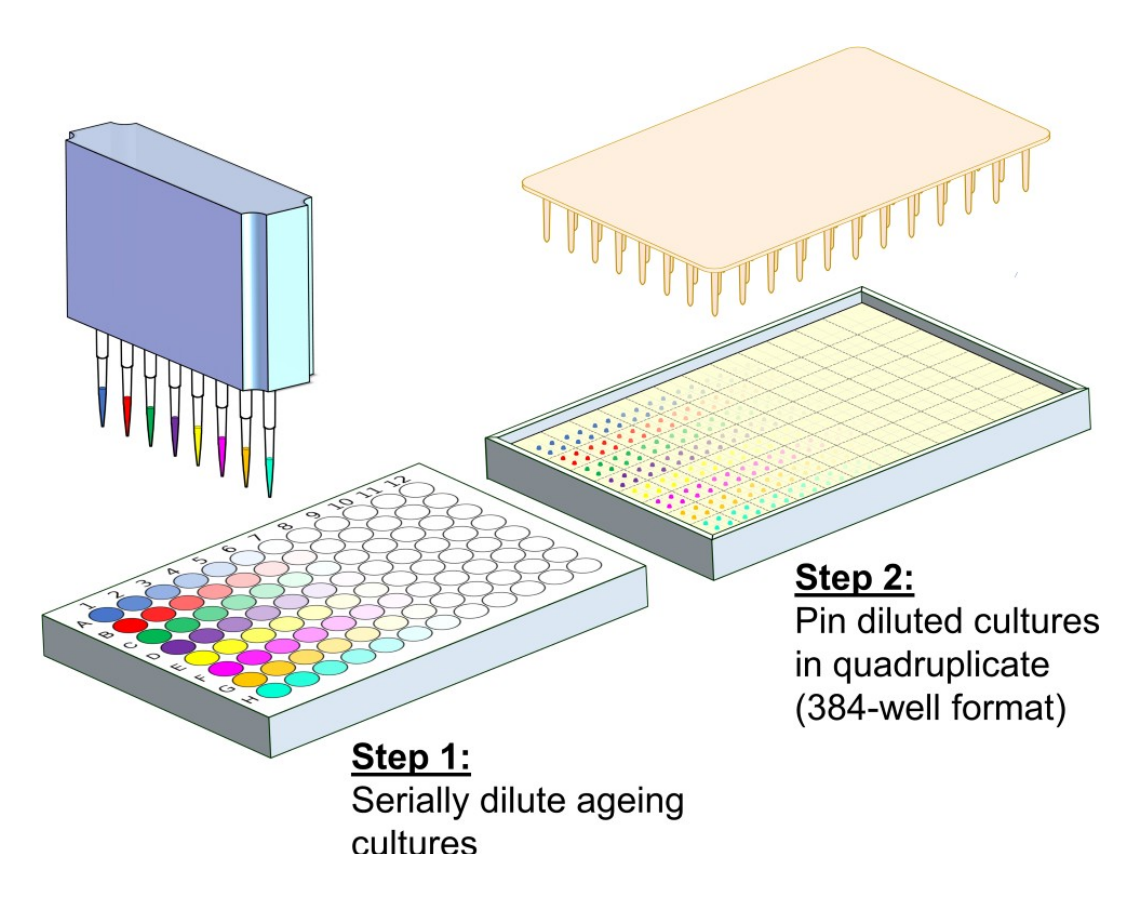


Figure 1: Schematic depiction of experimental protocol.

Image Analysis

In order to estimate the number of colony forming units for a particular sample, the pattern of colonies must first be analysed. colonyThreshold() will take a batch of images of agar plates and identify whether or not there is a colony in each position. For this, it is critical to provide a reference image to aid colony identification in sparsely populated regions of the plate (Figure 2A).

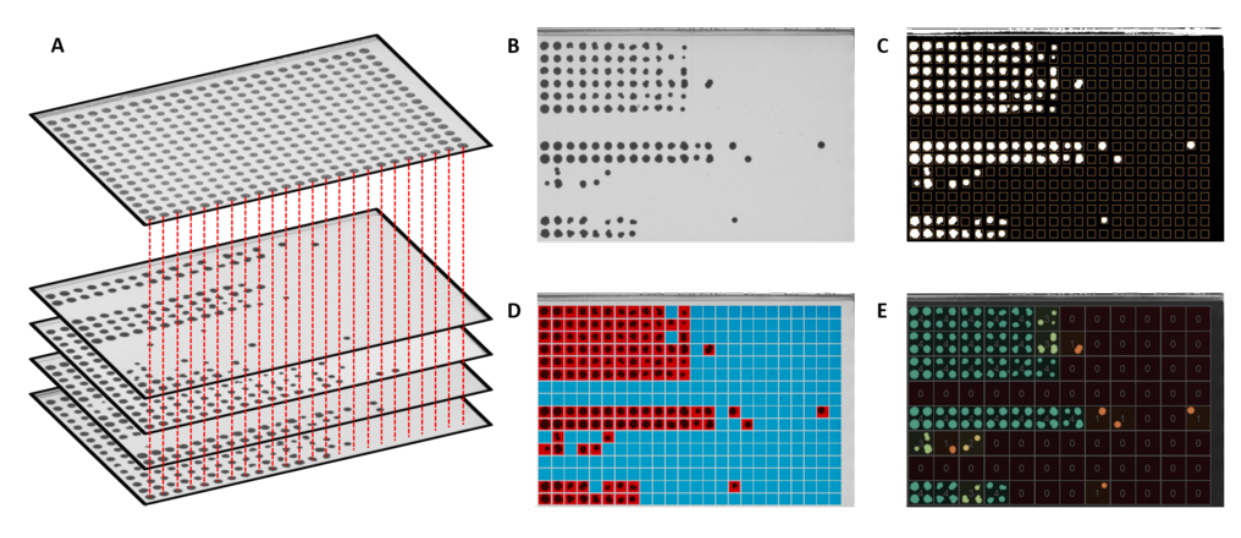


Figure 2: Outline of image analysis pipeline.

colonyThreshold() wraps the gitter() function in the gitter package in order to perform the image analysis. As such, all of the arguments used by gitter() are available in the colonyThreshold() function. Of particular importance are:

- plate.format the format of the agar plate
- well.plate.format the format of the plate used for serial dilutions
- inverse have colours in the image been inverted? For example, when a scanner is used to take images of the plate, the colonies will appear darker than the background

colonyThreshold() does not return any objects, but instead creates up to 4 files for each raw image processed (Figure 2B). These are:

- DAT file A tab delimited file containing quantified colony sizes, as described in gitter. A sixth column marking whether a colony has been classified as present (1) or absent (0) is added
- **Gridded image** Image showing colony identification by aligning colonies to the grid identified in the reference image, as described in gitter (Figure 2C)
- Threshold image Image showing whether a colony has been classified as present or absent for each position on the plate (Figure 2D)
- **Count image** Image showing how many colonies have been classified as present for each sample at each dilution factor (Figure 2E)

It is particularly important to manually check the **threshold image** in order to confirm that colonies have been correctly marked as present or absent. The software used to estimate the number of colony forming units from the pattern of colonies observed is robust to the occasional misclassification, so it does not matter if there are a few mistakes. However, any plates for which there are a substantial number of errors will need to be re-scanned and re-analysed.

There are some demo images stored within the package. The images can be accessed and image analysis performed using the following code:

```
#Get the directory of files to be analysed
dir <- system.file("extdata", "images", package="DeadOrAlive")

#View the files
list.files(dir)

#Get the reference image
reference <- system.file("extdata", "reference.jpg", package="DeadOrAlive")

#Analyse the files to identify whether there is a colony or not in each position
#Note: This will create a new directory called 'Image_Analysis'
colonyThreshold(dir=dir, reference=reference)
```

Extraction of Colony Patterns

The next objective is to collect the present/absent colony information and assemble it correctly based on the identity of the plates, time points and samples. This is achieved by supplying two supporting files – the plate reference file and the sample reference file – to the extractColonyVectors() function. This function will take a directory of processed DAT files generated by the colonyThreshold() function and extract a vector containing the number of colonies present at each dilution factor for each sample at each time point. For this to work, it is also necessary to provide the plate.format for the agar plate and the well.plate.format.

Demo files can be accessed from within the package. In this case, we are analysing an experiment where the lifespan of 48 different strains were measured at 7 different time points. Given that 8 strains can be measured in parallel on a single agar plate, this means that 6 agar plates are required per day. The **sample reference file** shows which strains are plated on each of the 6 plates. The **plate reference file** provides the identity of each image - i.e. which groups of strains at which time points are plated on each image. These two files, in

addition to the directory containing the processed **DAT files**, are passed to the extractColonyVectors() function as follows:

Estimation of Colony Forming Units

The next challenge is to estimate the number of colony forming units present for each sample at each time point. This is achieved via maximum likelihood estimation using the analyseColonyVectors() function – that is to say, the function determines what number of colony forming units in the culture is most likely to give rise to the pattern of colonies observed. This achieved as follows:

```
#Perform a maximum likelihood estimation of the number of viable cells

#Note: This will save a csv and markdown file in the current working directory

CFUsMLE <- analyseColonyVectors(myColonyVectors)
```

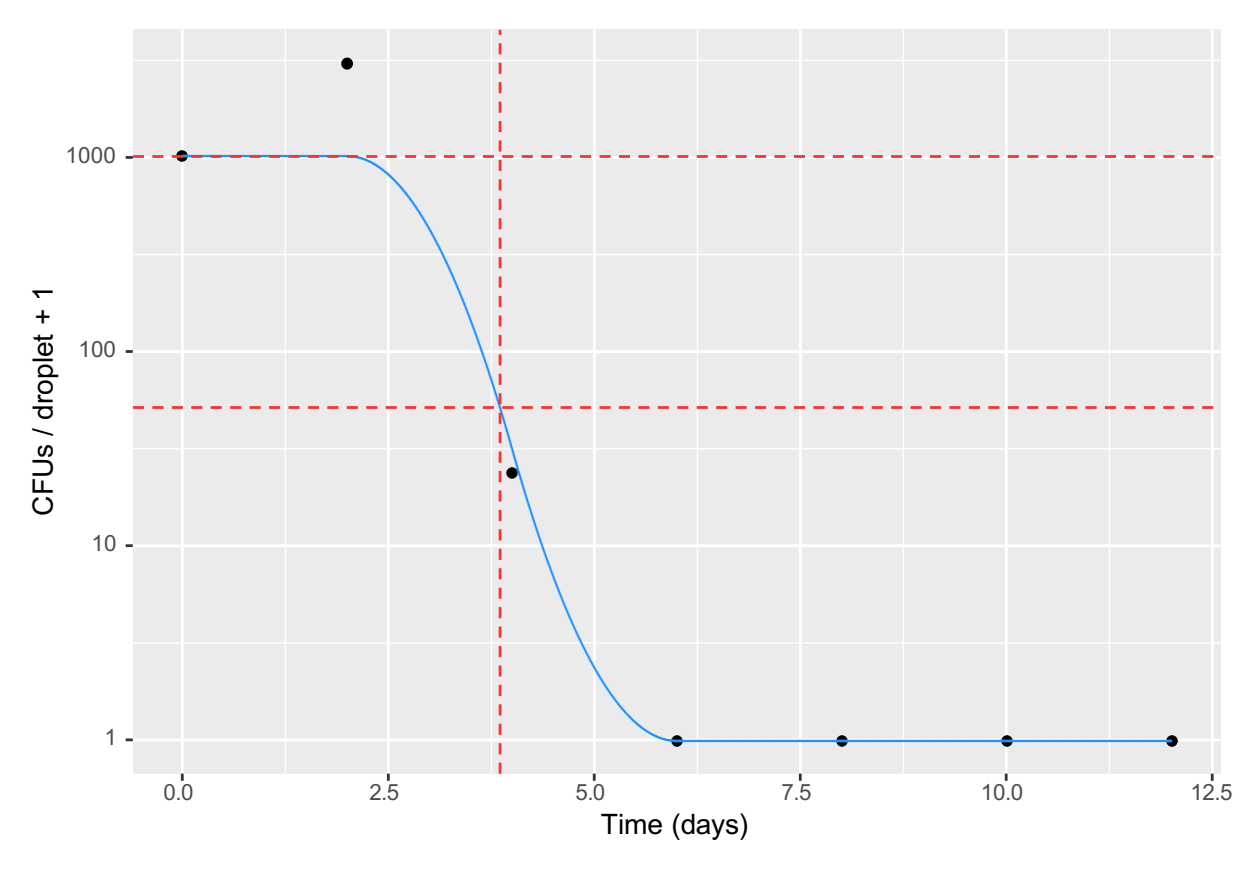
Analysis of Lifespan Curves

As a first step, it is advisable to perform some quality control steps. The maximum likelihood estimator is highly sensitive to outliers, and as such the analyseColonyVectors() function implements some quality control steps to remove outliers from the patterns of colonies. It is sensible to remove data points for which a lot of the colony pattern had to be excluded in order for a robust maximum likelihood estimation to be achieved:

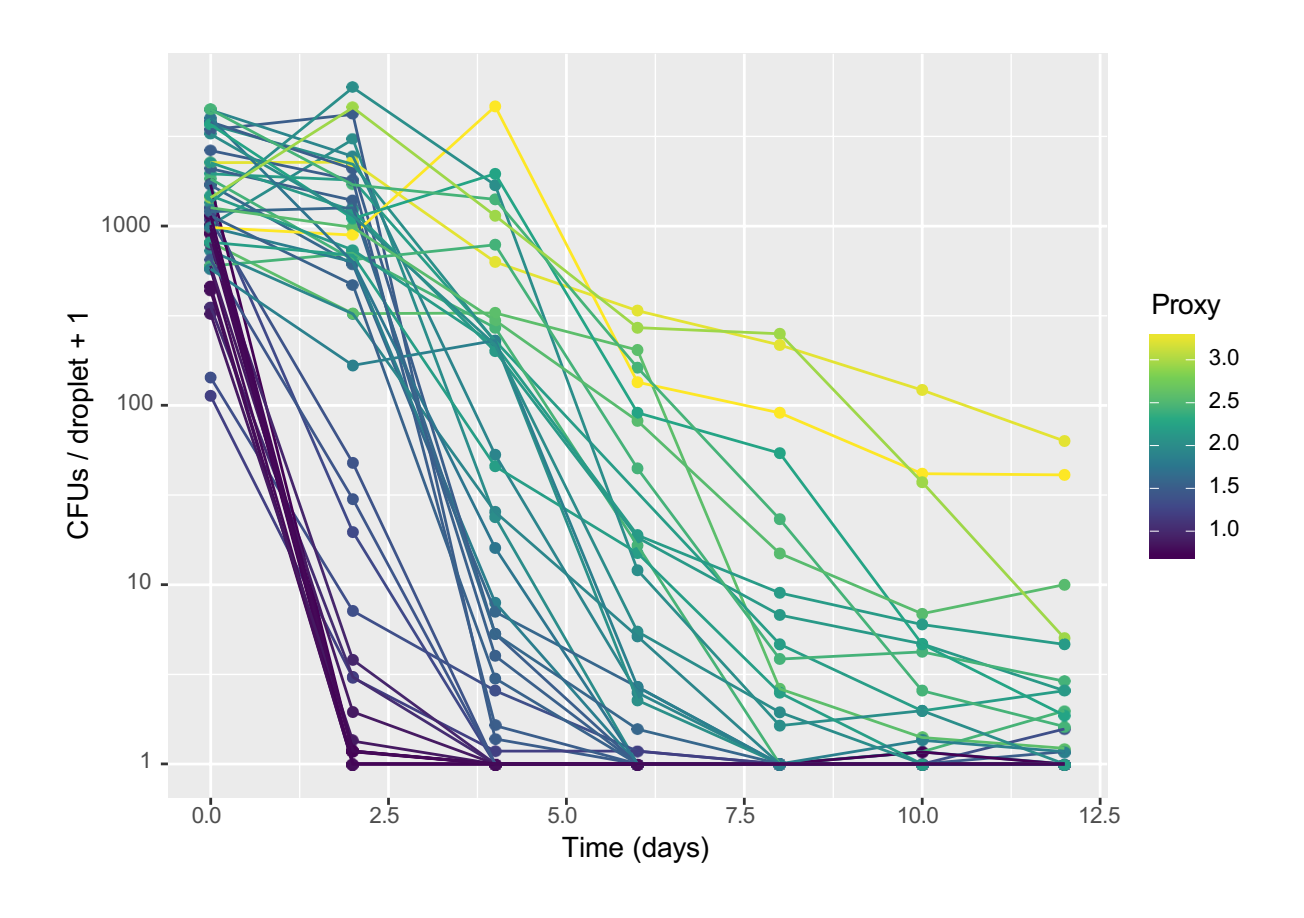
```
#Remove low quality data points
CFUsMLE <- CFUsMLE[CFUsMLE$TotalExclusions<=1,]
```

We can also calculate a proxy for each lifespan curve in order to summarise the lifespan of a culture with a single number. The plotProxy() function can be used to display how the proxy is calculated for a particular sample. For this, a spline is fitted to the data, and the default proxy is calculated as the square root of the amount of time taken for culture viability to decrease to 5%.

```
#Plot proxy calculation for the wt (972 h-)
g1 <- plotProxy(CFUsMLE, "972 h-")
print(g1)
```



Proxies for all samples can be calculated using the calculateProxy() function. We can then add an extra column in CFUsMLE and plot the lifespan curves according to proxy. This is always a recommended step in order to check that the proxy looks sensible.



References

- [1] United Nations. World population ageing 2015 (st/esa/ser. a/390), 2015.
- [2] Teresa Niccoli and Linda Partridge. Ageing as a risk factor for disease. *Current biology*, 22(17):R741–R752, 2012.
- [3] ERWIN Schrödinger. What is life (cambridge university press). *New York*, 1944.
- [4] Koutarou D Kimura, Heidi A Tissenbaum, Yanxia Liu, and Gary Ruvkun. daf-2, an insulin receptor-like gene that regulates longevity and diapause in caenorhabditis elegans. *Science*, 277(5328):942–946, 1997.
- [5] Scott Ogg, Suzanne Paradis, Shoshanna Gottlieb, Garth I Patterson, Linda Lee, Heidi A Tissenbaum, and Gary Ruvkun. The fork head transcription factor daf-16 transduces insulin-like metabolic and longevity signals in c. elegans. *Nature*, 389(6654):994–999, 1997.
- [6] Cynthia Kenyon. A conserved regulatory system for aging. *Cell*, 105(2):165–168, 2001.
- [7] Thomas BL Kirkwood, Martin Feder, Caleb E Finch, Claudio Franceschi, Amiela Globerson, Christian Peter Klingenberg, Kelly LaMarco, Stig Omholt, and Rudi GJ Westendorp. What accounts for the wide variation in life span of genetically identical organisms reared in a constant environment? *Mechanisms of ageing and development*, 126(3):439–443, 2005.

- [8] Gordon J Lithgow, Monica Driscoll, and Patrick Phillips. A long journey to reproducible results. *Nature*, 548(7668):387–388, 2017.
- [9] Mark Lucanic, W Todd Plummer, Esteban Chen, Jailynn Harke, Anna C Foulger, Brian Onken, Anna L Coleman-Hulbert, Kathleen J Dumas, Suzhen Guo, Erik Johnson, et al. Impact of genetic background and experimental reproducibility on identifying chemical compounds with robust longevity effects. *Nature communications*, 8(1):1–13, 2017.
- [10] Sadiya S Khan, Benjamin D Singer, and Douglas E Vaughan. Molecular and physiological manifestations and measurement of aging in humans. *Aging cell*, 16(4):624–633, 2017.
- [11] Thomas BL Kirkwood. Understanding the odd science of aging. *Cell*, 120(4):437–447, 2005.
- [12] Mark P Mattson. Hormesis defined. *Ageing research reviews*, 7(1):1–7, 2008.
- [13] Thomas BL Kirkwood. Systems biology of ageing and longevity. *Philosophical Transactions of the Royal Society B: Biological Sciences*, 366(1561):64–70, 2011.
- [14] Mikhail V Blagosklonny. Answering the ultimate question "what is the proximal cause of aging?". *Aging (Albany NY)*, 4(12):861, 2012.
- [15] Mikhail V Blagosklonny. Aging: Ros or tor. *Cell cycle*, 7(21):3344–3354, 2008.
- [16] Piotr Zimniak. What is the proximal cause of aging? *Frontiers in genetics*, 3:189, 2012.
- [17] Matt Kaeberlein. Lessons on longevity from budding yeast. *Nature*, 464(7288):513–519, 2010.

- [18] Antoine E Roux, Pascal Chartrand, Gerardo Ferbeyre, and Luis A Rokeach. Fission yeast and other yeasts as emergent models to unravel cellular aging in eukaryotes. *Journals of Gerontology Series A: Biomedical Sciences and Medical Sciences*, 65(1):1–8, 2010.
- [19] Antonia Lock, Kim Rutherford, Midori A Harris, Jacqueline Hayles, Stephen G Oliver, Jürg Bähler, and Valerie Wood. Pombase 2018: user-driven reimplementation of the fission yeast database provides rapid and intuitive access to diverse, interconnected information. *Nucleic acids research*, 47(D1):D821–D827, 2019.
- [20] V Wood, R Gwilliam, M-A Rajandream, M Lyne, R Lyne, A Stewart, J Sgouros, N Peat, J Hayles, S Baker, et al. The genome sequence of schizosaccharomyces pombe. *nature*, 415(6874):871–880, 2002.
- [21] Peter Laun, Mark Rinnerthaler, Edith Bogengruber, Gino Heeren, and Michael Breitenbach. Yeast as a model for chronological and reproductive aging—a comparison. *Experimental gerontology*, 41(12):1208–1212, 2006.
- [22] Robert K Mortimer and John R Johnston. Life span of individual yeast cells. *Nature*, 183(4677):1751–1752, 1959.
- [23] Eric C Spivey, Stephen K Jones Jr, James R Rybarski, Fatema A Sai-fuddin, and Ilya J Finkelstein. An aging-independent replicative lifespan in a symmetrically dividing eukaryote. *Elife*, 6:e20340, 2017.
- [24] Miguel Coelho, Aygül Dereli, Anett Haese, Sebastian Kühn, Liliana Malinovska, Morgan E DeSantis, James Shorter, Simon Alberti, Thilo Gross, and Iva M Tolić-Nørrelykke. Fission yeast does not age under favorable conditions, but does so after stress. *Current Biology*, 23(19):1844–1852, 2013.
- [25] Paola Fabrizio and Valter D Longo. The chronological life span of saccharomyces cerevisiae. *Aging cell*, 2(2):73–81, 2003.

- [26] Fumie Masuda, Mahiro Ishii, Ayaka Mori, Lisa Uehara, Mitsuhiro Yanagida, Kojiro Takeda, and Shigeaki Saitoh. Glucose restriction induces transient g2 cell cycle arrest extending cellular chronological lifespan. *Scientific reports*, 6:19629, 2016.
- [27] Theodora Sideri, Charalampos Rallis, Danny A Bitton, Bruno M Lages, Fang Suo, Mar'ıa Rodr'ıguez-López, Li-Lin Du, and Jürg Bähler. Parallel profiling of fission yeast deletion mutants for proliferation and for lifespan during long-term quiescence. *G3: Genes, Genomes, Genetics*, 5(1):145–155, 2015.
- [28] Jordan Gulli, Emily Cook, Eugene Kroll, Adam Rosebrock, Amy Caudy, and Frank Rosenzweig. Diverse conditions support near-zero growth in yeast: Implications for the study of cell lifespan. *Microbial Cell*, 6(9):397, 2019.
- [29] Sarah R Chadwick, Athanasios D Pananos, Sonja E Di Gregorio, Anna E Park, Parnian Etedali-Zadeh, Martin L Duennwald, and Patrick Lajoie. A toolbox for rapid quantitative assessment of chronological lifespan and survival in saccharomyces cerevisiae. *Traffic*, 17(6):689–703, 2016.
- [30] Zachery R Belak, Troy Harkness, and Christopher H Eskiw. A rapid, high-throughput method for determining chronological lifespan in budding yeast. *Journal of Biological Methods*, 5(4), 2018.
- [31] Charalampos Rallis and Jürg Bähler. Cell-based screens and phenomics with fission yeast. *Critical Reviews in Biochemistry and Molecular Biology*, 51(2):86–95, 2016.
- [32] Kenneth L Chen, Matthew M Crane, and Matt Kaeberlein. Microfluidic technologies for yeast replicative lifespan studies. *Mechanisms of ageing and development*, 161:262–269, 2017.
- [33] R Wilson Powers, Matt Kaeberlein, Seth D Caldwell, Brian K Kennedy, and Stanley Fields. Extension of chronological life span in yeast by

- decreased tor pathway signaling. *Genes & development*, 20(2):174–184, 2006.
- [34] Sergio E Campos, J Abraham Avelar-Rivas, Erika Garay, Alejandro Juárez-Reyes, and Alexander DeLuna. Genomewide mechanisms of chronological longevity by dietary restriction in budding yeast. *Aging Cell*, 17(3):e12749, 2018.
- [35] J Abraham Avelar-Rivas, Michelle Mungu'ıa-Figueroa, Alejandro Juárez-Reyes, Erika Garay, Sergio E Campos, Noam Shoresh, and Alexander DeLuna. An optimized competitive-aging method reveals gene-drug interactions underlying the chronological lifespan of saccharomyces cerevisiae. *Frontiers in Genetics*, 11, 2020.
- [36] Benjamin P Barré, Johan Hallin, Jia-Xing Yue, Karl Persson, Ekaterina Mikhalev, Agurtzane Irizar, Sylvester Holt, Dawn Thompson, Mikael Molin, Jonas Warringer, et al. Intragenic repeat expansion in the cell wall protein gene hpf1 controls yeast chronological aging. *Genome research*, 30(5):697–710, 2020.
- [37] Elizabeth A Winzeler, Daniel D Shoemaker, Anna Astromoff, Hong Liang, Keith Anderson, Bruno Andre, Rhonda Bangham, Rocio Benito, Jef D Boeke, Howard Bussey, et al. Functional characterization of the s. cerevisiae genome by gene deletion and parallel analysis. *science*, 285(5429):901–906, 1999.
- [38] Dong-Uk Kim, Jacqueline Hayles, Dongsup Kim, Valerie Wood, Han-Oh Park, Misun Won, Hyang-Sook Yoo, Trevor Duhig, Miyoung Nam, Georgia Palmer, et al. Analysis of a genome-wide set of gene deletions in the fission yeast schizosaccharomyces pombe. *Nature biotechnology*, 28(6):617–623, 2010.

- [39] Sarah E Pierce, Ron W Davis, Corey Nislow, and Guri Giaever. Genome-wide analysis of barcoded saccharomyces cerevisiae gene-deletion mutants in pooled cultures. *Nature protocols*, 2(11):2958–2974, 2007.
- [40] Andrew M Smith, Lawrence E Heisler, Joseph Mellor, Fiona Kaper, Michael J Thompson, Mark Chee, Frederick P Roth, Guri Giaever, and Corey Nislow. Quantitative phenotyping via deep barcode sequencing. *Genome research*, 19(10):1836–1842, 2009.
- [41] Tian Xu Han, Xing-Ya Xu, Mei-Jun Zhang, Xu Peng, and Li-Lin Du. Global fitness profiling of fission yeast deletion strains by barcode sequencing. *Genome biology*, 11(6):1–13, 2010.
- [42] Mirela Matecic, Daniel L Smith Jr, Xuewen Pan, Nazif Maqani, Stefan Bekiranov, Jef D Boeke, and Jeffrey S Smith. A microarray-based genetic screen for yeast chronological aging factors. *PLoS Genet*, 6(4):e1000921, 2010.
- [43] Roy Z Moger-Reischer and Jay T Lennon. Microbial ageing and longevity. *Nature Reviews Microbiology*, 17(11):679–690, 2019.
- [44] Audrey Menegaz Proenca, Camilla Ulla Rang, Andrew Qiu, Chao Shi, and Lin Chao. Cell aging preserves cellular immortality in the presence of lethal levels of damage. *PLoS biology*, 17(5):e3000266, 2019.
- [45] Cynthia J Kenyon. The genetics of ageing. *Nature*, 464(7288):504–512, 2010.
- [46] João Pedro de Magalhães and Robi Tacutu. Integrative genomics of aging. In *Handbook of the Biology of Aging*, pages 263–285. Elsevier, 2016.
- [47] Daniel L Smith Jr, Crystal H Maharrey, Christopher R Carey, Richard A White, and John L Hartman IV. Gene-nutrient interaction markedly

- influences yeast chronological lifespan. *Experimental gerontology*, 86:113–123, 2016.
- [48] Belém Sampaio-Marques, William C Burhans, and Paula Ludovico. Yeast at the forefront of research on ageing and age-related diseases. *Yeasts in Biotechnology and Human Health*, pages 217–242, 2019.
- [49] Hokuto Ohtsuka, Takafumi Shimasaki, and Hirofumi Aiba. Genes affecting the extension of chronological lifespan in schizosaccharomyces pombe (fission yeast). *Molecular Microbiology*, 2020.
- [50] Mevlüt Arslan, Burcu Turanli-Yildiz, Bahtiyar Yilmaz, Nazli Kocaefe, and Zeynep Petek Cakar. An improved semi-quantitative spot assay to analyse chronological lifespan in yeast. *Romanian Biotechnological Letters*, 23(3):13551, 2018.
- [51] Omar Wagih and Leopold Parts. Gitter: a robust and accurate method for quantification of colony sizes from plate images. *G3: Genes, Genomes, Genetics*, 4(3):547–552, 2014.
- [52] Nobuyuki Otsu. A threshold selection method from gray-level histograms. *IEEE transactions on systems, man, and cybernetics,* 9(1):62–66, 1979.
- [53] Richard P. Brent. An algorithm with guaranteed convergence for finding a zero of a function. *The Computer Journal*, 14(4):422–425, 1971.
- [54] Chris Fraley and Adrian E Raftery. How many clusters? which clustering method? answers via model-based cluster analysis. *The computer journal*, 41(8):578–588, 1998.
- [55] Art B Owen. Empirical likelihood ratio confidence intervals for a single functional. *Biometrika*, 75(2):237–249, 1988.
- [56] Charalampos Rallis, StJohn Townsend, and Jürg Bähler. Genetic interactions and functional analyses of the fission yeast gsk3 and amk2 single

- and double mutants defective in torc1-dependent processes. *Scientific reports*, 7(1):1–11, 2017.
- [57] Jürg Bähler, Jian-Qiu Wu, Mark S Longtine, Nirav G Shah, Amos Mckenzie III, Alexander B Steever, Achim Wach, Peter Philippsen, and John R Pringle. Heterologous modules for efficient and versatile pcr-based gene targeting in schizosaccharomyces pombe. *Yeast*, 14(10):943–951, 1998.
- [58] Charalampos Rallis, Sandra Codlin, and Jürg Bähler. Torc 1 signaling inhibition by rapamycin and caffeine affect lifespan, global gene expression, and cell proliferation of fission yeast. *Aging cell*, 12(4):563–573, 2013.
- [59] Catalina Romila, StJohn Townsend, Michal Malecki, Stephan Kamrad, Maria Rodriguez-Lopez, Olivia Hillson, Cristina Cotobal, Markus Ralser, and Jurg Bahler. Barcode sequencing and a high-throughput assay for chronological lifespan uncover ageing-associated genes in fission yeast. *bioRxiv*, 2021.
- [60] Pin Ng and Martin Maechler. A fast and efficient implementation of qualitatively constrained quantile smoothing splines. *Statistical Modelling*, 7(4):315–328, 2007.
- [61] Steven E Finkel. Long-term survival during stationary phase: evolution and the gasp phenotype. *Nature Reviews Microbiology*, 4(2):113–120, 2006.
- [62] Rostyslav Makarenko, Claire Denis, Stefania Francesconi, Serge Gangloff, and Beno^it Arcangioli. Nitrogen starvation reveals the mitotic potential of mutants in the s/mapk pathways. *Nature communications*, 11(1):1–13, 2020.
- [63] Alice Zuin, Mercè Carmona, Isabel Morales-Ivorra, Natalia Gabrielli, Ana P Vivancos, José Ayté, and Elena Hidalgo. Lifespan extension by

120

- calorie restriction relies on the sty1 map kinase stress pathway. *The EMBO journal*, 29(5):981–991, 2010.
- [64] Charalampos Rallis, Luis Lopez-Maury, Teodora Georgescu, Vera Pancaldi, and Jürg Bähler. Systematic screen for mutants resistant to torc1 inhibition in fission yeast reveals genes involved in cellular ageing and growth. *Biology open*, 3(2):161–171, 2014.
- [65] Kazuaki Takuma, Hokuto Ohtsuka, Kenko Azuma, Hiroshi Murakami, and Hirofumi Aiba. The fission yeast php2 mutant displays a length-ened chronological lifespan. *Bioscience, biotechnology, and biochemistry*, 77(7):1548–1555, 2013.
- [66] Susan L Forsburg and Leonard Guarente. Communication between mitochondria and the nucleus in regulation of cytochrome genes in the yeast saccharomyces cerevisiae. *Annual review of cell biology*, 5(1):153–180, 1989.
- [67] Antonin Thiébaut, Thierry Delaveau, Médine Benchouaia, Julia Boeri, Mathilde Garcia, Gaëlle Lelandais, and Frédéric Devaux. The ccaatbinding complex controls respiratory gene expression and iron homeostasis in candida glabrata. *Scientific reports*, 7(1):1–10, 2017.
- [68] Alexander A Goldberg, Simon D Bourque, Pavlo Kyryakov, Christopher Gregg, Tatiana Boukh-Viner, Adam Beach, Michelle T Burstein, Gayane Machkalyan, Vincent Richard, Sonia Rampersad, et al. Effect of calorie restriction on the metabolic history of chronologically aging yeast. *Experimental gerontology*, 44(9):555–571, 2009.
- [69] Alejandro Ocampo, Jingjing Liu, Elizabeth A Schroeder, Gerald S Shadel, and Antoni Barrientos. Mitochondrial respiratory thresholds regulate yeast chronological life span and its extension by caloric restriction. *Cell metabolism*, 16(1):55–67, 2012.

- [70] Michal Malecki, Stephan Kamrad, Markus Ralser, and Jürg Bähler. Mitochondrial respiration is required to provide amino acids during fermentative proliferation of fission yeast. *EMBO reports*, 21(11):e50845, 2020.
- [71] John P Aris, Ashley L Alvers, Roy A Ferraiuolo, Laura K Fishwick, Amanda Hanvivatpong, Doreen Hu, Christine Kirlew, Michael T Leonard, Kyle J Losin, Michelle Marraffini, et al. Autophagy and leucine promote chronological longevity and respiration proficiency during calorie restriction in yeast. *Experimental gerontology*, 48(10):1107–1119, 2013.
- [72] Charles Boone. Yeast systems biology: our best shot at modeling a cell. *Genetics*, 198(2):435–437, 2014.
- [73] Ben Langmead and Steven L Salzberg. Fast gapped-read alignment with bowtie 2. *Nature methods*, 9(4):357, 2012.
- [74] Aaron R Quinlan and Ira M Hall. Bedtools: a flexible suite of utilities for comparing genomic features. *Bioinformatics*, 26(6):841–842, 2010.
- [75] Shervi Lie, Peter Banks, Conor Lawless, David Lydall, and Janni Petersen. The contribution of non-essential schizosaccharomyces pombe genes to fitness in response to altered nutrient supply and target of rapamycin activity. *Open biology*, 8(5):180015, 2018.
- [76] Mark D Robinson, Davis J McCarthy, and Gordon K Smyth. edger: a bioconductor package for differential expression analysis of digital gene expression data. *Bioinformatics*, 26(1):139–140, 2010.
- [77] Yevhen Akimov, Daria Bulanova, Sanna Timonen, Krister Wennerberg, and Tero Aittokallio. Improved detection of differentially represented dna barcodes for high-throughput clonal phenomics. *Molecular systems biology*, 16(3):e9195, 2020.

- [78] Swati Parekh, Christoph Ziegenhain, Beate Vieth, Wolfgang Enard, and Ines Hellmann. The impact of amplification on differential expression analyses by rna-seq. *Scientific reports*, 6(1):1–11, 2016.
- [79] Claude Vezina, Alicia Kudelski, and SN Sehgal. Rapamycin (ay-22, 989), a new antifungal antibiotic i. taxonomy of the producing streptomycete and isolation of the active principle. *The Journal of antibiotics*, 28(10):721–726, 1975.
- [80] Ramasamy Selvarani, Sabira Mohammed, and Arlan Richardson. Effect of rapamycin on aging and age-related diseases—past and future. *GeroScience*, pages 1–24, 2020.
- [81] Joseph Heitman, N Rao Movva, and Michael N Hall. Targets for cell cycle arrest by the immunosuppressant rapamycin in yeast. *Science*, 253(5022):905–909, 1991.
- [82] Eric J Brown, Mark W Albers, Tae Bum Shin, Curtis T Keith, William S Lane, Stuart L Schreiber, et al. A mammalian protein targeted by g1-arresting rapamycin–receptor complex. *Nature*, 369(6483):756–758, 1994.
- [83] David M Sabatini, Hediye Erdjument-Bromage, Mary Lui, Paul Tempst, and Solomon H Snyder. Raft1: a mammalian protein that binds to fkbp12 in a rapamycin-dependent fashion and is homologous to yeast tors. *Cell*, 78(1):35–43, 1994.
- [84] M Isabel Chiu, Hillary Katz, and Vivian Berlin. Rapt1, a mammalian homolog of yeast tor, interacts with the fkbp12/rapamycin complex. *Proceedings of the National Academy of Sciences*, 91(26):12574–12578, 1994.
- [85] Matt Kaeberlein, R Wilson Powers, Kristan K Steffen, Eric A Westman, Di Hu, Nick Dang, Emily O Kerr, Kathryn T Kirkland, Stanley Fields, and Brian K Kennedy. Regulation of yeast replicative life span by tor and sch9 in response to nutrients. *Science*, 310(5751):1193–1196, 2005.

- [86] Tibor Vellai, Krisztina Takacs-Vellai, Yue Zhang, Attila L Kovacs, László Orosz, and Fritz Müller. Influence of tor kinase on lifespan in c. elegans. *Nature*, 426(6967):620–620, 2003.
- [87] Pankaj Kapahi, Brian M Zid, Tony Harper, Daniel Koslover, Viveca Sapin, and Seymour Benzer. Regulation of lifespan in drosophila by modulation of genes in the tor signaling pathway. *Current Biology*, 14(10):885–890, 2004.
- [88] David E Harrison, Randy Strong, Zelton Dave Sharp, James F Nelson, Clinton M Astle, Kevin Flurkey, Nancy L Nadon, J Erby Wilkinson, Krystyna Frenkel, Christy S Carter, et al. Rapamycin fed late in life extends lifespan in genetically heterogeneous mice. *Nature*, 460(7253):392– 395, 2009.
- [89] Joan B Mannick, Melody Morris, Hans-Ulrich P Hockey, Guglielmo Roma, Martin Beibel, Kenneth Kulmatycki, Mollie Watkins, Tea Shavlakadze, Weihua Zhou, Dean Quinn, et al. Torc1 inhibition enhances immune function and reduces infections in the elderly. *Science translational medicine*, 10(449), 2018.
- [90] Stephan Wullschleger, Robbie Loewith, and Michael N Hall. Tor signaling in growth and metabolism. *Cell*, 124(3):471–484, 2006.
- [91] Mathieu Laplante and David M Sabatini. mtor signaling in growth control and disease. *Cell*, 149(2):274–293, 2012.
- [92] Brian K Kennedy and Dudley W Lamming. The mechanistic target of rapamycin: the grand conductor of metabolism and aging. *Cell metabolism*, 23(6):990–1003, 2016.
- [93] Asier González and Michael N Hall. Nutrient sensing and tor signaling in yeast and mammals. *The EMBO journal*, 36(4):397–408, 2017.

- [94] Yoko Otsubo and Masayuki Yamamato. Tor signaling in fission yeast. *Critical reviews in biochemistry and molecular biology,* 43(4):277–283, 2008.
- [95] Robbie Loewith, Estela Jacinto, Stephan Wullschleger, Anja Lorberg, José L Crespo, Débora Bonenfant, Wolfgang Oppliger, Paul Jenoe, and Michael N Hall. Two tor complexes, only one of which is rapamycin sensitive, have distinct roles in cell growth control. *Molecular cell*, 10(3):457–468, 2002.
- [96] Christl Gaubitz, Taiana M Oliveira, Manoel Prouteau, Alexander Leitner, Manikandan Karuppasamy, Georgia Konstantinidou, Delphine Rispal, Sandra Eltschinger, Graham C Robinson, Stéphane Thore, et al. Molecular basis of the rapamycin insensitivity of target of rapamycin complex 2. *Molecular cell*, 58(6):977–988, 2015.
- [97] Margot Riggi, Beata Kusmider, and Robbie Loewith. The flipside of the tor coin–torc2 and plasma membrane homeostasis at a glance. *Journal of cell science*, 133(9), 2020.
- [98] Françoise M Roelants, Kristin L Leskoske, Maria Nieves Martinez Marshall, Melissa N Locke, and Jeremy Thorner. The torc2-dependent signaling network in the yeast saccharomyces cerevisiae. *Biomolecules*, 7(3):66, 2017.
- [99] Christl Gaubitz, Manoel Prouteau, Beata Kusmider, and Robbie Loewith. Torc2 structure and function. *Trends in biochemical sciences*, 41(6):532–545, 2016.
- [100] Suam Gonzalez and Charalampos Rallis. The tor signaling pathway in spatial and temporal control of cell size and growth. *Frontiers in cell and developmental biology*, 5:61, 2017.
- [101] Riko Hatakeyama, Marie-Pierre Péli-Gulli, Zehan Hu, Malika Jaquenoud, Guillermo Miguel Garcia Osuna, Alessandro Sardu, Jörn Dengjel,

- and Claudio De Virgilio. Spatially distinct pools of torc1 balance protein homeostasis. *Molecular cell*, 73(2):325–338, 2019.
- [102] Andreas Aufschnaiter and Sabrina Büttner. The vacuolar shapes of ageing: from function to morphology. *Biochimica et Biophysica Acta* (*BBA*)-*Molecular Cell Research*, 1866(5):957–970, 2019.
- [103] Chun-Yan Lim and Roberto Zoncu. The lysosome as a command-and-control center for cellular metabolism. *Journal of Cell Biology*, 214(6):653–664, 2016.
- [104] Yoko Otsubo, Akio Nakashima, Masayuki Yamamoto, and Akira Yamashita. Torc1-dependent phosphorylation targets in fission yeast. *Biomolecules*, 7(3):50, 2017.
- [105] KATSUHIKO Kitamoto, KIYOSHI Yoshizawa, YOSHINORI Ohsumi, and YASUHIRO Anraku. Dynamic aspects of vacuolar and cytosolic amino acid pools of saccharomyces cerevisiae. *Journal of bacteriology*, 170(6):2683–2686, 1988.
- [106] David M Hollenstein and Claudine Kraft. Autophagosomes are formed at a distinct cellular structure. *Current opinion in cell biology*, 65:50–57, 2020.
- [107] Xin Wen and Daniel J Klionsky. An overview of macroautophagy in yeast. *Journal of molecular biology*, 428(9):1681–1699, 2016.
- [108] Frank Madeo, Andreas Zimmermann, Maria Chiara Maiuri, Guido Kroemer, et al. Essential role for autophagy in life span extension. *The Journal of clinical investigation*, 125(1):85–93, 2015.
- [109] Kurt A Escobar, Nathan H Cole, Christine M Mermier, and Trisha A VanDusseldorp. Autophagy and aging: Maintaining the proteome through exercise and caloric restriction. *Aging cell*, 18(1):e12876, 2019.

References 126

- [110] Christian Ungermann and Fulvio Reggiori. Atg9 proteins, not so different after all. *Autophagy*, 14(8):1456–1459, 2018.
- [111] Martin Müller, Oliver Schmidt, Mihaela Angelova, Klaus Faserl, Sabine Weys, Leopold Kremser, Thaddäus Pfaffenwimmer, Thomas Dalik, Claudine Kraft, Zlatko Trajanoski, et al. The coordinated action of the mvb pathway and autophagy ensures cell survival during starvation. *Elife*, 4:e07736, 2015.
- [112] Jiajie Zhang, Kassian Kobert, Tomáš Flouri, and Alexandros Stamatakis. Pear: a fast and accurate illumina paired-end read merger. *Bioinformatics*, 30(5):614–620, 2014.
- [113] Brian Bushnell. Bbmap short-read aligner, and other bioinformatics tools, 2020.
- [114] Uku Raudvere, Liis Kolberg, Ivan Kuzmin, Tambet Arak, Priit Adler, Hedi Peterson, and Jaak Vilo. g: Profiler: a web server for functional enrichment analysis and conversions of gene lists (2019 update). *Nucleic acids research*, 47(W1):W191–W198, 2019.
- [115] Hayashi Yamamoto, Yuko Fujioka, Sho W Suzuki, Daisuke Noshiro, Hironori Suzuki, Chika Kondo-Kakuta, Yayoi Kimura, Hisashi Hirano, Toshio Ando, Nobuo N Noda, et al. The intrinsically disordered protein atg13 mediates supramolecular assembly of autophagy initiation complexes. *Developmental cell*, 38(1):86–99, 2016.
- [116] Tamiza Nanji, Xu Liu, Leon H Chew, Franco K Li, Maitree Biswas, Zhong-Qiu Yu, Shan Lu, Meng-Qiu Dong, Li-Lin Du, Daniel J Klionsky, et al. Conserved and unique features of the fission yeast core atg1 complex. *Autophagy*, 13(12):2018–2027, 2017.
- [117] Ben Zhou, Johannes Kreuzer, Caroline Kumsta, Lianfeng Wu, Kimberli J Kamer, Lucydalila Cedillo, Yuyao Zhang, Sainan Li, Michael C Kacergis,

- Christopher M Webster, et al. Mitochondrial permeability uncouples elevated autophagy and lifespan extension. *Cell*, 177(2):299–314, 2019.
- [118] Michelle E Maxson and Sergio Grinstein. The vacuolar-type h+-atpase at a glance–more than a proton pump. *Journal of cell science*, 127(23):4987–4993, 2014.
- [119] Jae Hong Seol, Anna Shevchenko, Andrej Shevchenko, and Raymond J Deshaies. Skp1 forms multiple protein complexes, including rave, a regulator of v-atpase assembly. *Nature cell biology*, 3(4):384–391, 2001.
- [120] Anne M Smardon, Maureen Tarsio, and Patricia M Kane. The rave complex is essential for stable assembly of the yeast v-atpase. *Journal of Biological Chemistry*, 277(16):13831–13839, 2002.
- [121] Dalibor Mijaljica, Mark Prescott, and Rodney J Devenish. V-atpase engagement in autophagic processes. *Autophagy*, 7(6):666–668, 2011.
- [122] Adam L Hughes and Daniel E Gottschling. An early age increase in vacuolar ph limits mitochondrial function and lifespan in yeast. *Nature*, 492(7428):261–265, 2012.
- [123] Henning J kleine Balderhaar and Christian Ungermann. Corvet and hops tethering complexes-coordinators of endosome and lysosome fusion. *Journal of cell science*, 126(6):1307–1316, 2013.
- [124] Gregory Segala, Marcela A Bennesch, Nastaran Mohammadi Ghahhari, Deo Prakash Pandey, Pablo C Echeverria, François Karch, Robert K Maeda, and Didier Picard. Vps11 and vps18 of vps-c membrane traffic complexes are e3 ubiquitin ligases and fine-tune signalling. *Nature communications*, 10(1):1–15, 2019.
- [125] Jinglan Zhang, Véronik Lachance, Adam Schaffner, Xianting Li, Anastasia Fedick, Lauren E Kaye, Jun Liao, Jill Rosenfeld, Naomi Yachelevich,

- Mary-Lynn Chu, et al. A founder mutation in vps11 causes an autosomal recessive leukoencephalopathy linked to autophagic defects. *PLoS genetics*, 12(4):e1005848, 2016.
- [126] William M Henne, Nicholas J Buchkovich, and Scott D Emr. The escrt pathway. *Developmental cell*, 21(1):77–91, 2011.
- [127] Robert C Piper and David J Katzmann. Biogenesis and function of multivesicular bodies. *Annu. Rev. Cell Dev. Biol.*, 23:519–547, 2007.
- [128] Tor Erik Rusten, Thomas Vaccari, Karine Lindmo, Lina MW Rodahl, Ioannis P Nezis, Catherine Sem-Jacobsen, Franz Wendler, Jean-Paul Vincent, Andreas Brech, David Bilder, et al. Escrts and fab1 regulate distinct steps of autophagy. *Current biology*, 17(20):1817–1825, 2007.
- [129] Tor Erik Rusten and Harald Stenmark. How do escrt proteins control autophagy? *Journal of cell science*, 122(13):2179–2183, 2009.
- [130] Matthew NJ Seaman, J Michael McCaffery, and Scott D Emr. A membrane coat complex essential for endosome-to-golgi retrograde transport in yeast. *The Journal of cell biology*, 142(3):665–681, 1998.
- [131] Matthew NJ Seaman. The retromer complex–endosomal protein recycling and beyond. *Journal of cell science*, 125(20):4693–4702, 2012.
- [132] Matthew NJ Seaman. Cargo-selective endosomal sorting for retrieval to the golgi requires retromer. *Journal of cell biology*, 165(1):111–122, 2004.
- [133] Eric G Marcusson, Bruce F Horazdovsky, Joan Lin Cereghino, Editte Gharakhanian, and Scott D Emr. The sorting receptor for yeast vacuolar carboxypeptidase y is encoded by the vps10 gene. *Cell*, 77(4):579–586, 1994.
- [134] Antony A Cooper and Tom H Stevens. Vps10p cycles between the lategolgi and prevacuolar compartments in its function as the sorting recep-

- tor for multiple yeast vacuolar hydrolases. *The Journal of cell biology*, 133(3):529–541, 1996.
- [135] Tamás Maruzs, Péter Lőrincz, Zsuzsanna Szatmári, Szilvia Széplaki, Zoltán Sándor, Zsolt Lakatos, Gina Puska, Gábor Juhász, and Miklós Sass. Retromer ensures the degradation of autophagic cargo by maintaining lysosome function in drosophila. *Traffic*, 16(10):1088–1107, 2015.
- [136] Wenhui Zheng, Jie Zhou, Yunlong He, Qiurong Xie, Ahai Chen, Huawei Zheng, Lei Shi, Xu Zhao, Chengkang Zhang, Qingping Huang, et al. Retromer is essential for autophagy-dependent plant infection by the rice blast fungus. *PLoS genetics*, 11(12):e1005704, 2015.
- [137] Scott A Small, Kelly Kent, Aimee Pierce, Conrad Leung, Min Suk Kang, Hirokazu Okada, Lawrence Honig, Jean-Paul Vonsattel, and Tae-Wan Kim. Model-guided microarray implicates the retromer complex in alzheimer's disease. *Annals of Neurology: Official Journal of the American Neurological Association and the Child Neurology Society*, 58(6):909–919, 2005.
- [138] Yoshihiko Kuchitsu and Mitsunori Fukuda. Revisiting rab7 functions in mammalian autophagy: Rab7 knockout studies. *Cells*, 7(11):215, 2018.
- [139] Takayoshi Kirisako, Misuzu Baba, Naotada Ishihara, Kouichi Miyazawa, Mariko Ohsumi, Tamotsu Yoshimori, Takeshi Noda, and Yoshinori Ohsumi. Formation process of autophagosome is traced with apg8/aut7p in yeast. *The Journal of cell biology*, 147(2):435–446, 1999.
- [140] Tomotake Kanki, KE Wang, Misuzu Baba, Clinton R Bartholomew, Melinda A Lynch-Day, Zhou Du, Jiefei Geng, Kai Mao, Zhifen Yang, Wei-Lien Yen, et al. A genomic screen for yeast mutants defective in selective mitochondria autophagy. *Molecular biology of the cell*, 20(22):4730–4738, 2009.

- [141] Levent Bas, Daniel Papinski, Mariya Licheva, Raffaela Torggler, Sabrina Rohringer, Martina Schuschnig, and Claudine Kraft. Reconstitution reveals ykt6 as the autophagosomal snare in autophagosome–vacuole fusion. *Journal of Cell Biology*, 217(10):3656–3669, 2018.
- [142] Henning J kleine Balderhaar, Henning Arlt, Clemens Ostrowicz, Cornelia Bröcker, Frederik Sündermann, Roland Brandt, Markus Babst, and Christian Ungermann. The rab gtpase ypt7 is linked to retromermediated receptor recycling and fusion at the yeast late endosome. *Journal of cell science*, 123(23):4085–4094, 2010.
- [143] Michael Mülleder, Enrica Calvani, Mohammad Tauqeer Alam, Richard Kangda Wang, Florian Eckerstorfer, Aleksej Zelezniak, and Markus Ralser. Functional metabolomics describes the yeast biosynthetic regulome. *Cell*, 167(2):553–565, 2016.
- [144] Minoo Razi, Edmond YW Chan, and Sharon A Tooze. Early endosomes and endosomal coatomer are required for autophagy. *Journal of Cell Biology*, 185(2):305–321, 2009.
- [145] CM Fader and MI Colombo. Autophagy and multivesicular bodies: two closely related partners. *Cell Death & Differentiation*, 16(1):70–78, 2009.
- [146] Sharon A Tooze, Adi Abada, and Zvulun Elazar. Endocytosis and autophagy: exploitation or cooperation? *Cold Spring Harbor perspectives in biology*, 6(5):a018358, 2014.
- [147] Yan G Zhao and Hong Zhang. Autophagosome maturation: an epic journey from the er to lysosomes. *Journal of Cell Biology*, 218(3):757–770, 2019.
- [148] Åsa B Birgisdottir and Terje Johansen. Autophagy and endocytosis—interconnections and interdependencies. *Journal of cell science*, 133(10), 2020.

- [149] Edward J Calabrese and Linda A Baldwin. U-shaped dose-responses in biology, toxicology, and public health. *Annual review of public health*, 22(1):15–33, 2001.
- [150] Edward J Calabrese and Linda A Baldwin. Reevaluation of the fundamental dose–response relationship: A new database suggests that the u-shaped, rather than the sigmoidal, curve predominates. *BioScience*, 49(9):725–732, 1999.
- [151] Qiang Zhang, Jingbo Pi, Courtney G Woods, Annie M Jarabek, Harvey J Clewell III, and Melvin E Andersen. Hormesis and adaptive cellular control systems. *Dose-Response*, 6(2):dose–response, 2008.
- [152] Qiang Zhang and Melvin E Andersen. Dose response relationship in anti-stress gene regulatory networks. *PLoS Comput Biol*, 3(3):e24, 2007.
- [153] Shusaku T Shibutani and Tamotsu Yoshimori. A current perspective of autophagosome biogenesis. *Cell research*, 24(1):58–68, 2014.
- [154] Nadia Jaber and Wei-Xing Zong. Class iii pi3k vps34: essential roles in autophagy, endocytosis, and heart and liver function. *Annals of the New York Academy of Sciences*, 1280:48, 2013.
- [155] Xinlei Yu, Yun Chau Long, and Han-Ming Shen. Differential regulatory functions of three classes of phosphatidylinositol and phosphoinositide 3-kinases in autophagy. *Autophagy*, 11(10):1711–1728, 2015.
- [156] Steve Jean and Amy A Kiger. Classes of phosphoinositide 3-kinases at a glance. *Journal of cell science*, 127(5):923–928, 2014.
- [157] Fei Xu, Lixin Na, Yanfei Li, and Linjun Chen. Roles of the pi3k/akt/mtor signalling pathways in neurodegenerative diseases and tumours. *Cell & bioscience*, 10:1–12, 2020.
- [158] Isabel Rodr'ıguez-Escudero, Francoise M Roelants, Jeremy Thorner, César Nombela, Mar'ıa Molina, and V'ıctor J Cid. Reconstitution of

- the mammalian pi3k/pten/akt pathway in yeast. *Biochemical Journal*, 390(2):613–623, 2005.
- [159] Julia Mar'ıa Coronas-Serna, Marta Valenti, Elba Del Val, Teresa Fernández-Acero, Isabel Rodr'ıguez-Escudero, Janire Mingo, Sandra Luna, Leire Torices, Rafael Pulido, Mar'ıa Molina, et al. Modeling human disease in yeast: recreating the pi3k-pten-akt signaling pathway in saccharomyces cerevisiae. *International Microbiology*, 23(1):75–87, 2020.
- [160] Keisuke Obara, Takayuki Sekito, and Yoshinori Ohsumi. Assortment of phosphatidylinositol 3-kinase complexes—atg14p directs association of complex i to the pre-autophagosomal structure in saccharomyces cerevisiae. *Molecular biology of the cell*, 17(4):1527–1539, 2006.
- [161] Zhong-Qiu Yu, Ling-Ling Sun, Zhao-Di Jiang, Xiao-Man Liu, Dan Zhao, Hai-Tao Wang, Wan-Zhong He, Meng-Qiu Dong, and Li-Lin Du. Atg38-atg8 interaction in fission yeast establishes a positive feedback loop to promote autophagy. *Autophagy*, 16(11):2036–2051, 2020.
- [162] Hai-Xin Yuan, Ryan C Russell, and Kun-Liang Guan. Regulation of pik3c3/vps34 complexes by mtor in nutrient stress-induced autophagy. *Autophagy*, 9(12):1983–1995, 2013.
- [163] Fen Liu, Weiming Hu, and Richard D Vierstra. The vacuolar protein sorting-38 subunit of the arabidopsis phosphatidylinositol-3-kinase complex plays critical roles in autophagy, endosome sorting, and gravitropism. *Frontiers in plant science*, 9:781, 2018.
- [164] Patricie Burda, Steven M Padilla, Srimonti Sarkar, and Scott D Emr. Retromer function in endosome-to-golgi retrograde transport is regulated by the yeast vps34 ptdins 3-kinase. *Journal of cell science*, 115(20):3889–3900, 2002.

- [165] Aamir S Mukadam and Matthew NJ Seaman. Retromer-mediated endosomal protein sorting: the role of unstructured domains. *FEBS letters*, 589(19):2620–2626, 2015.
- [166] Han Nim Lee, Xavier Zarza, Jeong Hun Kim, Min Ji Yoon, Sang-Hoon Kim, Jae-Hoon Lee, Nadine Paris, Teun Munnik, Marisa S Otegui, and Taijoon Chung. Vacuolar trafficking protein vps38 is dispensable for autophagy. *Plant physiology*, 176(2):1559–1572, 2018.
- [167] Peter V Schu, Kaoru Takegawa, Michael J Fry, Jeffrey H Stack, Michael D Waterfield, and Scott D Emr. Phosphatidylinositol 3-kinase encoded by yeast vps34 gene essential for protein sorting. *Science*, 260(5104):88–91, 1993.
- [168] Dave Bridges, Kaleigh Fisher, Sergey N Zolov, Tingting Xiong, Ken Inoki, Lois S Weisman, and Alan R Saltiel. Rab5 proteins regulate activation and localization of target of rapamycin complex 1. *Journal of Biological Chemistry*, 287(25):20913–20921, 2012.
- [169] Natalia V Varlakhanova, Michael J Mihalevic, Kara A Bernstein, and Marijn GJ Ford. Pib2 and the ego complex are both required for activation of torc1. *Journal of cell science*, 130(22):3878–3890, 2017.
- [170] Hirofumi Ukai, Yasuhiro Araki, Shintaro Kira, Yu Oikawa, Alexander I May, and Takeshi Noda. Gtr/ego-independent torc1 activation is achieved through a glutamine-sensitive interaction with pib2 on the vacuolar membrane. *PLoS genetics*, 14(4):e1007334, 2018.
- [171] Herbert M Sauro. Control and regulation of pathways via negative feedback. *Journal of The Royal Society Interface*, 14(127):20160848, 2017.
- [172] Alexander Y Mitrophanov and Eduardo A Groisman. Positive feedback in cellular control systems. *Bioessays*, 30(6):542–555, 2008.

- [173] Joëlle Morvan, Johan-Owen de Craene, Bruno Rinaldi, Vanessa Addis, Cédric Misslin, and Sylvie Friant. Btn3 regulates the endosomal sorting function of the yeast ent3 epsin, an adaptor for snare proteins. *Journal of cell science*, 128(4):706–716, 2015.
- [174] Hai Lan Piao, Iara MP Machado, and Gregory S Payne. Npfxd-mediated endocytosis is required for polarity and function of a yeast cell wall stress sensor. *Molecular biology of the cell*, 18(1):57–65, 2007.
- [175] Mouhamed Alsaqati, Rhian S Thomas, and Emma J Kidd. Proteins involved in endocytosis are upregulated by ageing in the normal human brain: Implications for the development of alzheimer's disease. *The Journals of Gerontology: Series A*, 73(3):289–298, 2018.
- [176] Claire E Richardson, Callista Yee, and Kang Shen. A hormone receptor pathway cell-autonomously delays neuron morphological aging by suppressing endocytosis. *PLoS biology*, 17(10):e3000452, 2019.
- [177] Michaela Conrad, Joep Schothorst, Harish Nag Kankipati, Griet Van Zeebroeck, Marta Rubio-Texeira, and Johan M Thevelein. Nutrient sensing and signaling in the yeast saccharomyces cerevisiae. *FEMS microbiology reviews*, 38(2):254–299, 2014.
- [178] CS Hoffman. Glucose sensing via the protein kinase a pathway in schizosaccharomyces pombe. *Biochemical Society Transactions*, 33(1):257–260, 2005.
- [179] Antoine E Roux, Alexandre Leroux, Manal A Alaamery, Charles S Hoffman, Pascal Chartrand, Gerardo Ferbeyre, and Luis A Rokeach. Proaging effects of glucose signaling through a g protein-coupled glucose receptor in fission yeast. *PLoS Genet*, 5(3):e1000408, 2009.
- [180] Joseph Kunkel, Xiangxia Luo, and Andrew P Capaldi. Integrated torc1 and pka signaling control the temporal activation of glucose-induced gene expression in yeast. *Nature communications*, 10(1):1–11, 2019.

- [181] Joseph S Stephan, Yuh-Ying Yeh, Vidhya Ramachandran, Stephen J Deminoff, and Paul K Herman. The tor and pka signaling pathways independently target the atg1/atg13 protein kinase complex to control autophagy. *Proceedings of the National Academy of Sciences*, 106(40):17049–17054, 2009.
- [182] Sonia Colombo, Pingsheng Ma, Liesbet Cauwenberg, Joris Winderickx, Marion Crauwels, Aloys Teunissen, David Nauwelaers, Johannes H de Winde, Marie-Françoise Gorwa, Didier Colavizza, et al. Involvement of distinct g-proteins, gpa2 and ras, in glucose-and intracellular acidification-induced camp signalling in the yeast saccharomyces cerevisiae. *The EMBO journal*, 17(12):3326–3341, 1998.
- [183] Reinhard Dechant, Matteo Binda, Sung Sik Lee, Serge Pelet, Joris Winderickx, and Matthias Peter. Cytosolic ph is a second messenger for glucose and regulates the pka pathway through v-atpase. *The EMBO journal*, 29(15):2515–2526, 2010.
- [184] Reinhard Dechant, Shady Saad, Alfredo J Ibáñez, and Matthias Peter. Cytosolic ph regulates cell growth through distinct gtpases, arf1 and gtr1, to promote ras/pka and torc1 activity. *Molecular cell*, 55(3):409–421, 2014.
- [185] SA Nadin-Davis, A Nasim, and D Beach. Involvement of ras in sexual differentiation but not in growth control in fission yeast. *The EMBO journal*, 5(11):2963–2971, 1986.
- [186] Brittney McInnis, Jessica Mitchell, and Stevan Marcus. Phosphorylation of the protein kinase a catalytic subunit is induced by cyclic amp deficiency and physiological stresses in the fission yeast, schizosaccharomyces pombe. *Biochemical and biophysical research communications*, 399(4):665–669, 2010.

- [187] Jolanda van Leeuwen, Charles Boone, and Brenda J Andrews. Mapping a diversity of genetic interactions in yeast. *Current opinion in systems biology*, 6:14–21, 2017.
- [188] Chris J Needham, James R Bradford, Andrew J Bulpitt, and David R Westhead. A primer on learning in bayesian networks for computational biology. *PLoS Comput Biol*, 3(8):e129, 2007.
- [189] Daniel C Jeffares, Charalampos Rallis, Adrien Rieux, Doug Speed, Martin Převorovský, Tobias Mourier, Francesc X Marsellach, Zamin Iqbal, Winston Lau, Tammy MK Cheng, et al. The genomic and phenotypic diversity of Schizosaccharomyces pombe. *Nature genetics*, 47(3):235–241, 2015.